Stony Brook University

The official electronic file of this thesis or dissertation is maintained by the University Libraries on behalf of The Graduate School at Stony Brook University.

Fault Detection and Diagnosis for
Multi-Actuator Pneumatic Systems

A Dissertation Presented

by

Kunbo Zhang

to

The Graduate School

in Partial Fulfillment of the

Requirements

for the Degree of

Doctor of Philosophy

in

Mechanical Engineering

Stony Brook University

May 2011

Stony Brook University

The Graduate School

Kunbo Zhang

We, the dissertation committee for the above candidate for the
Doctor of Philosophy degree, hereby recommend
acceptance of this dissertation.

Dr. Imin Kao - Dissertation Advisor
Professor, Mechanical Engineering

Dr. Jon Longtin - Chairperson of Defense
Associate Professor, Mechanical Engineering

Dr. Lei Zuo - Committee Member
Assistant Professor, Mechanical Engineering

Dr. Petar Djuric - Committee Member
Professor, Electrical and Computer Engineering, Stony Brook University

This dissertation is accepted by the Graduate School

Lawrence Martin
Dean of the Graduate School

Abstract of the Dissertation

Fault Detection and Diagnosis for

Multi-Actuator Pneumatic Systems

by

Kunbo Zhang

Doctor of Philosophy

in

Mechanical Engineering

Stony Brook University

2011

In pneumatic actuating systems, various kinds of faults are key factors in degrading system performance and increasing air consumption. It is therefore valuable to monitor pneumatic systems and implement predictive maintenance based on detection and diagnosis of fault conditions. This research investigates effects of leakages on a PLC control industrial multi-actuator (9 cylinders) pneumatic system. Leakages at 8 different levels and 9 different places are introduced in experimental tests. The dynamic models of actuators and control valves in pneumatic systems are discussed and extracted as system performance features in a quantitative study of leakage fault. Due to nonlinear properties of compressed air and friction force, derived dynamic model alone is not able to effectively indicate fault location and level with an expected accuracy. On the other hand, new qualitative methods using processed sensory information for recognizing fault and estimating its levels are devised. The reliability of fault detection and diagnosis solution in a pneumatic system offered by the mathematical tools is found to be highly dependent on the successful selection of input features those are extracted from original signals and the relationship between those extracted features. Finally we present the multi-actuator based vectorized map and a diagnostic features search method which are improvements of previous fault analysis research

in one-cylinder pneumatic system. The proposed method is also a good asset to pneumatic component selection applications. My research work concludes that it is possible to find suitable and reliable on-line monitoring solutions for multi-actuator pneumatic systems by means of locating and estimating compressed air leakage with a better confidence and a relatively small number of sensor installations.

Table of Contents

List of Figures

List of Tables

Acknowledgements

First and foremost, I would like to express my greatest appreciation to my advisor, Professor Imin Kao, for his guidance and devotion to my Ph.D. research throughout the past four years. Professor Kao provides me a perfect research environment, he involves in every step and improvement of my research, and offers expert insights into the subjects of dynamic modeling and fault detection and diagnosis in order to cultivate me to become a qualified Ph.D. from an undergraduate student knowing little about research.

It is my pleasure to acknowledge Professor Jon Longtin, Professor Lei Zuo, and Professor Petar Djuric for taking on the responsibilities of being my proposal and dissertation reading committee members. I sincerely appreciate their efforts in reading through my dissertation, providing comments and criticisms despite their busy schedules. The feedbacks from every committee member improved the quality and insight of my research along the whole fulfillment process of my dissertation.

I have also particularly enjoyed the friendship, many inspiring discussions, and collaborated experiment tests with my colleagues, Dr. Chia-Hung Dylan Tsai, Dr. Chunhui Chung, Dr. Roosevelt Moreno, ,Paul Arauz, Jun Nishiyama, and others in the lab. It was such a happy time to have everyone of them for four years.

Last but not least, I would like to express my greatest love to my family, especially my parents. Their continuous concern and encouragement are the power of pushing me up and full of my everyday life even though we are not living in the same continent. Without their spiritual and financial support, this dissertation would not even be able to start.

Chapter 1

INTRODUCTION

For actuation systems, pneumatics presents an alternative to traditionally limited electric motor and hydraulics technologies in major manufacturing industry. Compared with electric motors and hydraulic systems, pneumatic systems are generally clean, reliable in operation and able to directly coupled with the payload. Additionally, a pneumatic system can offer a high power-to-weight ratio, and can offer cost benefits as high as 10:1 over traditional technologies [2] [3]. Across all manufacturing industries, 70% of facilities have compressed air systems to drive a variety of equipment that accounts for 10% of all electricity and roughly 16% of all motor system energy use according to an assessment of 91 compressed air equipment distributor and 222 industrial end users in U.S. manufacturing industries [4].

There is hardly a factory that can function without compressed air. For many industrial applications, pneumatics is the preferred drive technology. Pneumatic technology is often selected due to its advantageous characteristics including simple construction, overload resistance, extraordinary service life, ease of assembly, reliability, economical cost factors and safety aspects. All these advantages might suggest that pneumatic applications is the best choice for actuation system and wouldnt require further monitoring technology for operation. The uncomfortable truth is compressed air is the most expensive energy available in production facilities. Manufacturers and machine builders are often surprised to learn that compressed air cost up to $ 0.30 / 1,000 scf. Consequently, it is crucial to save energy and optimize throughput. Successfully decreasing energy usage while increasing output depends on paying the greatest attention to the small details in

the way we design and operate manufacturing equipment and processes. For pneumatic systems, monitoring system operation and fault detection become more and more important, much of which has been summarized in Chapter 1.

1.1 Background of Leakage Detection and Diagnosis in Pneumatic Systems

A pneumatic system shown in Figure 1.1 usually has six basic required components [5]:

- An air tank to store a given volume of compressed air;

- A compressor to compress the air that comes directly from the atmosphere;

- An electric motor or other prime mover to drive the compressor;

- Valves to control air direction, pressure, and flow rate;

- Actuators to convert the energy of the compressed air into mechanical forces or torque to do useful work;

- Piping to carry the pressurized air from one location to another.

Wasting compressed air is usually seen as harmless. Actually, air leaks are often underestimated as a waste of energy and money. Leaks furthermore degrade machine performance because actuators produce less force, run slower, and less responsive. Furthermore, leaks require compressor to work on higher load in producing more air to compensate the leakage. Compressed air leaks can contribute to problems with system operations, including:

- Fluctuating system pressure, which can cause air tools and other air-operated equipment to function less efficiently, possibly affecting production,

- Excess compressor capacity, resulting in higher than necessary costs,

- Decreased service life and increased maintenance of supply equipment (including the compressor package) due to unnecessary cycling and increased run time.

A fact of operating cost for compressed air systems shows that 76% of the costs for compressed air are for electrical energy and maintenance, it becomes apparent that the cost of pneumatics is not the investment accounting for only 12% but the operation. Therefore, it makes sense to pay special attention to the proper usage of compressed air. Assuming that the compressors, the distribution system, and the pneumatic drives are all properly sized, steps must be taken to avoid the inefficient use of compressed air and/or air losses caused by leaks.

A little air lost here and there doesnt seem like a big deal. This may be the reason why air leaks are often not taken seriously. In existing installations, leaks are the primary cause of excessive compressed air consumption, as high as even 30% of the total air used. Wasted compressed air may be harmless to the environment, but it is not harmless to the bottom line. When cost is an issue, it is absolutely essential to recognize when compressed air is exhausting into the atmosphere. Very often, the cost of generation is not known; however, some companies use a value of \$ 18-30 per 1,000 cubic feet of compressed air. Leakage rates are a function of the supply pressure in an uncontrolled system and increase with higher system pressures. Leakage rates identified in cubic feet per minute (cfm) are also proportional to the square of the orifice diameter [6]. For various leakage diameter sizes and working pressure, the annual costs of compressed air are listed in Figure 1.2.

For example, assume leaks were found as follows: 100 leaks of 1/32 at 90 pounds per square inch gauge (psig), 50 leaks of 1/16 inch at 90 psig, and 10 leaks of 1/4 inch at 100 psig. The system has 7,000 annual operating hours, an aggregate electric rate of \$0.05 kilowatt-hour kWh, and compressed air generation requirement of approximately 18 KW /100 cfm.

$$\text{Cost savings} = \text{Leaks No.} \times \text{Leakage Rate (cfm)} \times \text{kW/cfm} \times \text{Hours} \times \text{Cost per KWh} \quad (1.1)$$

Using values of the leakage rates from the above table and assuming sharp-edged orifices, the total cost savings from eliminating these leaks are \$ 57,069. Note that the savings from the

3
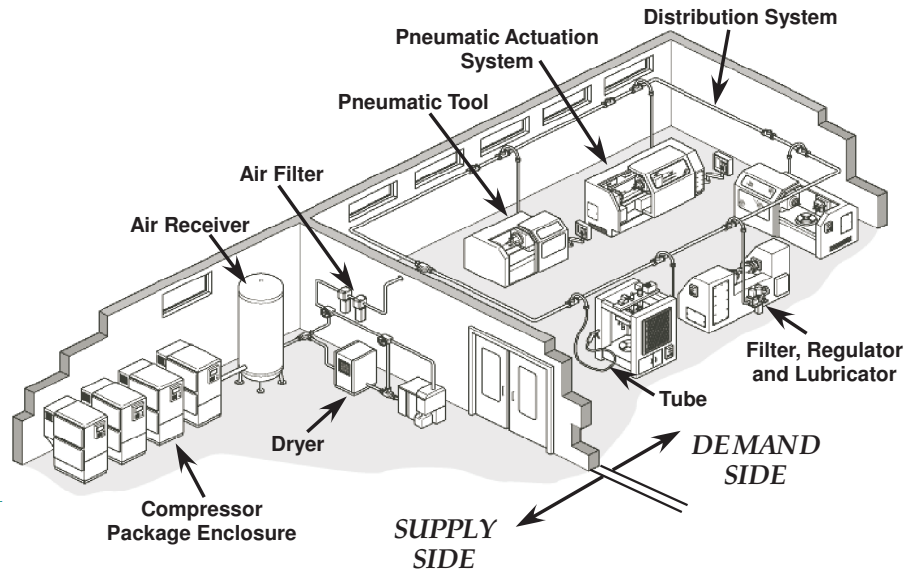
Figure 1.1: Components of a typical industrial compressed air system

Pressue (psig)	Orifice diameter (inches)					
	1/64	1/32	1/16	1/8	1/4	3/8
	Leakage flow rate (cfm)					
70	0.29	1.16	4.66	18.62	74.4	167.8
80	0.32	1.26	5.24	20.76	83.1	187.2
90	0.36	1.46	5.72	23.1	92	206.6
100	0.4	1.55	6.31	25.22	100.9	227
125	0.48	1.94	7.66	30.65	122.2	275.5

Figure 1.2: Leakage rate for different supply pressures and approximately equivalent orifice size.(For well-rounded orifices, values should be multiplied by 0.97 and by 0.61 for sharp ones.)
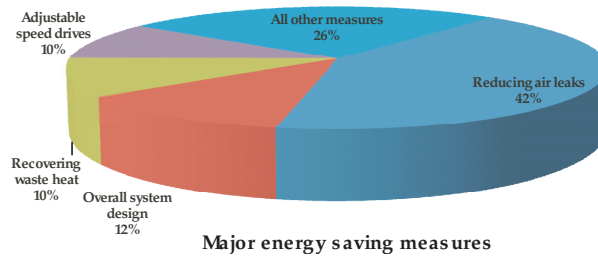
Figure 1.3: Share of major energy savings measures on the overall savings potential

elimination of just 10 leaks of 1/4 inch account for almost 70% of the overall savings. As leaks are identified, it is important to prioritize them and fix the largest ones first.

Another factor regarding leaks is something referred as artificial demand. The higher your supply pressure, the more air your leaks will consume, creating a greater demand on your compressor. By reducing the supply pressure, you can greatly reduce the amount of air that is required to be produced by your compressor. By simply reducing the main pressure the artificial demand created by this leak at 110 psi is reduced. Optimal leakage detection and management radically lowers the cost of compressed air, as leaky components are a great waste of energy and money. Figure 1.3 shows that the major share of the measures on the overall savings potential in pneumatic systems [7].

According to this EU study about 42 % of the total potential savings can be achieved in area of locating and eliminating leaks alone, when the applicability, effective cost and reduction in annual energy consumption is considered for 12 energy saving measures. Leakage detection and diagnosis becomes the dominant part and the most effective way in energy saving of compressed air system. The payback of investment in air leaks detection is also affirmative [4]. More than half of industrial plant air systems have large energy savings opportunities with relatively low project costs in United States. In small- to medium-sized industrial facilities, approximately 15% of compressed air system usage can be saved with simple paybacks of less than 2 years. In larger facilities, these savings could range from 30%-60% of current system usage. In addition to energy benefits, optimized compressed air systems frequently offer corresponding improvements in system reliability, product quality, and overall productivity. However, only 35% of those interviewed

during an assessment regularly conducted leaks prevention programs in their facilities. One reason for that is energy efficiency services sometimes is too costly and the other reason is there is no such an efficient fault detection and diagnosis technology applicable for a complicated compressed air driven plant.

Identification and repair of leaks in the air distribution system and end-use tools can often reduce system energy. The value of leak prevention seems intuitively obvious, given the exposed nature of air lines and the audible hiss of leaks. There several methods used in industrial fields to diagnose a leak. One common way to prevent waste is to regularly search for compressed-air leaks, Formal leak-detection programs usually involve complete, manual inspections of all air lines several time per year. Regular inspections find new leaks and also confirm that tagged leaks from past inspections have been repaired. Technicians typically diagnose pneumatic leaks by use an ultrasonic acoustic detector to recognize high frequency hissing sounds associated with air leaks, periodically inspecting tubes, and tightening fitting. One disadvantage of leak-detection programs is that depending on inspection frequency, leaks can go undetected for a long time. A simpler method is to apply soapy water with a paintbrush to suspect areas. Although reliable, inspections are usually time consuming and may be problematic in noisy industrial environments. Inspectors often miss small leaks, which prevents repair in the early stages before leakage becomes a major problem.

In summary, the most important energy saving measures appear to be reducing air leaks. The urgent necessity inspires our research on fault detection and diagnosis in pneumatic systems and the absence of applicable leaks detection methods under different situations impels us to focus on complicated practical pneumatic system analysis other than simulation and system modeling. There are always a financial savings potential and a theoretical research attraction in a pneumatic system leakage analysis. On the other hand, appropriate management of energy usage in pneumatic systems, including scrutinizing the efficiency of machines, optimizing systems that use pneumatic drive technology, selecting correctly sized component to perform the job, is also significant, which is not the coverage of this proposed study.

1.2   Statement of the Problem

When it comes to fault (leakage) detection and diagnosis in a pneumatic system, there are several major difficulties we need to deal with:

First, the nonlinear properties of pneumatic systems make it nearly impossible to establish an analytical mathematical model. Air is highly compressible, which makes the actuator compliant rather than stiff, introduces lag in the response. Air actuators also have relatively high friction with stick-slip effect that prevents smooth motion under many circumstances. These nonlinear behaviors of a compressed air cylinder preclude good modeling and control methods which work well for electro motor and hydraulic actuation systems. Most of the parameters and equations are derived empirically under certain conditions which means it is not applicable to a different pneumatic component or system.

Secondly, leaks in a compressed air system can be in various types due to diversified reasons. Although leaks can occur in any part of the system, the most common problem areas are couplings, hoses, tubes, seals, fittings, pipe joints, quick disconnects, FRLs (filter, regulator, and lubricator), condensate traps, valves, flanges, packings, thread seal-ants, and point-of-use devices. It is not practical to investigate every type of leak because some of them are unable to be simulated. In our study, we only introduce leakage on tubes which is easy to create and control at different locations.

Thirdly, the most important factor in deciding to invest in a compressed-air monitoring system is whether or not it makes financial sense. As the demand for technical advances and cost reduction in automation continues to increase, companies look for new methods to improve overall equipment efficiencyTo keep a machine running for millions of cycles, every component in its pneumatic system must continue to operate properly. Monitoring key system status indicators for the life of a machine -together with predictive information- can reduce unscheduled and lengthy downtime by eliminating time-consuming error identification and component testing and replacement. Currently, the available data describing machine status are still insufficient, so a new method must be developed to provide additional operating data from all system components. For example, a general rule of thumb is to install at least one flow sensor in the main supply line on every

machine with an average-size pneumatic system. It tracks air consumption over the long term and easily identifies sudden increases in demand. In this way, the proposed method should be fairly good enough to indicate leakage efficiently with a minimal cost of installation and operation.

To meet these specific characteristics, we have been working on developing new fault detection and diagnosis tools for pneumatic systems including model-based and signal-based methods based on the investigation of pneumatic actuation system models and sensory information. Eventually, this diagnostic tool is expected to offer a means of increasing productivity by identifying potential component or system-wide faults. Unlike traditional component based diagnostics, this approach incorporates the entire pneumatic process - from air supply line to actuators - by integrating valves, drives, and sensors into one system. Regardless of the degree of automation, pneumatic components and systems can be monitored and diagnosed under desired parameters in order to reduce service costs, improve the effectiveness of maintenance support teams, and preventive maintenance programs.
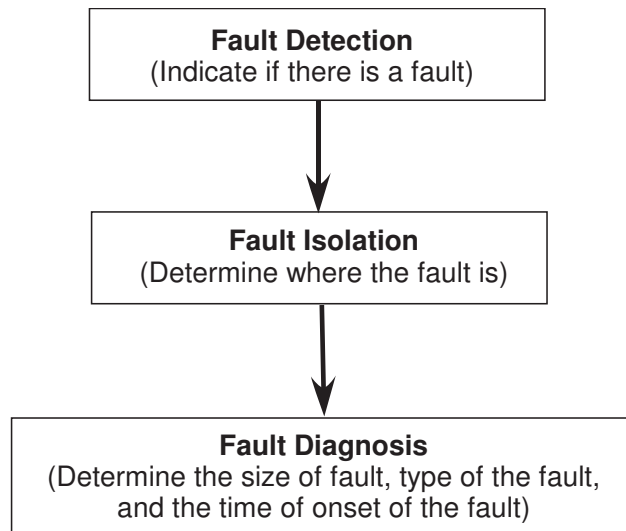
Figure 1.4: Tasks of fault detection and diagnosis

Fault detection and diagnosis systems consist of three major continuous tasks, Figure 1.4 explains the roles of the 3 major segments in FDD analysis. The detection performance of a diagnostic technique is characterized by several parameters including fault sensitivity, reaction speed, and robustness. The diagnosis performance is the ability to distinguish among faults (leakage in

our case) depending on physical properties of the hardware, the size of faults, noise, disturbances, model errors, and the design of the algorithm.

Our research focuses on pneumatic systems modeling, system performance analysis, signal processing and design of diagnostic algorithms. Meanwhile the proposed fault detection and diagnosis methods are expected to reach following objectives:

(1) detect leaks on individual machine and system or in the entire plant during operation,

(2) indicate the severity level for each specific leak,

(3) categorize and record leakage fault for future diagnosis,

(4) able to detect more than one fault existence at the same time,

(5) acceptable system model should be developed to assist in setting up threshold value and explain effects of leaks on system performance,

(6) adequate parameters should be introduced in order to increase the confidence and redundancy of diagnosis result, and

(7) smaller amount of sensors installation cost.

1.3   Outlines and Contribution of the Chapters

The introduction to importance of fault detection and diagnosis in pneumatic systems, statement of the problem, objectives of our research are presented in Chapter 1. A literature review of previous works in this filed is also included in Chapter 2. Chapter 3 describes the experimental setup of a PLC control multi-actuator pneumatic system, including hardware (sensors, valves, and actuators), software, and leakage level control. A brief explanation of recorded signals is presented to indicated the . Chapter 4 discusses the modeling of pneumatic components including valve, actuator, tube, and fault controller with experimental calculated parameters validation. Modal-based approaches of pneumatic analogy, logistic table, and system model are applied in detecting and

diagnosing leakage. In Chapter 5, signal-based approaches, wavelet in fault classification, vectorized map, and voronoi diagram, are introduced to analyze fault quantitatively and qualitatively. The topics of future work are proposed for three potential areas continuing from current research in Chapter 6: (1) Internal Leakage Detection and Diagnosis of Pneumatic Actuators and Valves, (2) Sensors Reduction, and (3)Fault Detection and Diagnosis in Pneumatic Systems Other Than Leakage.

Chapter 2

LITERATURE REVIEW

2.1   Fault Detection and Diagnosis

For the improvement of reliability, safety, efficiency, of supervision, fault detection and diagnosis (FDD) become increasingly important for many technical and industrial processes, such as power plants, chemical plants, steel mills, and airplanes heating equipment. The early detection of faults is critical in avoiding product deterioration, performance degradation, major damage to machinery and human health, or even loss of lives. For centuries the only way to learn about malfunctions and their locations was biological senses: looking, listening, touching and smelling. A dramatic development took place with the arrival of the computer and proliferation of its real-time applications [8]. The methods of fault detection and diagnosis may be classified into two major groups: *(i)signal-based methods: those which do not utilize the mathematical model of the plant*, and *(ii) model-based methods*. Some model-based FDD approaches have their origins from chemical process control. Some pioneers of this effort were D. Himmelblau [9], R. Mah (1976), G. Stephanopouls (1981), and V. Vaclavek (1974). Another root traced to aerospace related research sponsored by NASA, was spearheaded by A. Willsky (1976) and J. E. Potter and M. C. Suman (1977). In parallel, several researchers examined the possibility of applying the Kalman filters to perform FDD. The application of the Kalman filter idea can be traced to R. K. Mehra, and J. Peschon (1971), and A. Willsky (1976 and 1986). The original ideas of diagnostic observers probably came from R.V. Beard (1971) and Harold Jones (1973). They were followed by a other

researchers, including P. Frank (1980), M. A. Massoumnia (1986), N. Viswanadham (1987), J. Speyer (1987), R. Patton (1989), and G. Rizzoni (1994).

In development of process fault detection and diagnosis based on modeling, parameter, and state estimation, substantial work has been done by R. Isermann and his colleagues (1984, 1993, 1991). Other contributors also include A. Rault and coworkers (1984), B. Ninness and G. C. Goodwin (1991) in this area. The fundamental equivalence between parity relation and observer based designs was demonstrated by Gertler (1991). Similarly, some partial results and other supplementary were obtained by N. Viswanadham (1987), P. Frank (1990), J. F. Magni and P. Mouyon (1994). The clear link between parity relations and parameter estimation was pointed out by Gertler (1995). Furthermore, Akbaryan and Bishnoi presented fault diagnosis of multivariate systems using pattern recognition and multi-sensor data analysis technique [10]. Kumamoto *et al.* introduced the application of expert system techniques to fault diagnosis [11].

For the application of model-based fault detection and diagnosis(FDD) method, it is important to establish the exact or approximated model of system and components since the methods are developed based on fundamental understanding of physics. The earliest study on the modeling of a pneumatic servo system was published by Shearer in 1956 [12], who derived a set of nonlinear differential equations representing the system dynamics based on five law of physics. A similar model was presented in 1980 in [13]. These two reference formed the basis for most of the modeling research published to date. Derivations of similar nonlinear models have been presented in many recent publications for example [14, 15], in which a detailed mathematical model of dual action pneumatic actuators controlled with proportional spool valves and two nonlinear force controllers based on the sliding mode control theory were developed. In 2005 S. Ning and G. Bone [16] presented an experimental test of the "Standard Model" applicability to the hardware being modeled, and showed how to improve the accuracy of values.

Other nonlinear modeling approaches involved using neural networks or fuzzy logic. Fuzzy logic methods were used in [17, 18]. Balle and Fussel used a nonlinear fuzzy model with transparent inner structure for the generation of relevant symptoms in [17]. Chang *et al.* used dynamic fault

trees in a fuzzy diagnosis approach in [18]. Neural networks were used in [19, 20, 21, 22, 23, 24]. Chen *et al.* presented the neural networks of fault tolerant control scheme in flight control [19]. Kramer *et al.* presented an analysis and criticism on diagnosis using back-propagation neural networks in [20]. McGhee *et al.* introduced the application of neural networks for the identification and fault diagnosis of process valves and actuators in [21]. Tsai and Chang studied a generic scheme of integrated artificial neural networks for the purpose of fault detection and diagnosis in dynamic systems with varying inputs in [23]. Skoundrianos and Tzafestas studied the problem of plants with unknown description via a modeling techniques based on the local model network structure in [22].

Signal processing is also a promising approach for fault detection and diagnosis. Recently, Jin and Shi presented automatic feature extraction of waveform signals for in-process diagnostic performance improvement [25]. A fault detection and diagnosis for the continuous process with load-fluctuations using orthogonal wavelets was presented by Tsuge *et al.* [26]. Silveiria *et al.* presented an approach using wavelet transform for fault type identification in digital relaying [27]. Sun and Tang applied continuous wavelet transform for fault diagnosis of bearing [28]. More application of signal processing techniques in FDD can be found in various publications such as [29, 30, 31, 32]. Venkatasubramanian, Rengaswamy, and Kavuri reviewed process fault detection and diagnosis in [33, 34, 35].

A series of notable research has been performed by Xiaolin Li and I. Kao [36, 37, 38] for introducing an applicable FDD method based on an empirical one-actuator pneumatic system. Their presented diagnosis system focuses on the signal-based approaches which employed multi-resolution wavelet decomposition of various sensor signals such as pressure, flow rate, and flow to extract various useful features and determine leaks conditions. Additionally, pattern recognition technique, analytical vectorized maps, and fast search Voronoi method [39] were developed to diagnose an unknown leakage based on the established know feature vector classes. The limitation of this research include the relatively simple construction of the system with restricted leakage location, lack of complete dynamic model, applicability for various situations, and explanation

of candidate features selections. Our research, a continuation from Xiaolin's work applying and amending some of their methodologies, is based on a more complicated multi-actuator complex pneumatic system controlled by PLC, improving the applicability of vectorized map and feature extraction in multi-actuator situation, providing a solid theoretical backup for signal process steps, and combining model-based and signal-based technology to increase the reliability of the diagnostic methods.

2.2   Pneumatic System Models

The works generally recognized as the first significant presentation on pneumatic system modeling are a pair of papers authored by J. L. Shearer of MIT in 1956 [12]. In these papers, Shearer develops a linear mathematic model of a double-rod cylinder for small motions about its mid-stroke position. He also presents a theoretical model of the mass flow rate through a sliding-plate proportional valve, verifying the model experimentally. While the availability of modern computers has rendered his linear model obsolete, subsequent researchers in the field have copied his methodology towards the development of a model. A paper by Liu and Bobrow expands on Shearers work by developing a linear model based on an arbitrary operating point [40].

While linear models are preferable from the standpoint of controller design, pneumatic cylinders are highly nonlinear due to the effects of air compression, varying air volumes in the actuator, and friction. Wang and Singh investigate these nonlinearities in a study of a closed pneumatic piston chamber [41]. They find the nonlinear effects of friction and compressibility not only shift the resonant frequency of the mechanical system, but also induce asymmetric oscillatory behavior in the system. Nonlinear models are presented in a number of other papers, notably Richer and Hurmuzlu in [14, 15]. Their models includes the effects of propagation delay and friction losses in air hoses, which can be significant over long distances. While the model is qualitatively correct in predicting motion, many of the coefficients used in the model were engineering estimates of the actual values. This precludes a proper quantitative comparison of the simulation results with the experimental data. Figure 4.2 shows a typical valve-tube-cylinder system.

14

A recent approach to the modeling of pneumatic systems comes in the form of computer based simulators in which the engineer designs a virtual system. Hong and Tessman present a commercially available software package that models both pneumatic and hydraulic circuits [42]. Anglani, et al. present a similar package that works in a CAD environment, and allows the pneumatic system to interact with external mechanical elements [43]. Both systems are designed more for the practicing engineer as a tool for selecting components for a particular application, rather than for fundamental research into pneumatic systems.
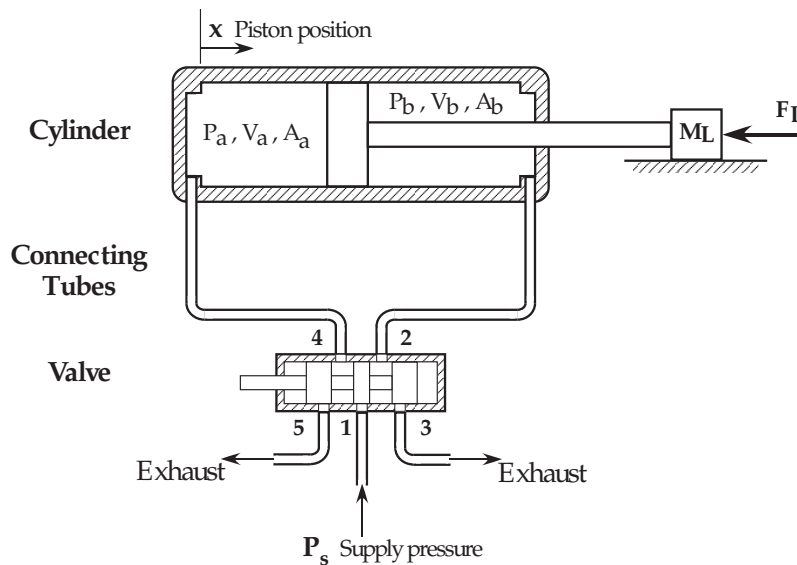
Figure 2.1: Schematic of a valve-tube-cylinder system

One issue in modeling of pneumatic processes is applying an isothermal model or an adiabatic model towards the expansion of air. The fundamental equations are similar, with the adiabatic expression being a factor of $1/k$ different than the isothermal expression. The term k refers to the ratio of specific heats ($k = 1.4$ for air). While a few researchers have applied the isothermal model, most assume the mechanical processes are significantly faster than the thermal processes, and thus use an adiabatic process. An exception worth mentioning is the study conducted by Pu and Weston in [44], in which the steady-state velocity of a pneumatic actuator may be predicted. In [14], Richer and Hurzumlu replace k with an intermediate term, α, in a hybrid model. The α term is bounded by 1 and k, and represents a compromise position between isothermal and adiabatic

15

processes, though they find the isothermal model better fits their experimental data. Backe and Ohligschlager investigate heat transfer in an air cylinder in detail [45]. They find a cylinder in motion initially behaves adiabatically, but heat flow works to restore isothermal conditions. The authors identify three experimentally determined parameters to describe the heat-transfer behavior: an air friction factor, a forced convention factor, and a natural convention factor. These factors may be determined by comparing simulated pressure- and temperature-time curves with measured data. Kawakami also investigate the differences between isothermal and adiabatic processes in a pneumatic cylinder in [46]. Their research indicates the practical differences between the two models is small enough as to be insignificant.

The mathematical modeling of flow through a valve is another concern in pneumatic systems. At least four flow models have been presented in previous literature: a model based on the theoretical flow through an orifice; the approximation of orifice flow in NFPA standard [47]; a model proposed by the ISA [48], and a model developed by ISO/JIS [49]. While different in their formulation, these models share a number of characteristics. Detailed discussions about modeling pneumatic components are presented in Chapter 4. In [50], Bobrow and McDonell tried a least-squares fit of experimental data with the theoretical flow through an orifice, trying to identify the flow coefficient. The authors ended up using an empirically-derived function to describe the valve flow. While most studies of pneumatic systems focus on linear actuators, Pu, Moore, and Weston develop a mathematical model of rotary air motors [51]. Another study of rotary actuators is performed by Wang, Pu, Moore, and Zhang in [52]. In it, the authors use Fourier series expansion to approximate discontinuous functions as continuous functions of the actuatorfs rotation. Generally, researchers assume the dynamics of the valves controlling a pneumatic actuator is significantly faster than the dynamics of the actuator and mass under control, so that the valve may be treated as a nonlinear gain function. Vaughan and Gamble create a detailed nonlinear model of the dynamics of a proportional valve in [53], accurately predicting the open-loop behavior of the valve. This study was conducted in order to apply a sliding mode controller to the valve in [54].

While the nonlinear dynamics of a pneumatic cylinder have been studied by numerous re-

searchers, the effects of friction draw particular attention. Friction has been identified as the most significant nonlinearity in a servo pneumatic actuator [55]. Stick-slip motion caused by friction can prevent certain motions from being realized. Any number of methods have been developed to model, analyze, and counteract the effects of friction. The works cited here are representative of the research being conducted in friction and tribology. Armstrong-Hlouvry, et al., perform an exhaustive survey of tribology and friction in a 1994 study that covers models, analysis tools, and compensation techniques for machines with friction. Their summary of friction models concludes with an integrated friction model having seven parameters for sliding contact between hard metal parts, lubricated by oil or grease. In many cases, this model may be extended to dry contact between surfaces. While there have been successful examples of servo controllers compensating for friction in both research and industry, the control and compensation tools are often more advanced than the techniques available to analyze the friction. In addition to Coulomb friction, stiction, and viscous friction, the author includes Stribeck friction, rising static friction, frictional memory, and pre-sliding displacement for a more complete model. Dimensional analysis permits a study of the effects of friction using five terms instead of ten. It also permits for an approximate, calculus-based analysis of control schemes, as opposed to numerical simulation of a specific system. Johnson and Lorenz map friction as a function of velocity, then perform a regression analysis to identify coefficients for static friction, Coulomb friction, viscous friction, and exponential friction [56]. A thorough model for friction includes five empirically-derived terms, but Canudas de Wit, et al. [57] present a three-term exponential approximation that is generally valid over the range of speeds considered. Wang and Longman study stick-slip friction in systems with learning controllers [58]. In sampled-data systems with significant friction, they find a minimum movement size is necessary to avoid limit cycling about the reference position. In [59], Dunbar, et al. present a methodology for identifying dry friction faults in a pneumatic actuator, though the method can be applied to other systems. An empirical fourth-order model for a pneumatic system is derived. Residuals calculated from the acceleration are proportional to the friction. The pneumatic muscle actuators of [60] are single-piece devices that mimic biological muscle, and have no sliding contacts within

the actuator.

Even though it is difficult to obtain a perfect analytical description, modeling of pneumatic system could be extremely useful for fault detection and diagnosis. Because it is the bridge between sampled signals and pneumatic components, without knowledge of physical meaning behind the signal information we are not be able to explain what we process. And it offers qualitative detection results which determine the system situation deviation from normal case. System models also assist in selecting and generating appropriate diagnostic features we can't directly capture from sensory information. It is simple to correlate system performance changes with monitored parameters via the help of pneumatic system models.

2.3   Applications of FDD in Industrial Pneumatic Systems

Besides all the FDD research attempts mentioned above, there are also several successful applications of leakage diagnosis in industrial field. One of the pioneers is Festo, a supplier of automation technology in compressed air systems offering services of leakage detection, energy saving and compressed air consumption analysis [61]. Festo claims by identifying and eliminating leaks, by optimizing the compressed air generation and distribution layout, plant operators can expect to save up to 50% of energy costs. With savings of that order, a full optimization and maintenance program will pay for itself within two years [62].

Festo's concept is to deploy sensors across the pneumatic system regarding problem areas to be diagnosed. The information collected from these analog and digital sensors is fed to Festo PLC, which not only performs machine control functions but also runs custom pre-programmed diagnostic algorithms to process this data and display the results on an operator panel with alarms when thresholds are violated. Information used for diagnosis includes analog signal, time of actuator travel, time of valve switching, counting of actuator stroke, and air consumption calculation [63]. Diagnosis uses characteristics and symptoms to identify the existence of actual or impending faults - and locate them. It analyzes directly measurable signals using cause and effect mechanisms. Diagnosis may alternatively be model-based, enabling the number of sensors and the

Energy Monitoring Package – Contents

Plant wide asset and energy management system

FED Operator Interface

SCADA - VipWin Software

SDE1 Pressure Sensor

FDC Module

SFE1 Flow Sensor

MS6-SFE Flow Sensor

Technical Data	
Monitoring	flow, pressure and air consumption
Power supply	24 V DC
Flow measuring ranges	SFE1: 10 to 200 l/min, MS6-SFE: 200 to 5,000 l/min
Pressure sensor	SDE1: 0 to 10 bar
Measuring rate	approx. 10 ms
Update rate	approx. 2 s
Visualization	SCADA or FED
Monitoring statuses Status display	Green Normal operation Yellow Warning Orange Maintenance reminder Red Alarm Grey No signal available
History	trend data for air consumption and flow data export option as an .csv file
Process coupling	digital interface for • operating status • product number • status/trigger signals Profibus/DeviceNet* OPC
Systems of units available	SI units or U.S. customary units

Figure 2.2: Festo Compressed Air Energy Management - A standard product package for monitoring air consumption, pressure and flow

costs to be significantly reduced. In order to localize faults in pneumatic systems, personnel rely on existing data from drive units and valves as well as additional key sensors such as pressure and flow, analyzing this data using controllers and software solutions. Malfunctions here may include inadmissible leakage due to tubing damage. The maintenance staffs are guided to the location of the problem.

For an example of real fault detection and diagnosis at work, an American ophthalmic lenses manufacturer Davis Vision uses remote monitoring and diagnostic systems from Festo to contribute to the trouble-free production of ophthalmic lenses on CNC machines [64]. Sensors for pressure (SDE1) and flow (SFE1) monitor the pneumatic gripping mechanism of a spindle, which is used to grind the shape of the optical lenses. Using a pressure profile, daily checks are performed on the PC and via the front-end display to determine whether there are any leaks in the compressed air system. A predictive maintenance program helps the company to identify any irregular increase in compressed air and therefore replace the gripping mechanism before it comes to a standstill.

Moreover, energy savings also increases by checking every pneumatic component for correct sizing and application. A suitable example of saving energy through ideally sizing pneumatic components to optimally perform the function required was one discovered during a recent Festo Energy Saving Service. The recommendation offered was to replace the double acting cylinders with single acting, spring return cylinders. As a result, the total air consumption was reduced by nearly 50%, and the potential sources of leaks were reduced by 44%.

Other industrial fault diagnosis applications include usage of enhanced positioner firmware EXPERT for early faults detection of control valve with pneumatic actuators giving maintenance recommendations from SAMSON which performs online monitoring [65], and LeakMate devices from Enertech able to identify leak components and quantify gas leaks of a test volume based on pressure decay, makeup flow, and sonic nozzle technologies [66].

2.4   Terms in Fault Detection and Diagnosis

In order to keep the terminology consistent in this dissertation, definitions related to the fault detection and diagnosis are listed in the following. Most of the terminology used in the following chapters were first introduce and defined at SAFEPROCESS Technical Committee. Some basic definitions can be found, for example in the RAM (Reliability Availability and Maintainability) dictionary (1988), in contributions to IFIP (1983), and in German standards such as the DIN standards and VDI/VDE-Richtlinien [67, 68].

(i) *States and Signals*

- Fault: An unpermitted deviation of at least one characteristic property or parameter of the system from the acceptable/usual/standard condition.

- Failure: Permanent interruption of a system's ability to perform a required function under specified operation conditions.

- malfunction: An intermittent irregularity in the fulfillment of a system's desired function.

20

- Error: A deviation between a measured or computed value (of an output variable) and the true, specified or theoretically correct value.

- Residual: A fault indicator, based on deviation between measurements and model-equation-based computations.

- Symptom: A change of an observable quantity from normal behavior.

(ii) *Functions*

- Fault detection: Determination of faults present in a system and the time of detection.

- Fault isolation: Determination of the kind, location and time of detection of a fault. Follows fault detection.

- Fault identification: Determination of the size and time-variant behavior of a fault. Follow fault isolation.

- Fault diagnosis: Determination of the kind, size, location and time of detection of a fault. Follows fault detection. Includes fault isolation and identification.

- Monitoring: A continuous real-time task of determining the conditions of a physical system, by recording information, recognizing and indicating anomalies in the behavior.

(iii) *Models*

- Quantitative model: Use of static and dynamic relations among system variables and parameters in order to describe a system's behavior in quantitative mathematical terms.

- Qualitative model: Use of static and dynamic relations among system variables and parameters in order to describe a system's behavior in qualitative terms such as causalities or if-then rules.

- Diagnosis model: A set of static dynamic relations which link specific input variables - symptoms - to specific output variables - faults.

- Analytical redundancy: Use of two or more (but not necessarily identical) ways to determine a variable, where one way uses a mathematical process model in analytical form.

(iv) *System Properties*

- Reliability: Ability of a system to perform a required function under stated conditions, within a given scope, during a given period of time.

- Safety: Ability of a system not to cause danger to persons or equipment or the environment.

Chapter 3

EXPERIMENTAL SETUP

The goal of this study is to establish a detection and diagnosis method, which generates information and maintenance suggestions based on the conditions of the pneumatic system components by using available sensory information. The complete range of sensor signals and information of pneumatic actuators and valves are available from the real-time control of the system. Thus, these signals can be used for the diagnosis of local components and system and entire plant. Finally, this intelligent fault detection and diagnosis methodology can be integrated with the real-time control system in order to contribute to a energy efficient and condition-based monitoring tool implementation. The rest of this chapter explains experimental setup of this multi-actuator pneumatic system, including valve, actuator, sensor, control module, DAQ, and how we introduce leakages , and give a brief introduction to the signal we capture from various sensors.

3.1   Introduction

A multi-actuator PLC control industrial pneumatic system has been constructed with customized settings in order to study the effect of different manually introduced faults/leakages on this complex system. This system facilitates us to extend the previous research work performed on a one-cylinder pneumatic system [39] where more accurate signals due to system design based on industrial standards and the complexity of multiple actuators moving respectively and simultaneously can't be realized. This pneumatic system is controlled by PLC and executes an assigned

movement sequence cyclically using power of compressed air. Numerous sensors are deployed on every possible faulty place to provide sufficiently localized or systemic information for fault detection and diagnosis.

3.2 Experimental Equipment and Setup

3.2.1 Schematic of the Multi-Actuator Pneumatic System

The schematic of the configuration of the multi-actuator-pneumatic system is shown in Figure 3.1. The PLC-based real-time control and data acquisition system includes hardware, software, and HMI control panel to make up this mechatronic system. The system executes a prescribed sequence of movements and control which becomes, at the high-level task level, an automated robotic system performing several inter-related pick-and-place assembly tasks. It is intentional to design the actuators following a cyclic sequence due to the purpose of research convenience.

The manufacturing automation system consists of a total of *16* control valves, *12* flow control valves, *52* sensors (including both digital and analog types), *10* pneumatic actuator (including linear and rotary cylinders and vacuum gripper) and *3* pressure regulators. The input pressure is set to be lower than *80 psi* (*5.5 bar*) and the maximum working flow rate is about *200 l/min* due to limitation of flow meters measuring range. A snapshot photo of this research system in our lab is shown in Figure 3.2 with the corresponding schematic of the whole system in Figure 3.1. Part of the pneumatic circuit, which we primarily work on, including subsystems of two cylinders from this manufacturing automation system is illustrated in Figure 3.1.

3.2.2 Pneumatic and Mechanical Setup

The system was constructed by the Festo(US) Corporation in collaboration with our research team from Stony Brook University. Initial data acquisition and experiments were also designed and conducted at Festo using their high quality house air system. Later, the system was donated to Stony Brook. We continue to use this system to conduct experiments, add more sensors, change
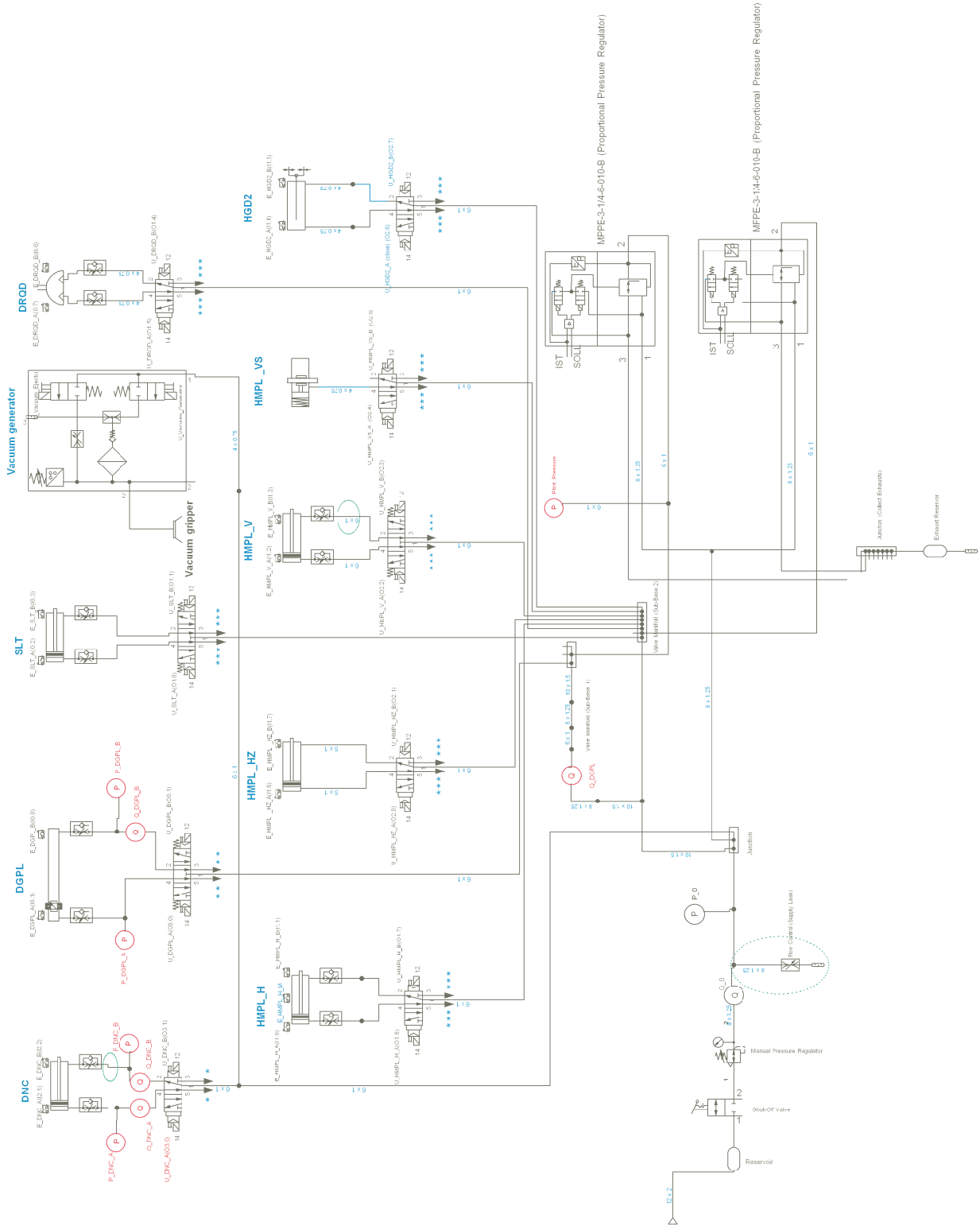
Figure 3.1: Schematic of the pneumatic system setup
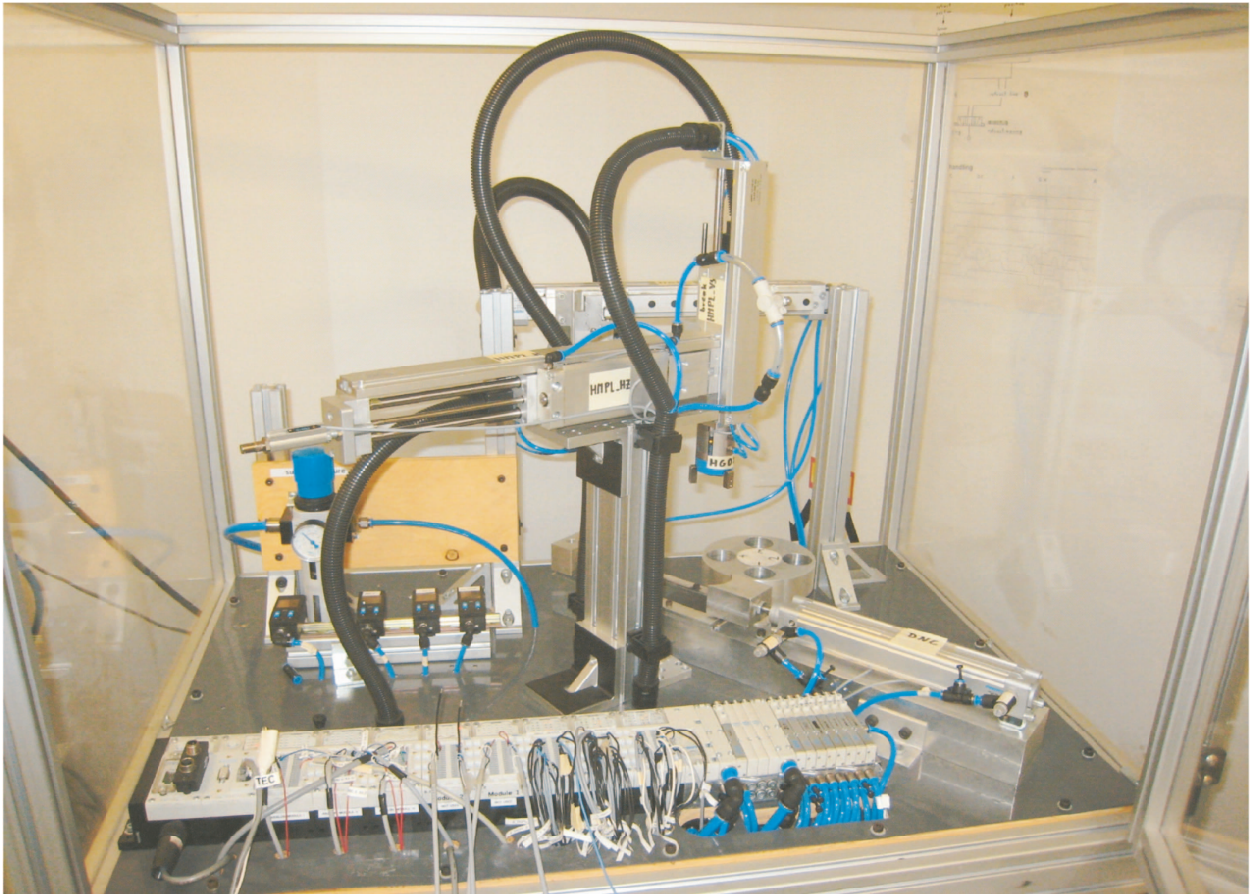
Figure 3.2: A photo of automated manufacturing system for experimental study

the ways of introducing leakage, and adjust flow control parameters in the system in order to meet our research purposed at different stages.

This integrated system performs the pick-and-place task of cylindrical pegs using robot arms, putting it in the tray with 4 different choices (rotatory actuator), picking it up, placing it on a slider (linear actuator), moving it to mother location, picking it up and placing it at another location. The process reverse itself and repeats for other pegs. During the prescribed operations, the pistons move back and forth between the extending and retracting positions. There are totaly five different types of actuator, including double-rod cylinder, rotatory cylinder, rodless cylinder, and spring-return cylinder, applied in the system, giving us the opportunity to investigate properties of various

cylinders and their interaction characteristics. Table 3.1 outlines major hardware components of the system and their specifications as shown below.

System Component	Specifications	
Air Compressor	Model NO.	WL65001AJ
	Major Parameters	13 gallon tank 5.5 SCFM@90 psi 125 MAX psi
	Manufacturer	Campbell Hausfeld
	Function	Compressed Air Supply
Air Filter	Model NO.	H2A-6C10-050
	Major Parameters	MAX pressure 300 psig MAX temperature 225 °F
	Manufacturer	Finite filter Co.
	Function	Filter Air
Tubing	Model NO.	PUN
	Major Parameters	Outer diameter 3-16 mm Internal diameter 2.1-11 mm
	Manufacturer	Festo
	Function	Transfer Compressed Air
Filter Regulator	Model NO.	LFR-D-5M-MIDI
	Major Parameters	Regulation range 0.5-12 bar
	Manufacturer	Festo
	Function	Pressure regulation and filter
Pressure Regulator	Model NO.	MPPE-3-1/4-6-D10-B
	Major Parameters	Regulation range 0-6 bar Flow rate 0-1600 l/min@6 bar
	Manufacturer	Festo
	Function	Regulate pressure
Reservoir	Model NO.	CRVZS-2
	Major Parameters	Volume 2 l operating pressure -0.95-16 bar
	Manufacturer	Festo
	Function	Compensate pressure fluctuations
DNC Cylinder	Model NO.	DNC-32-200-PPV-A
	Major Parameters	Piston diameter 32 mm stroke 200 mm position sensing
	Manufacturer	Festo
	Function	Linear actuator
SLT mini slide	Model NO.	SLT-010-08-A-CC-B
	Major Parameters	Piston diameter 25 mm stroke 230 mm
	Manufacturer	Festo
	Function	Double-acting drives

Table 3.1: A list of pneumatic and mechanical parts and their specifications

3.2.3   Motion Control Components

The movement of the actuators of this pneumatic system is controlled by host computer through a Festo modular electrical I/O valve terminal CPX, which is an integration of PLC controller, signal I/O modules and valves. The electrical CPX terminal is a modular peripheral system for valve terminals. The system is specifically designed so that the valve terminal can be adapted to suit different applications. The modular system allows one to control and monitor the status of valves which drive the movement of actuators with pre-uploaded program developed using FESTO *statement List Programming Language*. Figure 3.3 shows the CPX components connection diagram and the functional explanation of the components.

During operation, signals from proximity sensors are used to assist control of extending and retracting movement of the piston. When the proximity signal switches from 0 to 5 *V* (from 0 to 1 in digital signal state), it means the piston is reaching one side, where the proximity sensor is attached, of the cylinder; when the proximity signal switches from 5 *V* to 0, it mean the piston is moving away from the corresponding side of the cylinder. If the proximity signal does not change, it indicates either the piston is staying out or it has not arrived at the location. Control signal of valve is sent out only when the desired proximity sensor signal is detected. The solenoid valves operate with a 24 *VDC* power supply, with a sampled digital signal 1 (0 *V*) indicating the corresponding side solenoid being stimulated and the valve opens and a value 0 (5 *V*) indicating the corresponding side valve is closed. All the valves used here are on/off directional valves which means the orifice area of a valve is not able to control like proportional valve.

For a linear pneumatic cylinder, the piston moves back and forth between the extreme left position and the extreme right position during operation. As shown in Figure , when the piston is fully extended from its folded configuration, it is said to take the extended position. On the other hand, when the piston retracts from the extreme right position to the extreme left position, it is said to take the retracted position. The extending and retracting motions of the pneumatic cylinder are controlled by the two solenoids of the control valve. When the piston reaches the end the the stroke, the proximity sensor detects the arrival of the piston rod and send the signal to the

computer [69]. The computer in turn will determine the next action and send control signals to respective solenoid valves.
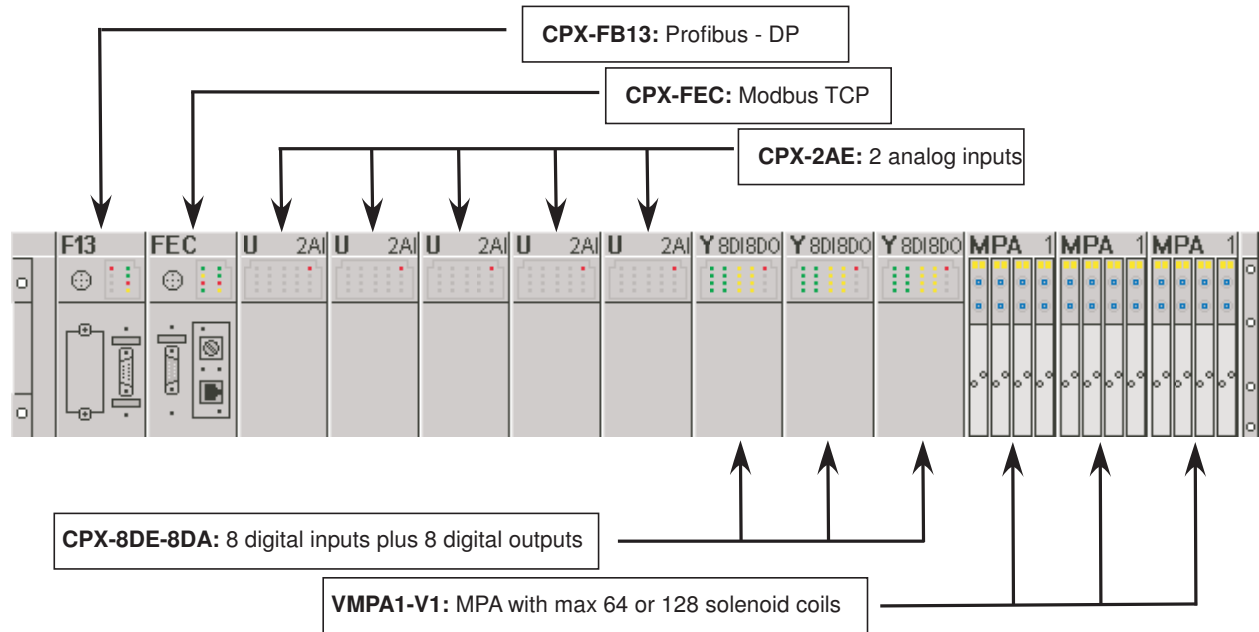
Figure 3.3: CPX terminal connection diagram

The movement sequences of this pneumatic system are listed in Figure 3.4 including the first and last five steps.

Besides open/closed control valves to control actuators, there are several flow control valve placed on lines of both sides connected to cylinders. This throttling device is adjustable to permit regulation of the air flow through the valve, with throttling in one direction of the flow only. In the other direction, free flow is provided through the check valve [70]. In our system, the flow control valves regulate the rate of flow of air exhausting to the atmosphere and the speed of cylinder movement, which gives an initial rapid movement followed by a slowing down as air is compressed on the exhaust side of the piston. However, one needs to notice that the dynamic behavior of the piston will change after introducing the flow control valve because the pressure information measured after the control valve can't assist in analyzing cylinder chamber dynamics. In this way, we take out flow control valves to study the true performance of an actuator first and then put them

Step 1	U_DRQD_A (reach 90° move CW)
Step 2	U_DNC_B (move in)
	U_DRQD_B (reach 0° move CCW)
	U_HMPL_H_A (Extend to DRQD position)
Step 3	U_DRQD_A (reach 90° move CW)
	U_SLT_A suction (move down)
Step 4	Vacuum generation
Step 5	U_SLT_B suction(move up)

Step 54	U_HMPL_V_A (move down)
Step 55	U_HGD2_B (open gripper at HMPL)
Step 56	U_HMPL_V_B \ (move up)
Step 57	U_HMPL_VS_B (close clamb-cylinder)
Step 58	U_DNC_A (push out)
	U_DRQD_A (reach 90° move CW)

Note - Multiple transitions occurring within the same step indicates that these are parallel movements (initiated at the same time).

Figure 3.4: The movement descriptions of the first 5 steps and last 5 steps and their corresponding valve control signals

back to better investigate the actuator performance under different situations.

3.2.4   Sensors and Data Acquisition

A data acquisition (DAQ) system lies in the heart of the control and sampling subsystem of the experimental setup. The data acquisition system in this test consists of *(i) sensors (transducers)*, *(ii) data acquisition hardware (break-out box for connection interface)*, and *(ii) a computer*. The flow chart of data acquisition process is depicted in Figure 3.5. And components of the DAQ system are described as follows.

Five different types of sensors are employed in the system. They are described in the following.

- *Flow meter*: Flow meter can be placed in the path of air flow to measure the flow rate
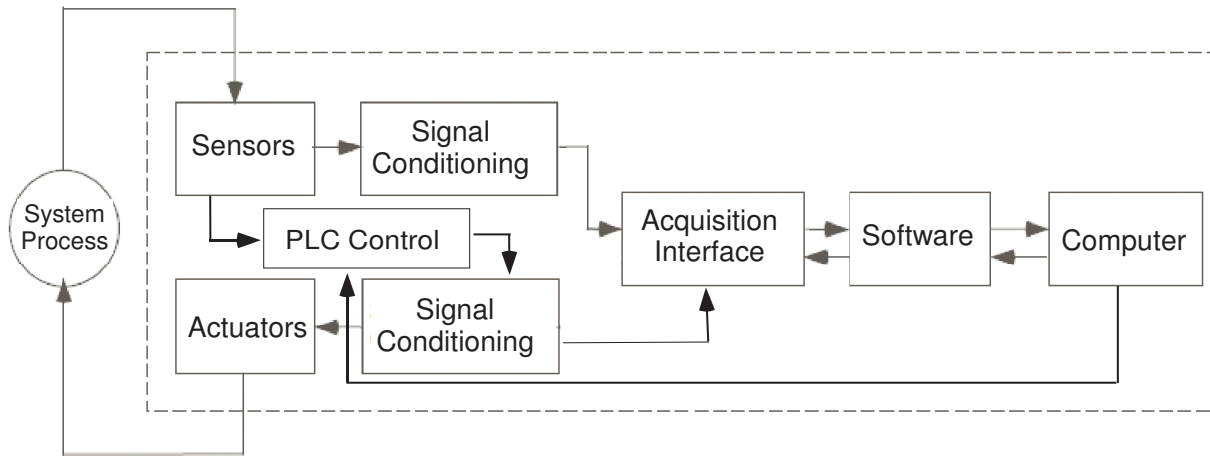
Figure 3.5: The data acquisition system of the pneumatic system

- *Pressure sensor*: Pressure sensors are connected to the location within the pneumatic system at which the pressure is to be measured

- *Proximity sensor*: Proximity sensors are installed at the extending and retracting sides of pneumatic cylinders to detect the location of piston rod movement

- *Solenoid valve sensor*: Solenoid valves are used to control the movement of compressed air. The valves are opened or closed by electro-magnetic means of actuators with line signals of 0 or 1 that can be sampled by the DAQ system.

- *LVDT* : This LVDT sensor attached to the rod head of the studied cylinder to offer linear displacement signal which can be derived to velocity and acceleration information.

Flow sensors used in the system is designed based on thermal technology of measuring of temperature change at two places of laminar flow warmed up by a heater. With a measuring rang between 0   200 l/min, the flow meter output analog signals of flow rate in unit of SLPM (standard liter per minute) and accumulated flow measurement in unit of Standard Liter.

The contacting proximity sensor SME is built according to magnetic reed measuring principle. It consist of a reed switch whose contacts close when a magnetic field (cylinder piston) approaches, thus generating a switching signal. Festos proximity sensors are position sensors and they are mounted on placed of the end of a cylinder stroke. As soon as the cylinder piston returns to this desired position, the switching signal status changes. A demonstration of how a cylinder stroke is defined and how a proximity sensor functions is shown in Figure.

Displacement information is offered by the help of an Omega Linear Variable Displacement Transducer (LVDT) attached to the cylinder piston rod. It is installed on two wooden clamping supports to avoid interference of magnetic materials . All of the captured sensory information is directly used for analysis except the LVDT signal. From Figure 3.6 you can see the original displacement signal of a stroke full of noise, this is due to the high sensitivity of the LVDT, vibration of testing system, and the nonlinear stick-slip effect when the piston is moving. We use Butterworth filter to filter out undesired noise. Figure 3.7 and Figure 3.8 compare the plots derived velocity and acceleration signals signals from cylinder DNC before and after filtering. Compare the LVDT result calculated from equation (3.1) with actual cylinder DNC stroke length 200 *mm*, the very good approximation validated the help of filtering in processing LVDT signal.

$$0.517 \ \frac{m}{s} \ \text{(average speed)} \times 0.38 \ s \ \text{(stroke time)} = 196.46 \ mm \approx 200 \ mm \qquad (3.1)$$

The DAQ board is set with $0 \sim 10 \ V$ unipolar input since most analog sensors have unipolar output in this range. However, the signal from the proximity and solenoid valve control sensors are 12 *V* and 24 *V*, respectively. They are conditioned to become digital signals to be acquired by the digital input channels of the DAQ system. The communication between the PLC and computer is done by an ethernet cable.We employ the NI-PCI-6025E DAQ card to interface to the PLC with which the sensor signals are directly connected. The NI-PCI-6025E DAQ has 16 single-ended analog inputs, two 12-bit analog outputs and 32 digital I/O lines, with a sampling rate as high as 200 *kS/s*. It comes with a compatible SCB-100 shielded I/O connector break-out box having as many as 100 terminals. The sampling frequency is 1000 *Hz* for analog signal and 100*Hz* for digital
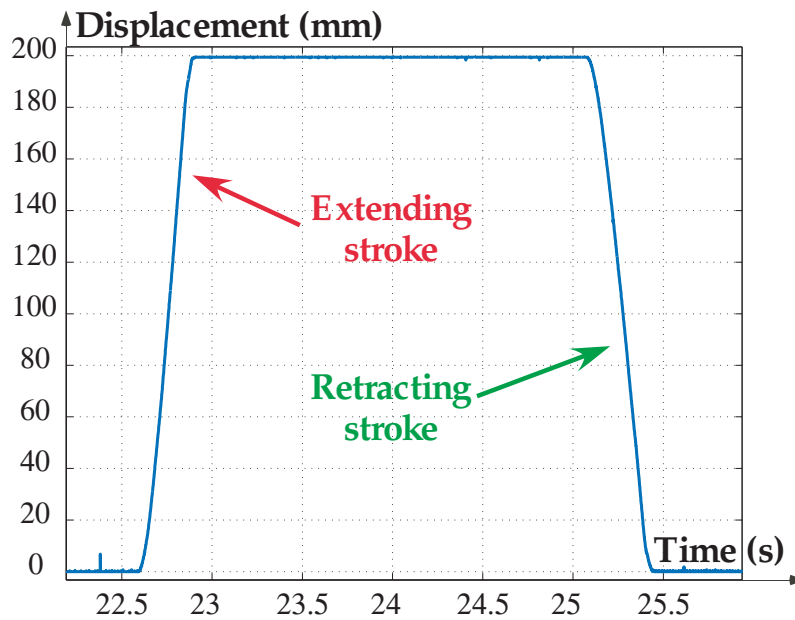
Figure 3.6: Displacement measure from LVDT in extending stroke and retracting stroke of cylinder DNC
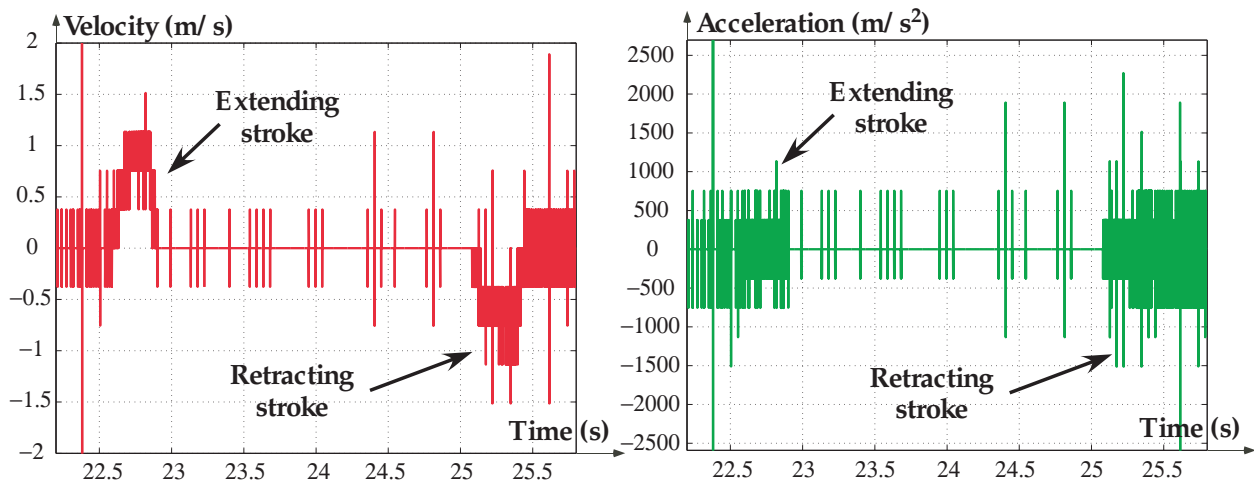
Figure 3.7: Velocity (left) and acceleration (right) derived from displacement signal of LVDT

signal.

The data can be classified in two categories: analog (flow rate, pressure, and displacement)
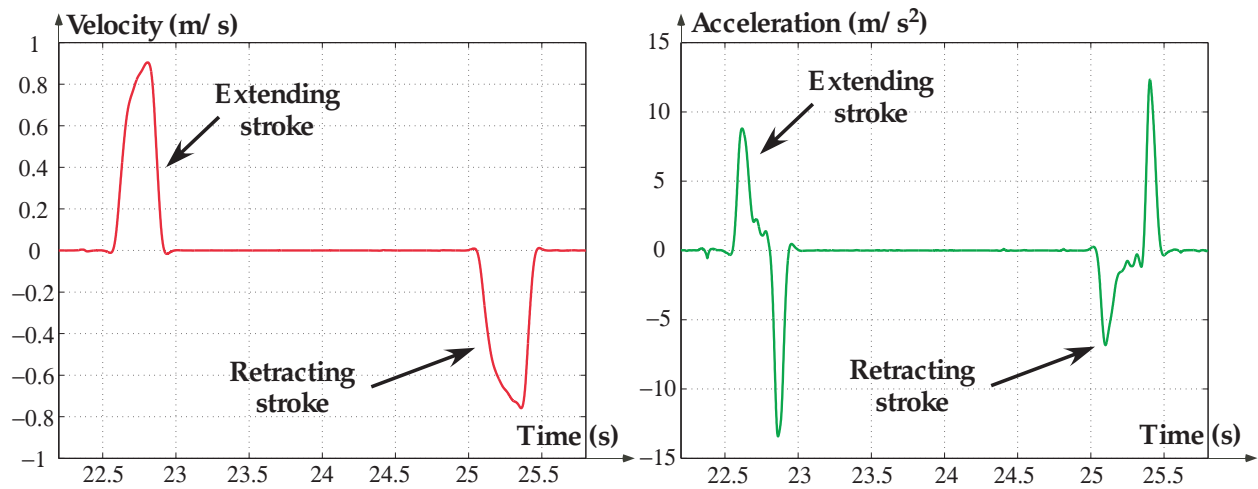
Figure 3.8: Filtered velocity (left) and acceleration (right) derived from displacement signal of LVDT

System Component	Specifications	
DAQ	Model NO.	NI-PCI-6025E
	Major Parameters	16 SE analog inputs, 32 digital I/O lines
	Manufacturer	National Instruments
I/O Connector Block	Model NO.	SCB-100
	Major Parameters	100 pin connectors shielded cable
	Manufacturer	National Instruments
Flow Meter	Model NO.	SFE1-LF-F200-HQ8-P2U-M12
	Major Parameters	Flow measure 0-200 l/min, analog output 0-10 V
	Manufacturer	Festo
Pressure sensor	Model NO.	SDE1-D10-G2-W18-L-PU-M8
	Major Parameters	Pressure measure 0-10 bar output 0-10 V
	Manufacturer	Festo
Proximity sensor	Model NO.	SME-8-K-LED-24
	Major Parameters	Magnetic reed, operating at 24 VDC
	Manufacturer	Festo

Table 3.2: Data acquisition hardware list. (Source: NI and Festo Documentations)

and digital (valve control and proximity data). Connections from the stack interface to the break-out box are described in Figure 3.9 with the explanation of names defined for parameters. Some of the input ports are not used because they are reserved for future use when new types of sensors are introduced.

PIN #	SIGNAL	INPUT
1	AI GND	1- 84
2	AI GND	
3	AI 0	
4	AI 8	P_DNC_A
5	AI 1	Q_DGPL_A
6	AI 9	Q_DNC_A
7	AI 2	
8	AI 10	E_DGPL_A
9	AI 3	Q_DNC_B
10	AI 14	E_DGPL_B

PIN #	SIGNAL	INPUT
11	AI 4	P_DNC_B
12	AI 12	U_DGPL_A
13	AI 5	P_DGPL_A
14	AI 13	U_DGPL_B
15	AI 6	P_O
16	AI 14	E_SLT_A
17	AI 7	Q_0
18	AI 15	E_SLT_B
19	AI SENSE	
20	AO 0	
21	AO 1	
22	AO EXT REF	
23	AO GND	

PIN #	SIGNAL	INPUT
51	AI 16 (P3.7)	U_SLT_A
52	AI 24 (D GND)	U_HMPL_H_A
53	AI 17 (P3.6)	U_SLT_B
54	AI 25 (D GND)	U_HMPL_H_B
55	AI 18 (P3.5)	E_DRQD_A
56	AI 26 (D GND)	E_HMPL_V_A
57	AI 19 (P3.4)	E_DRQD_B
58	AI 27 (D GND)	E_HMPL_V_B
59	AI 20 (P3.3)	U_DRQD_A
60	AI 28 (D GND)	U_HMPL_V_A
61	AI 21 (P3.2)	U_DRQD_B
62	AI 29 (D GND)	U_HMPL_V_B
63	AI 22 (P3.1)	E_HMPL_H_A
64	AI 30 (D GND)	E_HGD2_A
65	AI 23 (P3.0)	E_HMPL_H_B
66	AI 31 (D GND)	E_HGD2_B

PIN #	SIGNAL	INPUT
67	AI 32 (P2.7)	U_HGD2_A
68	AI 40 (D GND)	33 - 38 - 68 E_DNC_B
69	AI 33 (P2.6)	U_HGD2_B
70	AI 41 (D GND)	U_DNC_A
71	AI 34 (P2.5)	E_HMPL_HZ_A
72	AI 42 (D GND)	U_DNC_B
73	AI 35 (P2.4)	E_HMPL_HZ_B
74	AI 43 (D GND)	U_VAC_REL
75	AI SENSE (P2.3)	
76	AI GND (D GND)	
77	AI 36 (P2.2)	U_HMPL_HZ_A
78	AI 44 (D GND)	U_VAC_GEN
79	AI 37 (P2.1)	U_HMPL_HZ_B
80	AI 45 (D GND)	U_HMPL_VS_A
81	AI 38 (P2.0)	E_HMPL_H
82	AI 46 (D GND)	U_HMPL_VS_B

E_HMPL_V_A

A-extending side
B-retracting side

Cylinder

E-proximity sensor signal / U-valve control signal

Pin #: Numbers on connector block box
Signals: AI X = analog signal input
P X.X = digital signal input

P_XXX —— Pressure Data

Q_XXX —— Flow Rate Data

P_0 = supply pressure

Figure 3.9: SCB-100 connector break-out box inputs

3.2.5 Fault Introduction and Level Control

The experimental setup includes a manual leakage control valves to generates leakage in the system with different levels at various locations of the system. This manually adjusted fault control subsystem allows for the study of fault detection and diagram with controlled fault situation. The initial experimental setup by Festo is shown in Figure 3.10 with a 8 *on/off* valves combination providing 8 different leak levels by turning on and off different valves. However, the leakage

system has a relative smaller flow rate of less than 20 *l/min*, which is not able to cover the full range of our research interest.
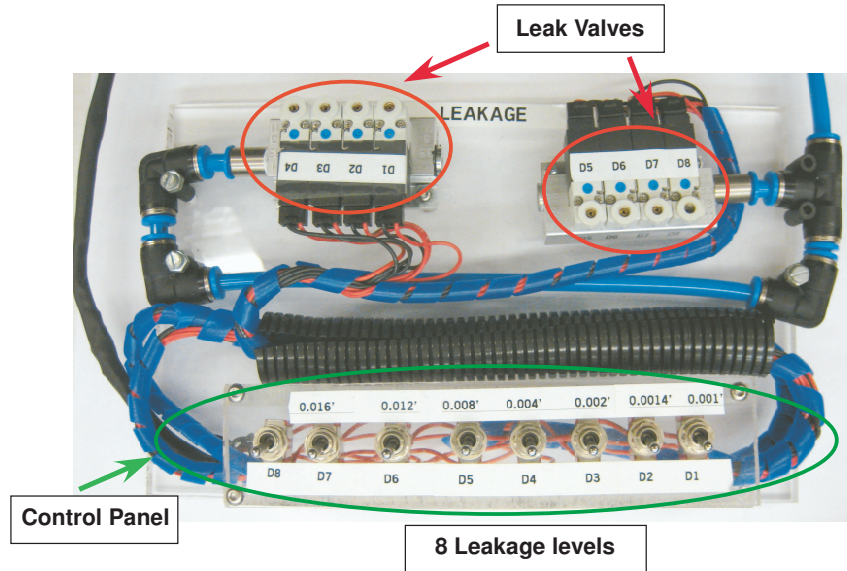
Figure 3.10: Fault (leakage) introduction component
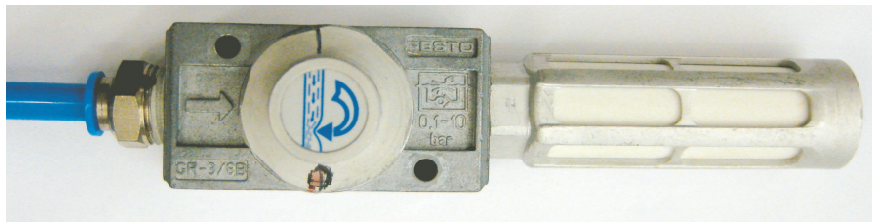
Figure 3.11: Leakage control valve with a silencer

To conquer this disadvantage, we introduce another leakage level control device with higher amount as shown in Figure 3.11 .This is a one way flow control valves (Festo GR-3/8B), which is able to offer max. 1000 *l/min* leakage with 20 rotation turns. The GR-3/8B valves is placed on both retract and extend lines connecting to studied cylinder and the supply line of the system. All possible locations where leakage could be introduced in the system are listed in Table 3.3. And Figure 3.12 indicates the 3 possible introduced leakages places at the retracting side of DNC and HMPLV cylinders and the supply line. The maximum turn is set to be 6 is because the limitation of

Actuator	Leakage Potential Location	Leakage Level (number of turns)
All actuators	Supply Line	1 - 6
DNC	Retracting, Extending Line	1 - 6
DRQD	Retracting, Extending Line	1 - 6
DGPL	Retracting, Extending Line	1 - 6
SLT	Retracting, Extending Line	1 - 6
HMPL_H	Retracting, Extending Line	1 - 6
HMPL_HZ	Retracting, Extending Line	1 - 6
HMPL_V	Retracting, Extending Line	1 - 6
HMPL_VS	Retracting, Extending Line	1 - 6
HGD2	Retracting, Extending Line	1 - 6
Regulator	Pilot Line	1 - 6

Table 3.3: Leakage locations and levels in the pneumatic system

flow meter measuring range (200 *l/min*), if higher flow rate value is expected practical case, more investment is needed.

The GR-3/8B valve can be turned *n* turns counterclockwise from its completely closed position to simulate the leakage. In this way different levels of leakage are relied on The relationship between the number of turns and the nominal flow rate is shown in Figure 3.13 as well as the our test shows the similar property in Figure 3.14. It is noticed that the curve in Figure 3.14 is not linear so the flow rate and pressure do not change linearly with the number of turns. To further understand the variations of pressure and flow rate values under different turns of the valve, relationship of flow rate and pressure is measured and plotted in Figures .

3.3 A Brief Discussion of Captured Signals

A massive amount of data is collected from this multi-actuator system including normal situation (no fault) data to create models and extract features and faulty conditions to be diagnosed using various sensors. An overview of the whole system situation is shown in Figure 5.4 and Figure 5.5 presented by pressure and flow rate signals in supply line. Whole cycle of 58 steps is completed in around . If we choose to pick cylinder DNC as our first focus, the sensors locating on DNC lines are plotted in Figures 3.12. The reason to choose DNC is because it has the biggest geometry size
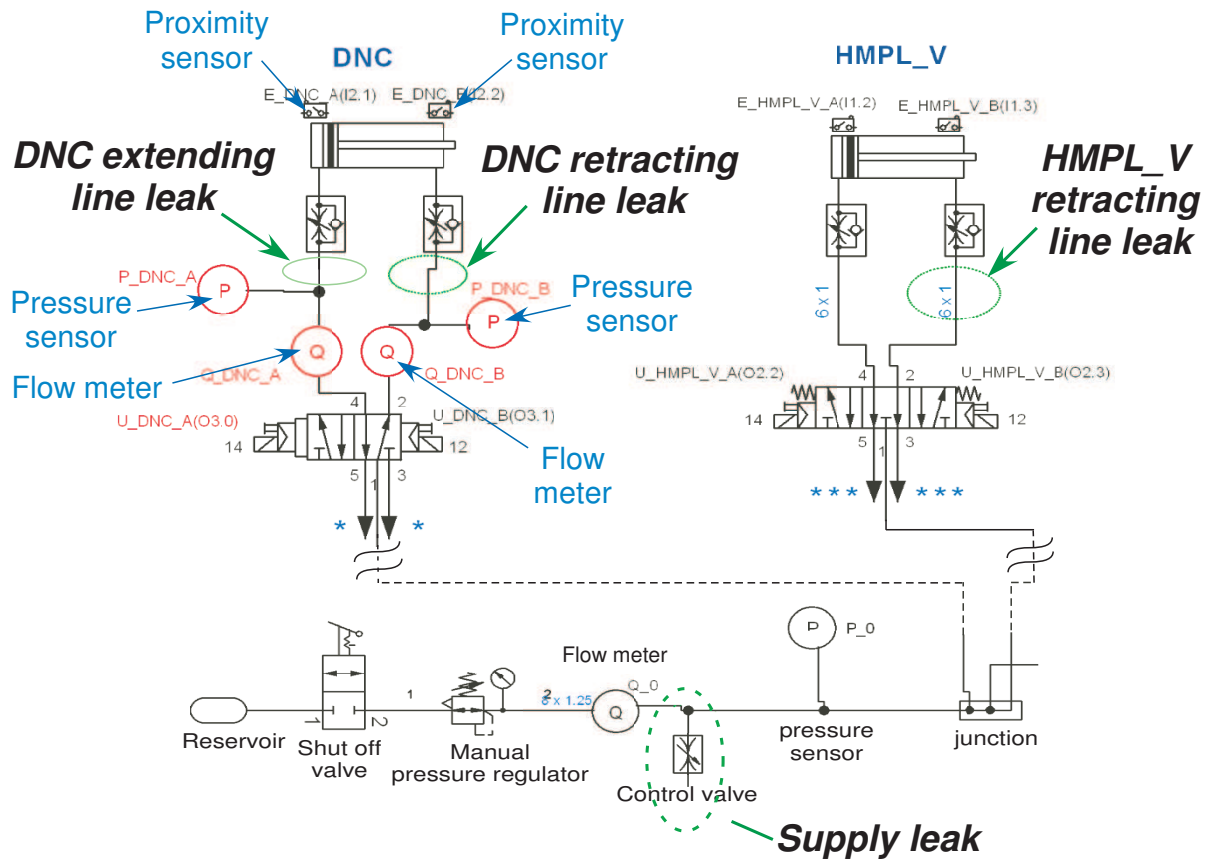
Figure 3.12: Three different leakages introduced at DNC-retracting side, HMPLV-retracting side and supply line (in green circle)

and the variations of parameters governing dynamics of cylinder DNC are not changing that fast. Figure 3.15 shows the one complete cycle of cylinder DNC. A full cycle is defined as stating from fully retracted position, moving to fully extended position, and then move from fully extended position back to fully retracted position. The PLC control codes is programmed that DNC retracting stroke is following DNC extending stroke to offer continuous study convenience in our research. The time duration between the two strokes is the DNC cylinder stays at the fully retracted position to wait for motion of other cylinders to be completed.

To better understand what is happening inside one stroke time, we need to zoom in to a specific strokes of cylinder DNC. Figures and show typical pressure and flow rate profiles with
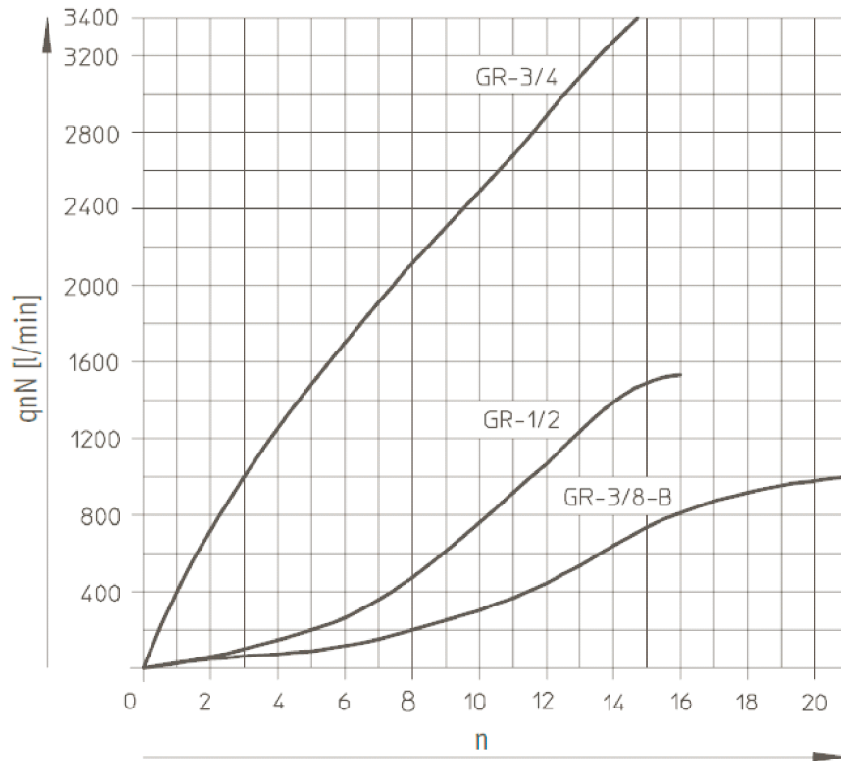
Figure 3.13: Flow versus adjustment screw rotation. (Courtesy of Festo Company)

displacement during extending and retracting strokes of cylinder DNC which are sampled from our testing system. It is advisable to treat one full stroke of a pneumatic cylinder to several continuous segments based on dynamic status of valve and piston. Some terms regarding cylinder's motion characteristics are defined as [71]:

(1) Positioning time / Piston start-up time (t_p): It is the time between the solenoid valve is energized (de-energized) and the piston (rod) of a cylinder starts traveling. The accurate judgment is done by the start-up of acceleration curve.

(2) Stroke time (t_s): It is the time between the piston (rod) of a cylinder starts traveling and the piston (rod) reaches at the stroke end. Additionally, we define full operating time $t_o = t_p + t_s$.

(3) Maximum velocity: It is the maximum values of the piston velocity which occurs during

39

Flow rate: l/min

Pressure: bar
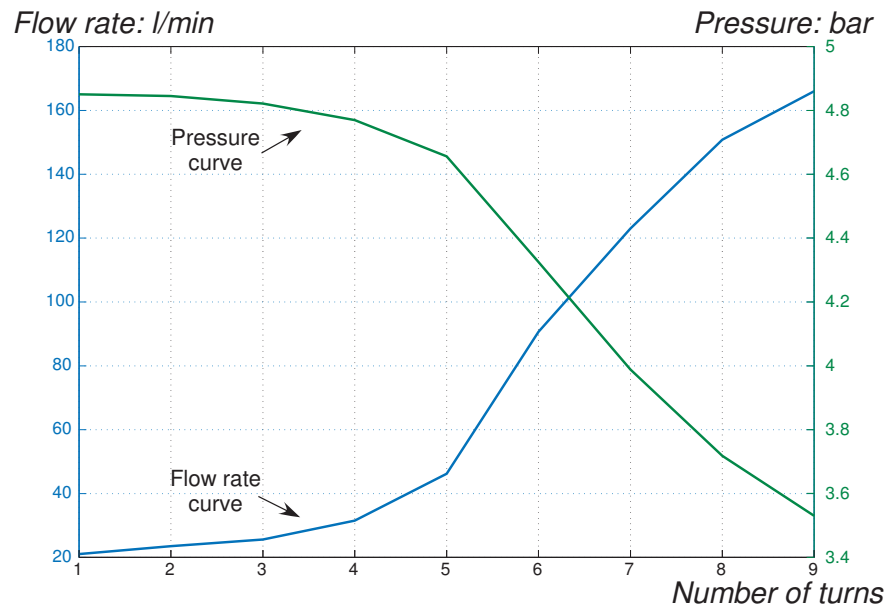
Number of turns

Figure 3.14: Plot of flow rate and pressure versus the number of turns for leakage control

the stroke. If when lurching or stick-slipping occurs, velocity may reach the largest value.

(4) Maximum exhaust flow rate: It is the maximum flow rate value measured from exhaust line of a cylinder during a stroke duration.

(5) Balancing velocity: If a cylinder having enough longer stroke is driven by meter-out the latter half of a stroke will be in an uniform motion. Regardless of the supply pressure or a load, the piston speed for the time will be dependent only on effective area of the exhaust circuit and the piston area.

(6) Balancing pressure: It is the pressure value in each chamber of a cylinder when the acceleration curve is starting up from zero.

At the same time we denote the signals acquired from sensors following classification codes as shown in Figure 3.16 in this dissertation.
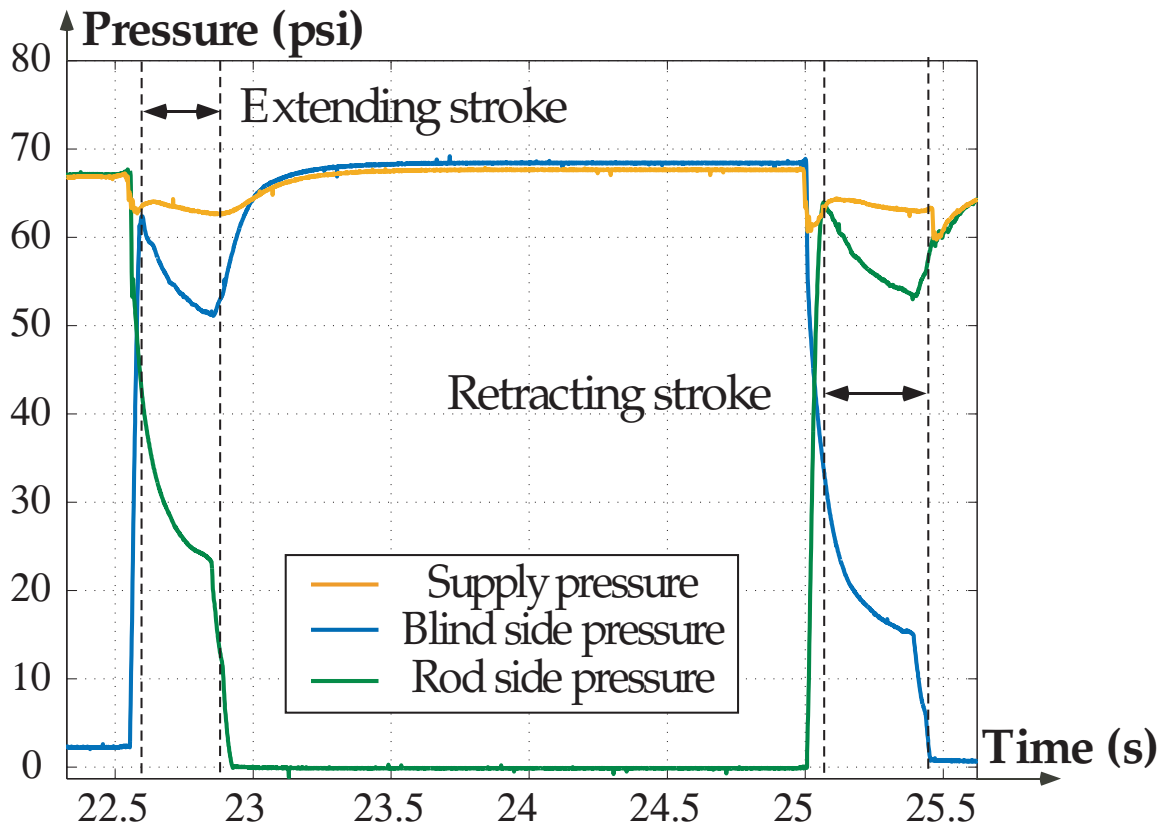
Figure 3.15: The overlaid typical data for extending pressure, retracting pressure, and supply pressure during the extending stroke and retracting stroke of cylinder DNC

3.4   Discussions

3.4.1   Flow Meter

The flow meter is an intrusive device and can affect the characteristics of the flow because the compressed air flow is forced to pass through the flow meter testing region to form a laminar flow and thereby restricting or altering the flow. The flow meter can be installed at the inlet, extending, or retracting line of pneumatic cylinders. In addition, flow meter can be placed before or after the leakage location which brings impacts on property of flow. And the flow meter is only able to measure flow rate value in one direction because of the design principle. So we need to switch

the mounting direction a flow meter on the same time to redo the test again if the flow rate on the reverse direction is desired.

Since Festo flow meter measures mass flow rate and the output is in unit of SLPM, a standard condition for air should be defined. In this dissertation, standard conditions refer to temperature 0 °C, pressure 1013 mbar, and atmosphere density 1.294 kg/m^3.

Pneumatic System Sensor Signal
Type codes

Analog signal
Example: **P_In**
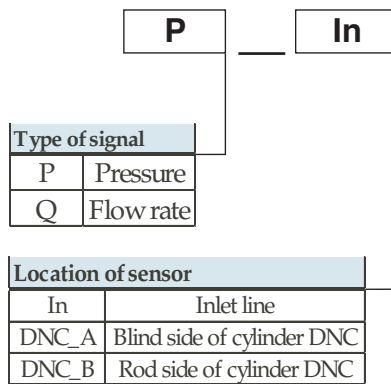
Digital signal
Example: **U_DNC_B**

P		In

U		DNC		A

Type of signal

P	Pressure
Q	Flow rate

Type of signal

U	Proximity sensor
E	Valve control signal

Location of sensor

In	Inlet line
DNC_A	Blind side of cylinder DNC
DNC_B	Rod side of cylinder DNC

Actuator

DNC	HMPL_HZ
DGPL	HMPL_V
SLT	HMPL_VS
DRQD	HGD2
HMPL_H	

Location of sensor

A	Rod side of cylinder/valve
B	Blind side of cylinder/valve
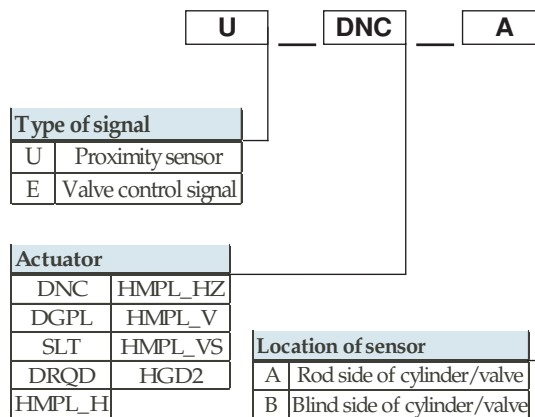
Figure 3.16: Type codes of sensors signals

3.4.2   Sampling Rate

By visual inspection of the sampled data, the curve of data is smooth and nearly continuous. Compare sampled signal curves with typical profile from industrial company manual, it is confirmed this is no important information lost. The sampling frequency of the data acquisition system is 1000 *Hz*, with a sampling time of 1 milliseconds between two sampling points. Since the typical time span of operation is from 0.4 seconds to 2.2 seconds (under 80 *psi*) for the pneumatic cylinders in extending and retracting strokes, we surmise that the rate of data acquisition is fast enough for this application. A potential concern is the difference of the sampling rates between the digital data (100 *Hz*) and analog data (1000 *Hz*). However, this concern is minimal with

synchronization of data points in analysis.

3.4.3   Others

No system is in perfect condition without any fault in practice and our testing pneumatic system is also not guaranteed leak free. So the recorded normal situation should be considered relatively leak free after running thousands of cycles even though it is built under strict industrial standards. That is why both reference data and fault data are captured to derive different between them.

Compressed air supply for this pneumatic system is from house air line in out lab which is not as good as the air quality in Festo. Due to the limitation of tank volume, compressed is not be able to keep at a constant level when there is relatively large amount air consumed in the system. Fluctuation of pressure value is observed during the whole motion process.

There is also a tank placed on all the exhaust lines from every valve. Purpose of this design is to eliminate the noise of hiss sound when air exhausts to atmosphere. This tank would not change the characteristics of actuator and valve.

3.5   Summary

In this chapter, we discuss the experimental setup and the major components of the system, including mechanical parts, pneumatic parts, sensors, and the control and data acquisition. The terms related to the motion characteristic of a linear cylinder is defined. The redundant definitions can provide foolproof of system operation. The manually adjusted leakage control values are used to control the different levels of leakage for the study of FDD. Data acquisition system with details of signals and sampling rate are also discussed. Analysis of the acquired data for FDD will be discussed in the next two chapters.

Chapter 4

MODEL-BASED FAULT DETECTION AND DIAGNOSIS FOR PNEUMATIC SYSTEMS

4.1   Introduction

The overall concept of fault detection and diagnosis (FDD) consists in the following three essential tasks:

- Fault detection: detection of the occurrence of faults in the functional units of the process, which leads to undesired or intolerable behavior of the whole system;

- Fault isolation: localization (classification) of different faults; and

- Fault analysis or identification: determination of the type, magnitude and cause of the fault.

The intuitive idea of the model-based fault diagnosis technique is to replace the hardware redundancy by a process model which is implemented in the software form on a computer. A process model is a quantitative or a qualitative description of the dynamic and steady-state behavior, which can be obtained using the well-established process modeling technique. This model usually represents the nominal behavior of the system, without any fault. In the general framework of diagnosis, this is known as *consistency-based diagnosis* [72] or *model-based diagnosis* [25]. Deviation from normality was recognized based on the knowledge of how normal components work. In this

way, we are able to reconstruct the process behavior on-line, when associated with the concept of hardware redundancy, this is called **software redundancy** concept. Software redundancy is also called **analytical redundancy**.

Similar to the hardware redundancy schemes, the process model will run in parallel to the process and be driven by the same process inputs in the framework of the software redundancy concept. It is reasonable to expect that the re-constructed process variables delivered by the process model will follow well the corresponding real process variables in the fault-free operating states and show an evident derivation by a fault in the process. In order to receive this information, a comparison of the measured process variables (output signals) with their estimates delivered by the process model will then be made. The difference between the measured process variables and their estimates is called the **residual**. Roughly speaking, a residual signal carries the most important message for a successful fault diagnosis:

$$\text{if residual} \neq 0 \text{ then fault, otherwise fault-free} \tag{4.1}$$

The procedure of creating the estimates of the process outputs and building the difference between the process outputs and their estimates is called the residual generation. Correspondingly, the process model and the comparison unit build the so-called residual generator, as shown in Figure 4.1. Classical approaches use models to generate residuals with an observer, with a parity space approach, or with the a detection filter. The main practical difficulties arise from the model precision and unknown disturbances of the system. This leads to the trade-off between the false alarm and missed detection..

Model-based fault detection methods use residuals which indicate changes between the process and the model. One general assumption is that the residuals are changed significantly so that detection is possible. In other words, the residual size after the appearance of a fault is large enough and long enough to be detected. The most important issue in model-based fault detection is the accuracy of the model describing the behavior of the monitored system. Figure 4.1 shows the basic structure of model-based fault detection procedure. Based on the measured input and output signals, the detection methods generate residuals, parameter estimates, or state estimates,
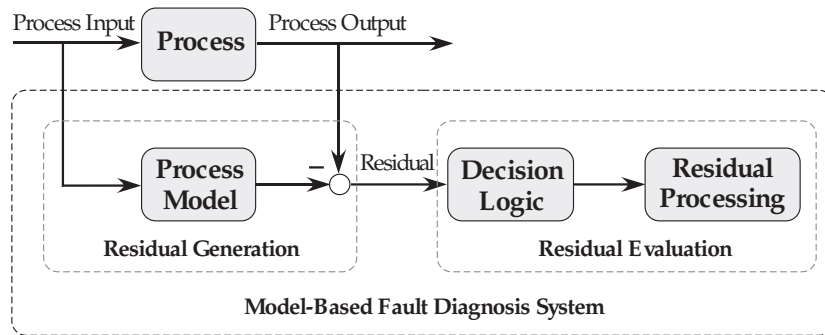
Figure 4.1: Description of model-based fault diagnosis scheme

which are called features. Following that, changes of features are detected—leading to symptom-s [73, 74]. Most contributions in the field of quantitative model-based FDI (fault detection and isolation; see Section 2.4) focus on the residual generation problem since the decision-making problem is relatively straightforward if the residuals are well defined.

In the most general sense, a system is a collection of objects designed to perform tasks. In a somewhat simplified sense, a signal can be any mechanism (mechanical or electrical or any type of transducers) that is used to transmit information. For the purpose of the pneumatic system under study, all sampled data of our study shown in Figure 3.15 are treated as waveform signals. The characteristic of these waveform signals are summarized as follows:

(1) Not stationary

(2) Working cycle-based

(3) Segmental signal

For this kind of signals in the model-based approach, observation are considered as a time ordered stochastic process. The critical concern of using this approach is to have an appropriate process model which is sensitive to process faults but robust to process noise [25]. In such systems, features are considered as random variables or as a random set.

In this chapter, system modeling for pneumatic systems is discussed. An approach based on pneumatic analogy to detect and diagnose leakage will be studied. Finally, the application of

FDD on the experimental data using system models will be presented. This approach is a signal model-based approach according to Isermann [73].

4.2 System Model
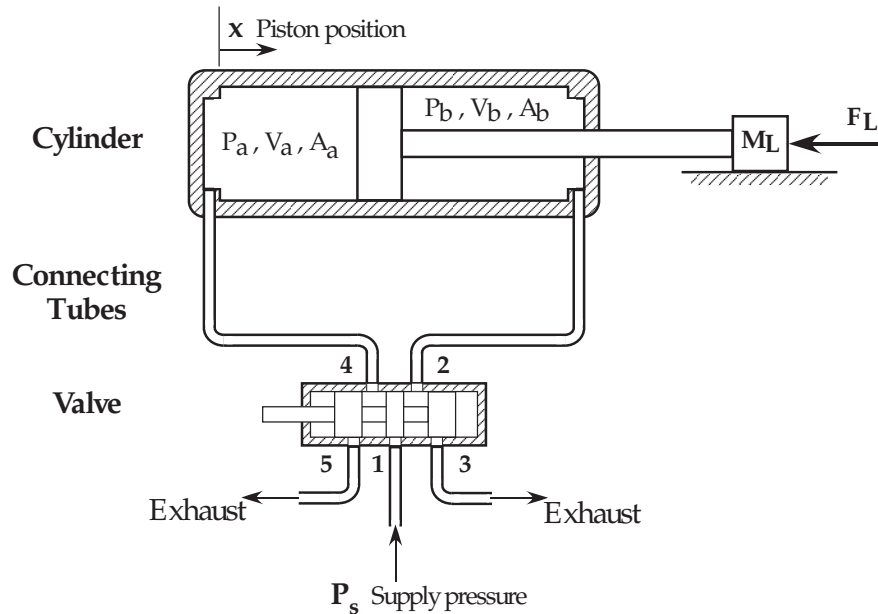
Figure 4.2: Schematic representation of the pneumatic cylinder-valve system

To establish an analytical process model for FDD of this testing system, a relatively accurate system model of a pneumatic actuator controlled by a directional valve needs to be provided. However, compressibility of air and highly nonlinear flow and friction of the pneumatic system components add difficulties in establish model and identify parameters. Richer and Hurmuzlu introduced a nonlinear mathematical model in 2000 [14] [15] and validated models of pneumatic components by identifying unknown characteristics, such as valve discharge coefficient, valve spool viscous friction coefficient, and discharge coefficient. Thomas conducted successful experiments in deriving a conventional state representation and a mass-based system representation models to assist in advanced servo control of a pneumatic actuator [47]. In 2005, Ning and Bong succeeded in obtaining accurate values for model parameters and experimentally tested applicability of their model to

the hardware being modeled, still for a pneumatic servo positioning system [16]. So far there is no presentation of an appropriate system model of the leakage detection and diagnosis for pneumatic systems.

A typical pneumatic system includes a force element (the pneumatic actuator), a command device (valve), connecting tubes, and position, pressure and force sensors. The external load consists of the mass of external mechanical elements connected to the piston and a force produced by an environmental interaction. A schematic representation of the pneumatic actuator system is shown in Figure 4.2, with variables of interest specified for each component. In order to obtain the accurate model of each component in our study, this valve-cylinder subsystem is separated into three components: (1)valve, (2)tube and (3)cylinder.

4.2.1   Model of Directional Control Valve

The pneumatic valve is a critical component of the actuator system and is also the interface between electronic controllers and pneumatic systems. It is the command element, and should be able to provide fast and precisely controlled air flows through the actuator chambers. There are many designs for pneumatic valves, which differ in geometry of the active orifice, type of the flow regulating element, number of paths and ports, actuation type, etc. We restricted our study to a spool valve, actuated by solenoid. It is usually considered that a valve has a very fast response compared with motion of a cylinder thus the control delay can be omitted for the valve in a pneumatic system.

A Festo solenoid valve controls the pneumatic cylinder used in this study. Figure 4.3 shows the internal structure of a spool valve and lists the characteristics and specification of this valve. Figure 4.4 illustrates the control of the extending and retracting strokes and shows the ports and their connections. There is a mid-position status for this valve which is normally closed when there is no control signal on either side. Port 1 is always the port for air supply; port 3 and port 5 are two exhaust ports linking to the atmosphere; and port 4 and port 2 are connected to cylinder's blind side (A side) and rod side (B side) separately as demonstrated in Figure 4.4. During the operation
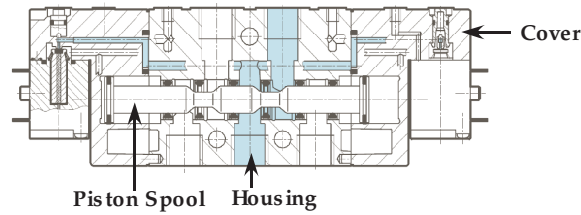
Festo Solenoid Valve CPE 14	
Type number	196937 CPE14-M1BH-5/3G-1/8
Type	Solenoid direction 5/3 way mid position valve
Normal position	Closed
Design	Piston spool
Exhaust function	Flow control
Nominal diameter	6 mm
Standard nominal flow rate	410 1/min
Switching time on/off	20/42 ms
Operating pressure	3-8 bar

Figure 4.3: Sectional view and specification of Festo directional control valve

of system, this valve is placed either at the left position or right position, mid-position is never set in any cycle of operation.

For simulation purposes, it is desirable to have an accurate mathematical model of flow through the solenoid valve. The flow rate is a complex function, and os influenced by of multiple variables: upstream pressure, downstream pressure, and temperature. Generally there are three mathematical models that define flow-rate characteristics of pneumatic components under compressible fluids. Each model contains two regimes, chocked (sonic) and unchocked (subsonic), for a compressible flow through a valve. In the subsonic flow regime, the flow rate increases as the ratio of downstream pressure to upstream pressure decreases. In the choked flow regime, the flow through the valve is sonic and does not increase as the downstream pressure drops. The differences and application criteria of these three models are discussed as following.

Modeling of the valve involves two aspects: the dynamics of the valve spool, and the mass flow through the valve's variable orifice. However, the dynamics of the valve spool is not our research concern because the valve is not the actuation component. A mass flow characteristic is sufficient to represent the working situation of a valve by input and output pressures and the flow rate. Furthermore, the mass flow rate is a bridge linking all other components cylinder and tube in
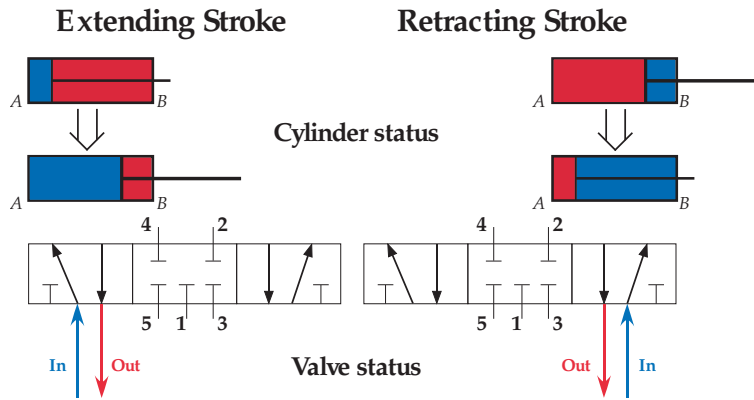
Figure 4.4: Valve control and cylinder strokes

this subsystem.

Flow through a valve is treated as flow through an orifice. The area of the valve is given by the spool position relative to the radial holes in the valve sleeve, as it is shown in Figure 4.5. Since we are using a on/off directional valve, the orifice area is fixed. One direct mathematical model for the flow of air through a valve is derived from compressible flow through a fixed orifice. The equation is divided into two regions based on the ratio of the downstream pressure (P_2) to upstream pressure (P_1), P_2/P_1. The pressure drop across the valve orifice is usually large, and the flow has to be treated as compressible and turbulent. If the upstream to downstream pressure ratio is larger than a critical value P_{cr}, the flow will attain sonic velocity (choked flow) and will depend linearly on the upstream pressure. If the pressure ratio is smaller than P_{cr}, the mass flow depends nonlinearly on both upstream and downstream pressures. The critical pressure is calculated using the ratio of specific heats for air, k, as follows

$$P_{cr} = (\frac{P_2}{P_1})_{cr} = (\frac{2}{k+1})^{\frac{k}{k-1}} \tag{4.2}$$

For air k = 1.4, the critical pressure ratio is found to be 0.528. When the pressure ratio is higher than the critical pressure ratio, flow through the orifice is subsonic, and increases as the pressure ratio decreases. At the critical pressure ratio, flow through the orifice is sonic. At this point the orifice is said to be choked, and further decreases in [75], [76], and [77] given as

equation(4.3),

$$\dot{m}_v = \begin{cases} C_D A C_1 \frac{P_1}{\sqrt{T}}, & \text{if } \frac{P_2}{P_1} \leq P_{cr} \\ C_D A C_2 \frac{P_1}{\sqrt{T}} (\frac{P_2}{P_1 1})^{\frac{1}{k}} \sqrt{1 - (\frac{P_2}{P_1})^{\frac{(k-1)}{k}}}, & \text{if } \frac{P_2}{P_1} > P_{cr} \end{cases} \tag{4.3}$$

where $\dot{m}_v$ is the mass flow rate through orifice area, C_D is a nondimensional, discharge coefficient, R is an ideal gas constant, and where

$$C_1 = \sqrt{\frac{K}{R}(\frac{2}{k+1})^{\frac{k+1}{k-1}}}, \quad C_2 = \sqrt{\frac{2k}{R(k-1)}}$$

The upstream and downstream pressures are absolute pressures, rather than gauge pressures. The discharge coefficient reflects a contraction of the flow path downstream of the orifice, reducing the effective flow area. This equation does not include the flow coefficient C_V , which is the most often used parameter describing the flow capacity of a given valve becomes the orifice area is very difficult to measure accurately. The critical ratio value is fixed at 0.528 which differs from the experimental test.

The maximum mass flow rate reached by the Festo valve is around 350 *SLPM* when pressure is around 4 bar in a PUN 6 x 1 tube (outside diameter: 6 *mm* and inside diameter: 4 *mm*). To calculate the flow velocity in experimental condition. At 20 °C, we use

$$Q_S = Q \frac{P T_S}{P_S T} \tag{4.4}$$

where Q_S is the measured flow rate in *SLPM*, Q is volumetric flow rate, P is absolute pressure in experimental condition, T is temperature in °K, P_S is absolute pressure in standard condition, and T_S is temperature in °K of standard condition. The maximum accessible flow rate is 100.7 m/s, which is far from the sonic speed 340 m/s. This implies that no sonic flow exists in our tests.

In 1989, the International Organization for Standardization published ISO 6358 [49], a standard that succeeded in expressing the flow characteristics for pneumatic equipment using sonic conductance C and critical pressure ratio b. Sonic conductance represents the maximum flow rate

51
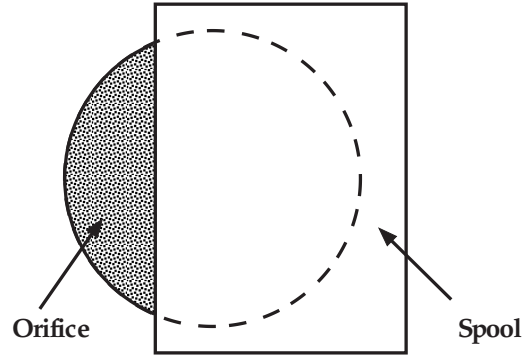
Figure 4.5: Orifice area versus spool position

at choked flow, and has much the same definition as that of effective area S. A JIS B 8390 standard [78] published in 2000 is consistent with the ISO standard. These published empirical flow equations of the two standards are summarized purely based on experimental tests, the incorporated factor sonic conductance offers information of flow capacity, and critical pressure ratio can be changed. However, there is one disadvantage preventing us from applying them to measured data. Since there is never a sonic region in our experiments as demonstrated above, a sonic conductance C value is not expected and cannot obtained from experiments. However, we draw a conclusion from these two standards that the critical pressure ratio P_{cr} can vary from one type of valve to another, which shows that subsonic-flow characteristics depend on valve construction. The ISO/JIS model of valve flow is shown in equation(4.5),

$$
Q_{SLPM} = \begin{cases} 600 \times CP_1 \sqrt{\frac{T_S}{T}}, & \text{if } \frac{P_2}{P_1} \leq b \\ 600 \times CP_1 \sqrt{1 - (\frac{\frac{P_2}{P_1}-b}{1-b})^2} \sqrt{\frac{T_S}{T}}, & \text{if } \frac{P_2}{P_1} > b \end{cases}
\tag{4.5}
$$

where C is sonic conductance and b is critical pressure ratio (equal to P_{cr}).

At the same time, the process-control industry was applying the term "coefficient of volume flow" or C_V to gases, after applying a density conversion factor. The parameter C_V is a measure of water flow rate at a minimum differential pressure (1 *psi*) through the valve. Correspondingly a less complicated equation for flow through a valve is presented by the Instrumentation, Systems,
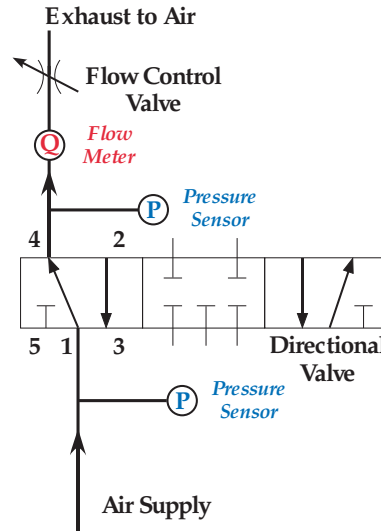
Figure 4.6: Valve flow measurement apparatus

and Automation Society in 2002 [48] and 2007 [79], named Flow Equations for Sizing Control Valves as an American National Standard. The ISA equation incorporates the flow coefficient C_V and an experimentally determined pressure differential ratio factor X_T. Like the orifice equation, flow is divided into the regions of sonic (choked) and subsonic (unchoked) flow. The ISA equation calculates the mass flow rate, measured in standard cubit feet per minute. It is used to model the control valve because Festo offers the specific flow coefficient C_V value which is easy to validate, and the critical pressure ratio is adjustable in order to match our unchocked situation. For compressible air, the ISA flow equation is defined as

$$Q_{SLPM} = \begin{cases} 11.51 \times C_V P_1 \sqrt{\frac{X_T}{T}}, & \text{if } X \geq X_T \\ 22.67 \times C_V P_1 (1 - \frac{X}{3X_T}) \sqrt{\frac{X_T}{T}}, & \text{if } X < X_T \end{cases} \quad (4.6)$$

where $X_T = \frac{P_1 - P_2}{P_1} = 1 - \frac{P_2}{P_1}$

This model was developed to account for the observation that two valves with identical flow coefficients can exhibit different flow rates under identical pressure conditions. The complexity of any valve in the geometry of the flow path corresponds to X_T, with more complex geometries

53

yielding higher values. For example, a study [77] presents two valves having identical flow coefficients. For a ball valve with a straight flow path, $X_T = 0.14$; for a needle valve with a Z-shaped flow path, $X_T = 0.84$.

Figure 4.6 shows a schematic of an equipment used to determine the flow rates. The path from port 1 to port 4 is measured, with the considered path of port 1 to port 2 having the same characteristic. All plumbing is TPE-U (PU) tubing with a 10 *mm* outside diameter and a 1 *mm* wall thickness. At any given voltage setting, the flow control valve was adjusted as to vary the pressure drop across the valve. The steady-state flow rate was measured using a mass flow meter.

The experimental data lacks the choked-flow region predicted by each of these models. Examination of the ISA equation, though, shows that values of the flow coefficient C_V and the critical pressure drop ratio X_T may be selected so that the ISA model can predict the flow rate. Figure 4.7 compared the standard ISA model of flow, assuming a supply pressure of 80 psig and a temperature of $528°R$, and the experimental data. It is obvious that the critical pressure drop is not shown in the test and the curve still has an increasing trend near the left end with lower $\frac{P_2}{P_1}$. Especially when the flow control valve is closed with no flow rate, a pressure drop between upstream line and downstream line is observed. This does not comply with any standard which states that $Q = 0$ when $\frac{P_2}{P_1} = 1$. In order to apply experimental data to confirm valve parameters, additional tests are conducted to measure the pressure drop when there is no flow at different levels supply pressure. After subtracting the pressure drop at no flow from original upstream pressure P_1, a real pressure ratio and flow rate relationship is derived and depicted in Figure 4.8.

By minimizing the RMS (root mean square) error between the data and the model at each data point, the values of C_V and X_T are estimated in Matlab using ten repeated tests data with average. Figure 4.9 shows an example of minimizing the RMS error for one test. Finally the parameters of the ISA model, flow coefficient C_V and pressure drop ratio X_T, are 0.3988 and 1.0, respectively. The value $X_T = 1.0$ indicated that the flow rate always stays in subsonic / unchocked region for any pressure ratio $\frac{P_2}{P_1}$ between 0 and 1. To validate the flow coefficient value, we need to refer to Festo specification of this valve. It is mentioned that the standard nominal flow rate
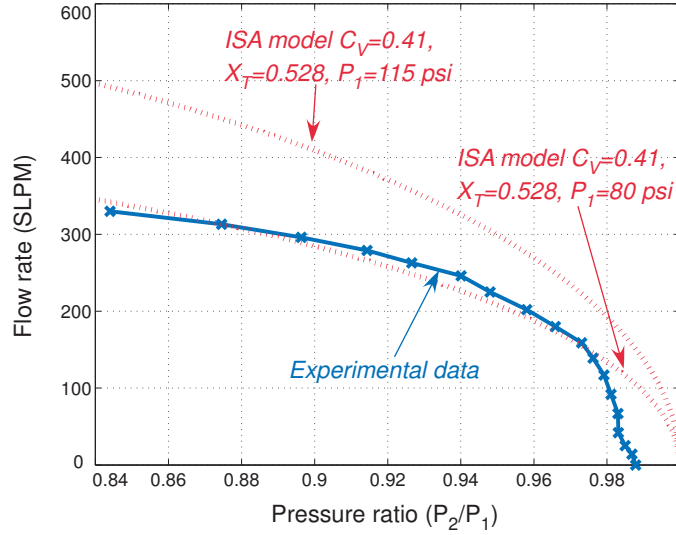
Figure 4.7: Compare the experimental data with ISA model for flow through a valve

is 410 l/min under the standard condition (temperature $T = 20°$C, upstream pressure $P_1 = 6$ bar, and downstream pressure $P_2 = 5$ bar). Substituting the standard conditions into equation(4.6) with previously developed C_V and X_T values, the nominal flow rate is calculated as 413.6 l/min which is very close to 410 l/min found in the product literature. Thus, the calculated valve model with the derived parameters $C_V = 0.3971$ and $X_T = 1.0$ can be applied in the system modeling and leakage diagnosis.

4.2.2   Model of Pneumatic Cylinder Chamber

In this section, we seek to develop a differential equation that links the chamber pressures to the mass flow rate through the valve and the translational speed of piston. In the previous works [40], [75], and [80], the authors derived this equation by assumption that the charging and discharging processes were both adiabatic. Al-Ibrahim [81] found experimentally that the temperature inside the chambers lays between the theoretical adiabatic and isothermal curves when the temperature inside the chamber is examined by thermocouple. The experimental values of the temperature were close to the adiabatic curve only for the charging process. For the discharging of the chamber the isothermal assumption was closer to the measured values. In this article we derive
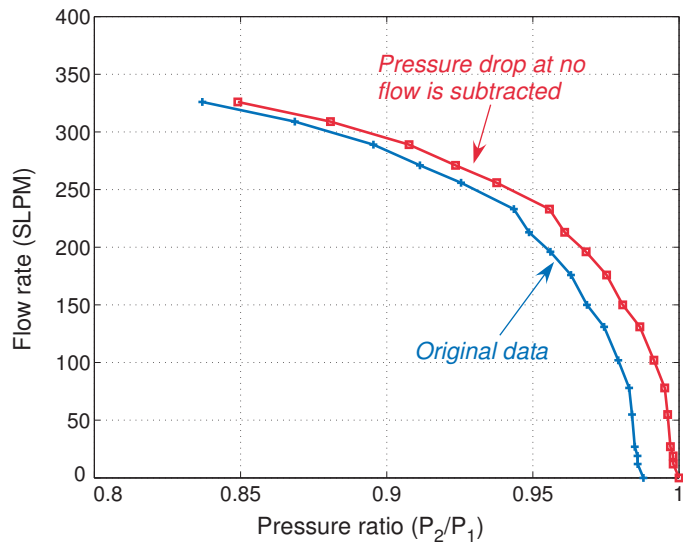
Figure 4.8: Subtract pressure drop when flow rate is zero from original signal
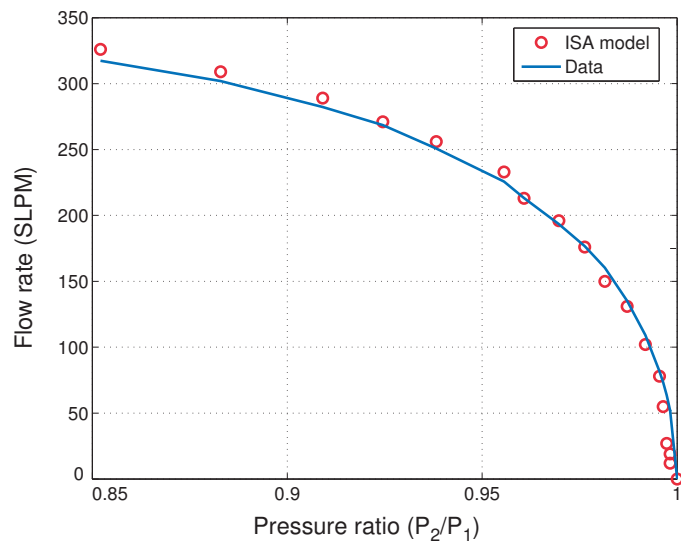
Figure 4.9: Predicted flow rate using ISA model, $C_V = 0.3988$, $X_T = 1.00$

the pressure dynamics equation in a way that accounts for the different thermal characteristics of the charging and discharging processes of the cylinder chambers. The most general model for a volume of gas consists of three equations: an equation of state, the conservation of mass equation, and the energy equation [82] [14]. To facilitate the analysis of air in pneumatic systems, the following conditions are often assumed in modeling a pneumatic system:

(i) the gas is ideal gas,

(ii) the pressures and temperature within each chamber are homogeneous,

(iii) kinetic and potential energy terms are negligible, and

(iv) the leakage in the cylinder can be neglected for initial modeling.
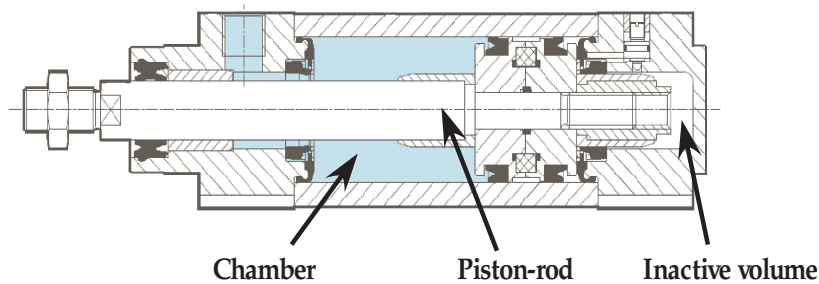
Festo cylinder DNC	
Stroke	200 mm
Piston diameter	32 mm
Rod diameter	12 mm
Piston-rod weight	0.6 lb
Load weight	0.7 lb

Figure 4.10: Sectional view and specification of Festo cylinder DNC

these equations can be written for each chamber. Considering the control volume V, with density ρ, mass m, pressure P, and temperature T, the ideal gas law can be written as

$$P = \rho R T \tag{4.7}$$

where, R is the ideal gas constant. Using the continuity equation the mass flow rate can be expressed as

$$\dot{m} = \frac{d}{dt}(\rho V) \qquad \text{or} \qquad \dot{m}_{in} - \dot{m}_{out} = \dot{\rho} V + \rho \dot{V} \tag{4.8}$$

where $\dot{m}_{in}$ and $\dot{m}_{out}$ are the mass flows entering and leaving a chamber. Combine the energy equation

$$\dot{q}_{in} - \dot{q}_{out} + kC_V(\dot{m}_{in}T_{in} - \dot{m}_{out}T_{out}) - \dot{W} = \dot{U} \tag{4.9}$$

where $\dot{q}_{in}$ and $\dot{q}_{out}$ are heat transfer terms, k is the specific heat ratio ($k = 1.4$ for air), C_v is the specific heat at constant volume, T_{in} is the temperature of incoming flow, W is the rate of change in the work, and U is the change of internal energy. The pressure dynamics inside a cylinder chamber can be written as

$$\dot{P} = \frac{RT}{V}(\alpha_{in}\dot{m}_{in} - \alpha_{out}\dot{m}_{out}) - \alpha \frac{P}{V}\dot{V} \tag{4.10}$$

where α_{in} and α_{out} have values between 1 and k, depending on the actual heat transfer during the process. In equation(4.10), a value of α_{in} close to k is recommended for the charging process and α_{out} should be chosen close to 1 during the discharging process. The thermal characteristic of compression/expansion process due to the piston movement is suggested to be $\alpha = 1.2$, according to the research from Al-Ibrahim and Otis [83].

Choosing the origin of piston displacement at the end of blind side as shown in Figure 4.2, the volume of each chamber can be expressed as

$$V_i = \begin{cases} V_{ci} + A_i x, & \text{for chamber A;} \\ V_{ci} + A_i(L-x), & \text{for chamber B;} \end{cases} \tag{4.11}$$

where $i = a, b$ is the cylinder chambers index (a is blind side and b is rod side), V_{ci} is the inactive volume at the end of stroke for cushion and admission ports, A_i is the piston effective area, L is the piston stroke, and x is the piston displacement. The difference between the piston's effective areas for each chamber A_a and A_b is the piston rod. Substituting equation(4.11) into equation(4.10), the time derivative for the pressure in the pneumatic cylinder chambers becomes

$$P_i = \begin{cases} \frac{RT}{V_{ca}+A_a x} k\dot{m}_{in} - 1.2\frac{PA_a}{V_{ca}+A_a x}\dot{x}, & \text{for extending stroke in chamber A;} \\ \frac{RT}{V_{cb}+A_b(L-x)}(-\dot{m}_{out}) - 1.2\frac{PA_b}{V_{cb}+A_b(L-x)}\dot{x}, & \text{for extending stroke in chamber B;} \\ \frac{RT}{V_{ca}+A_a x}(-\dot{m}_{out}) - 1.2\frac{PA_a}{V_{ca}+A_a x}\dot{x}, & \text{for retracting stroke in chamber A;} \\ \frac{RT}{V_{cb}+A_b(L-x)}(k\dot{m}_{in}) - 1.2\frac{PA_b}{V_{cb}+A_b(L-x)}\dot{x}, & \text{for retracting stroke in chamber B;} \end{cases} \tag{4.12}$$

In this new form, the pressure equation accounts for the different heat transfer characteristics of the charging and discharging processes, air compression or expansion due to piston movement, the difference in effective area on the opposite sides of the piston, and the inactive volume at the end of stroke and admission ports. The flow entering a cylinder chamber is from the pressure tank, through the pneumatic valve and connecting tube (leaking between neighboring chamber is not considered) and the air can flow out to the atmosphere through the valve.

In order to validate the cylinder model derived in different stroke situations for the two chambers, experimental tests are conducted with no leakage, as shown in Figure 4.11. The air cylinder used in this study was manufactured by Festo corporation. An LVDT is mounted to move with the rod of the cylinder is used as a position sensor.
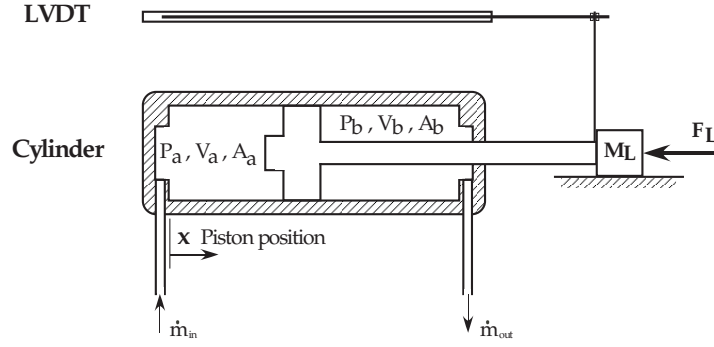
Figure 4.11: Schematic of cylinder model test system

4.2.3   Piston-Load Dynamics and Friction Estimation

The equation of motion for the piston-rod-load assembly can be expressed as

$$P_a - P_b - F_f = (M_L + M_P)\ddot{x} \tag{4.13}$$

where M_L is the external load mass, M_P is the piston and rod assembly mass, x is the piston position, and F_f is the friction force. The left-hand side of equation(4.13) represents the actuator active force, produced by the pressure differential acting across the piston and the friction force. In order to control the actuator force, one has to finely tune the pressure levels in the cylinder chambers using the command element, pneumatic valve, and flow control valve for exhaust. This requires detailed models for the dynamics of pressure in both chambers of the actuator, valve dynamics, and connecting tubes, which we have derived and will derived in this Chapter.

Knowledge of the friction in the cylinder is important in modeling its dynamic motion. Various models for friction between sliding parts have been presented [84]. In this work, the friction force is modeled by the traditional combination of stick-slip, Coulomb and viscous friction.

$$F_f = \begin{cases} F_{sf}, & \text{if } \dot{x} = 0 \text{ and } \ddot{x} \neq 0; \\ F_{cf} + C_{vf}\dot{x}, & \text{if } \dot{x} \neq 0; \end{cases} \tag{4.14}$$

where F_{sf} is the stick-slip friction force, F_{cf} is the Coulomb friction force, and C_{vf} is the coefficient of viscous friction. These parameter depend on the cylinder, and can be estimated from the experimental data. A method for estimating the parameters F_{sf} and C_{vf} is described in the following.

Initially the cylinder rests at the position $x = 0$. During the extending stroke (cylinder rod moves from the end of blind side to the end of rod side), the valve is actuated to allow the air to enter chamber A and leave chamber B to atmosphere. However, there is a time delay (δt) between the time of valve control command (t_1) and the time when the piston starts to move (t_2). The time duration δt is also called the start-up time. During this process, compressed air is accumulated in the inactive volume of the cylinder and tube. The pressure in chamber A increases to generate force to overcome the friction force and force generated by air in chamber B. Therefore, stick-slip friction force can be estimated by the following equation:

$$F_{sf} = (P_a|_{t=t_2}A_a) - (P_b|_{t=t_2}A_b) \tag{4.15}$$

From Figure 4.12, P_a at time t_2 is 61.37 psi and P_b at time t_2 is 40.22 psi. Substituting these values into equation(4.15) yields the result: $F_{sf} = 150$ N. We assume that the stick-slip friction force during extending stroke and retracting stroke are same.

$$P_a|_{t=t_3}A_a - P_b|_{t=t_3}A_b - F_{cf} - C_{vf}\dot{x} = (M_L + M_P)\ddot{x}|_{t=t_3} \tag{4.16}$$

From the velocity and acceleration data derived from the displacement signal of LVDT, one can see that the velocity is approximately constant during the extending stroke motion of piston-rod. In addition, the pressures inside the two chambers of the cylinder do not change much. Using the data in this constant speed interval and equations(4.14) and (4.16) to define the friction force when piston is in motion. The Coulomb friction force F_{cf} and viscous friction coefficient C_{vf} can be found: $F_{cf} = 158.6N$ and $C_{vf} = 17.88\frac{Ns}{m}$. Calculation of retracting stroke also agrees with this number. The pressures are plotted in Figure 4.12.
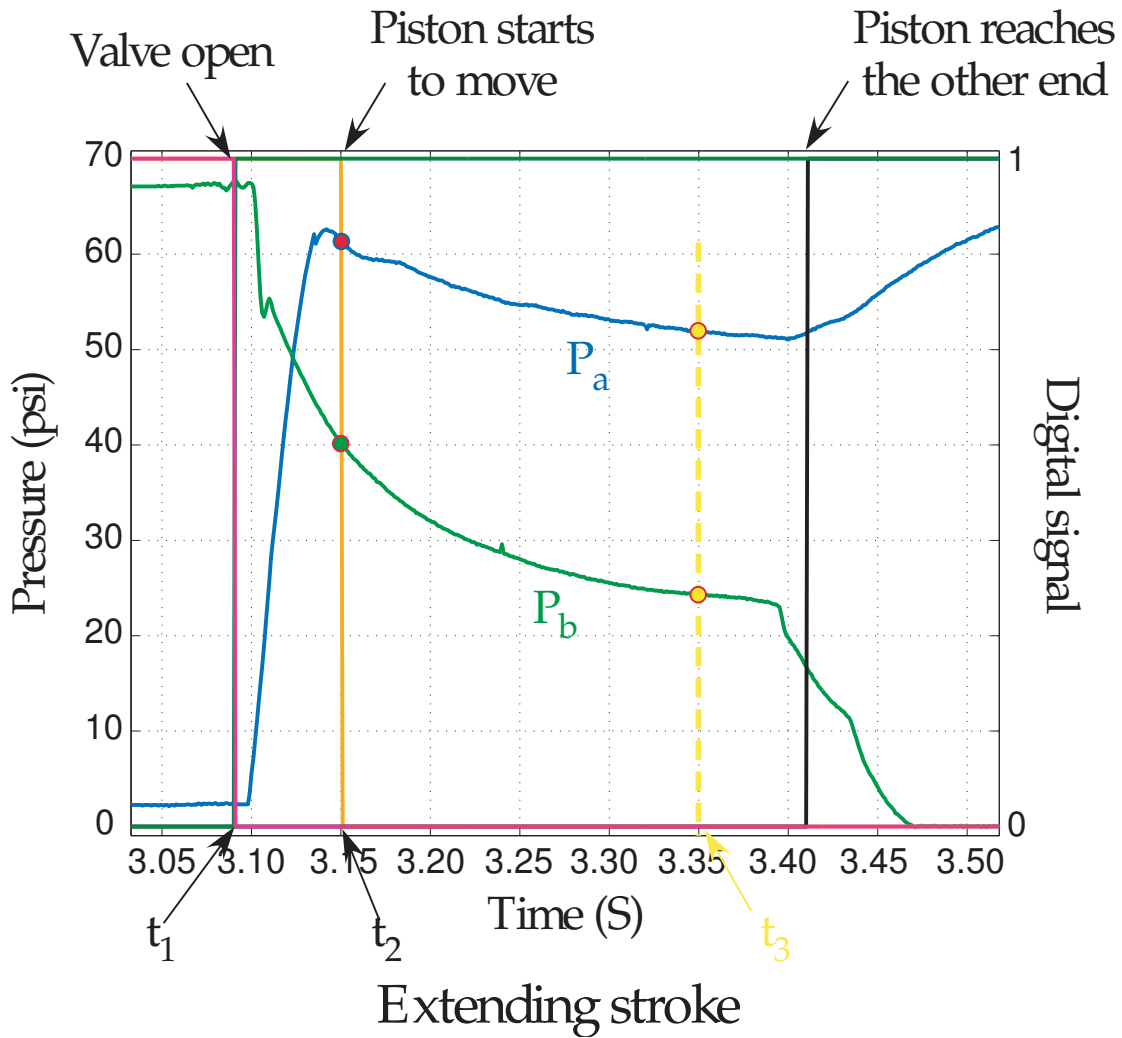
Figure 4.12: Pressure measurement with valve and proximity sensor signals for estimating the parameters of friction forces: F_{sf}, F_{cf}, and C_{vf}

4.3 Fault Detection and Diagnosis using Model-Based Approaches

In this section, we apply various methods to perform model-based fault detection and diagnosis for pneumatic systems. They are:

- Electro-Pneumatic equivalence

- Logistic table

- System model

4.3.1 Electro-Pneumatic Equivalence

Flow rate was found to be an important parameter in diagnosis of pneumatic systems found through our study. The flow rate, Q in SLPM (standard liter per minute), can be measured directly by a mass flow meter. The volume of flow, U, is an accumulation of flow rate over a duration which is equal to the area under the curve of flow rate across the time interval. They are defined and related by the following equation

$$U = \int Q dt = \sum Q \Delta t, U_c = U/N \tag{4.17}$$

where U_c is the average flow per cycle for N cycles.

In the consideration of linear characteristics of a pneumatic system, the analogy between the parameters of a pneumatic and a mechanical system or electrical circuit has been recognized using the one-port discrete lumped-parameter model [1]. Employing the expanded Maxwell or impedance analogy, the power conjugate variables for flow are volume velocity (flow variable) and pressure (effort variable). Hamilton variables are the system descriptors which, when differentiated in time, yield the power conjugate variables. For examples, in mechanical system these will be the displacement and linear momentum. In pneumatic systems, they are volume, U, and pressure-momentum, γ, with

$$\Delta P = \frac{\rho l}{A}\frac{dQ}{dt} \qquad and \qquad \Gamma = \frac{\rho l}{A}Q \qquad\qquad (4.18)$$

where ρ is the mass density of the fluid, l is the pipe length, A is the cross-sectional area, and Q is the flow rate. The three types of passive energic elements for pneumatic system are [1]

- Fluid inertance (kinetic energy): The pipe fluid inertance can be obtained as $I = (\rho l)/A$,

- Fluid capacitance (potential energy): the two common forms of fluid capacitance are spring-like compressibility and pressure increases with depth due to the presence of a gravitational field,

- Fluid resistance (energy loss): flow friction in pipes, leakage, flow around bends or through orifices and valves.

Such correlation of inertance, capacitance, and resistance provides us with intuitive and helpful insights into the behavior of pneumatic systems. The analogous relationship is summarized in Table 4.1 for the purpose of comparison and analysis.

Parameters/type	Pneumatic	Electrical	Mechanical
Effort	pressure, P	voltage, V	force, F
Flow	flow rate, Q	current, i	velocity, v
Displacement	flow, U	charge, q	distance, x
Power	$\Delta P \cdot Q$	$V \cdot i$	$F \cdot v$

Table 4.1: Comparison of equivalent parameters in pneumatic system versus electrical and mechanical systems [1]

Based on the electro-pneumatic analogy in Table 4.1, we regard the flow rate as equivalent to the current, i, and the pressure as equivalent to the electrical potential, V. The pressure measured at the location of the flow meter is labeled as V_m. The resistors represent the flow resistance along the flow path, causing drop in pressure (voltage). This can be confirmed from the experimental results described above. In Figure 4.13, the introduction of leakage is modeled as another branch of air

64

flowing along the path in addition to the initial R_c with added flow resistance of R_{ls} in parallel. The introduction of such parallel flow branch reduces the effective resistance by combining R_c and R_{ls} in parallel. That is,

$$i_{ls} = \frac{V}{R_1 + \frac{R_c R_{ls}}{R_c + R_{ls}}} > i = \frac{V}{R_1 + T_c} \tag{4.19}$$

$$V_{m,ls} = V - R_1 i_{ls} < V_m = V - R_1 i \tag{4.20}$$
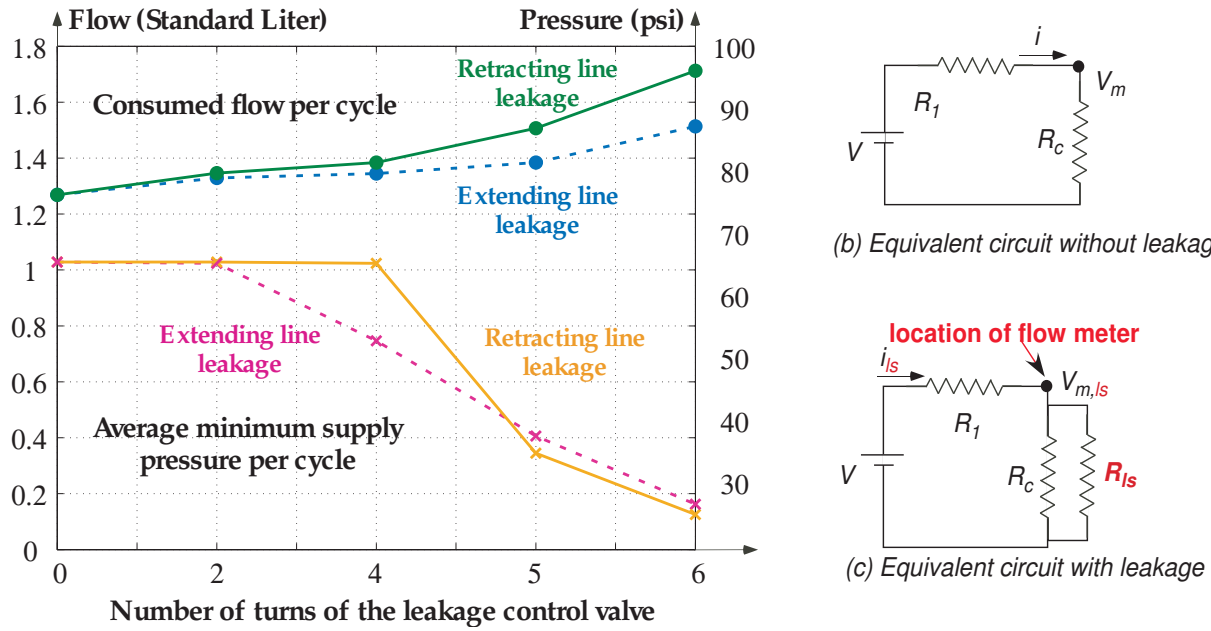
Figure 4.13: Experimental results of leaks vs. pressure and flow changes per cycle(*left*). Equivalent circuit of the flow leakage effect for pneumatic system (*right*)

As a result, the total current i_{ls} increases, causing a larger voltage drop across the same resistor R_1. Hence, the introduction of leakage results in a smaller $V_{m,ls}$. That is,

$$i_{ls} > i \ \& \ V_{m,ls} < V_m \Leftrightarrow Q_{ls} > Q \ \& \ P_{ls} < P \tag{4.21}$$

where Q_{ls} is the flow rate with leakage level control, Q is the regular flow rate without leak, P_{ls} is the pressure with leakage level control, and P is the regular pressure without leak. Thus, the analytical model presented in equations 4.21 is consistent with the experimental results, which show that the pressure (voltage) is decreased when a leak is introduced, while the flow rate (current) is increased. With manually adjusted leakage control, a circuit analogous to the pneumatic system is constructed and illustrated in Figure 4.13.

Number of turns	0	2	4	5	6
Consumed flow of extending stroke (SL)	0.6306	0.6986	0.7193	0.7624	0.9093
Consumed flow of retracting stroke (SL)	0.6379	0.6300	0.6256	0.6221	0.6042
Minimum supply pressure in extending (psi)	62.48	62.19	38.01	29.56	22.67
Minimum supply pressure in retracting (psi)	60.5	60.37	59.96	38.15	23.35

Table 4.2: The results and comparison of leakage on the extending side, with the flow meter in both lines and pressure sensor in inlet line. The flow of extend stroke increases as the number of leakage turns at 0, 2 ,4, 5, and 6 turns. (SL stands for standard liter)

Number of turns	0	2	4	5	6
Consumed flow of extending stroke (SL)	0.6306	0.6180	0.6099	0.5904	0.5609
Consumed flow of retracting stroke (SL)	0.6379	0.7285	0.7740	0.9165	1.1515
Minimum supply pressure in extending (psi)	62.48	62.41	62.14	27.85	22.74
Minimum supply pressure in retracting (psi)	60.5	60.57	60.44	34.4	20.01

Table 4.3: The results and comparison of leakage on the retracting side, with the flow meter in both lines and pressure sensor in inlet line. The flow of extend stroke increases as the number of leakage turns at 0, 2 ,4, 5, and 6 turns. (SL stands for standard liter)

The experimental data with leakage in extending line is listed Table 4.2 and leakage in retracting line is shown in Table 4.3. The recorded pressure values are the minimum supply pressure during each stroke. The results in Figure 4.13 shows that the consumed flow per cycle increases when the amount of leak is increased (controlled by leak control knob). At the same time, the pressure measured along the same line drops. When the flow increases more, the drop in pressure is larger. This can be clearly seen from the pairs of of extend and retract curves in Figure 4.13.

There is a close correlation in leak and parameter of the pneumatic system and further analysis reveals that there are also changes associated with the profiles of pressure and flow rate. However, it is only a linear first-order relationship for qualitative analysis. A further discussion of the quantitative changes will be presented in details in Section 4.3.2 and Chapter 5.

4.3.2   Logistic Table

Tt is convenient in FDD to form a logistic table consisting of selected features of the parameters or processes to be diagnosed. The selection of the features depends on the process and expertise knowledge of the system. In the following, we will illustrate such method of FDD using an example from the experiments. Table 4.4 lists 13 features selected to construct the logistic table.

Element of feature	Description of the feature
1	Minimum supply pressure P_s
2	Minimum blind side line pressure P_a during extending stroke
3	Maximum blind side line pressure P_a during retracting stroke
4	Maximum rod side line pressure P_b during extending stroke
5	Minimum rod side line pressure P_b during retracting stroke
6	Consumed flow in chamber A during extending stroke
7	Exhaust flow in chamber B during extending stroke
8	Consumed flow in chamber A during retracting stroke
9	Exhaust flow in chamber B during retracting stroke
10	Maximum exhaust flow rate from chamber A during retracting stroke
11	Maximum exhaust flow rate from chamber B during extending stroke
12	Time of extending stroke
13	Time of retracting stroke

Table 4.4: Features selected to construct logistic table

In each class of leakage (location), we can divide the analysis into a series of subclasses corresponding to different sizes of leakage. The leakage is regulated by the leakage control valve shown in Figure 3.1. A template for each class was created, and a template pattern recognition

Feature	1	2	3	4	5	6	7	8	9	10	11	12	13
Extend line	−	−	−	0	+	+	0	0	+	+	−	+	−
Retract line	−	+	0	−	−	−	−	−	−	−	+	−	+
Both(Extend + Retract) lines	−	0	0	0	0	+	−	0	0	+	0	+	0
Supply line	−	−	0	−	0	+	0	+	0	−	−	+	+

Table 4.5: Logistic table of the 13 features defined in Section 4.3.2 vs. the 4 classes of leakage (extend, retract, both sides, and supply line)

technique was employed to classify unknown leakage into different configuration (location and size) of leakage [85].

A logistic table for FDD based on the variation features in response to the three classes of leakage is presented in Table 4.5. In Table 4.5, "+" means the feature value is increased with an increasing level of leakage, "−" means the feature value is decreased with an decreasing level of leakage, "0" means the there is no correlation between the feature and a leakage or leakage influence on the feature is uncertain (this feature can't be applied to diagnose the corresponding leakage). The logistic table can be used to determine 4 possible locations of an unknown fault (in this case, the leakage), by examining the variation of the 13 features.

4.3.3 System Model Applications in Diagnosis and Prognosis of Leakage

The dynamic model of a cylinder chamber can also be applied in explaining the variation of the pressure and flow rate due to the movement of a piston. Take the retracting stroke shown in Figure 4.14as an example. (For this test, the inlet pressure sensor denoted by signal P_{in} in the figure is placed just on the inlet line of cylinder DNC control valve, after the manifold connecting to other cylinders.) First, the value spool is actuated and the control valve is set for air entering the rod side and air leaving the blind side. At this time t_1 the piston-rod is not moving yet because the differential forces generated by pressures on the two sides of the piston is not big enough to overcome the friction force. At time t_2, the piston-rod leaves the rod side wall, goes through the cushioning areas and accelerates towards the blind-side. The stroke is too short to have a constant speed area when the piston reaches the cushioning area on the other side with the piston movement

decelerated and stopped by the cylinder wall in blind side.

Three important time instances deserve to be treated carefully, as indicated in Figure 4.14 with a yellow circle and numbers *I*, *II* and *III*. At time t_1, the rod-side line is connected to the supply line and the pressure is supposed to drop immediately. The delay between the drop staring edge of P_{in} and the valve control signal is due to the valve response time (20 *ms*). The delay between P_{in} and P_b is due to the length of the connecting tube. At time t_2, the pressure in chamber *B* reaches the same value as the supply pressure, causing the pressure and the flow rate drop. Check Equation(4.12) during retracting stroke, $x = L$ and $\dot{x} = 0$. For chamber *B*, the flow rate change $\dot{m}_{in} < 0$ and the second part in the right-hand side is 0; thus $\dot{P}_b < 0$. For chamber *A*, the flow rate change $\dot{m}_{out} > 0$ and the second part in the right-hand side is 0; thus $\dot{P}_a < 0$. This reflects the right trend in Figure 4.14. At time t_3, increase of P_b attributes to the increase of supply pressure P_{in} and the control volume in chamber *B* is fixed with a decreasing speed of entering flow.
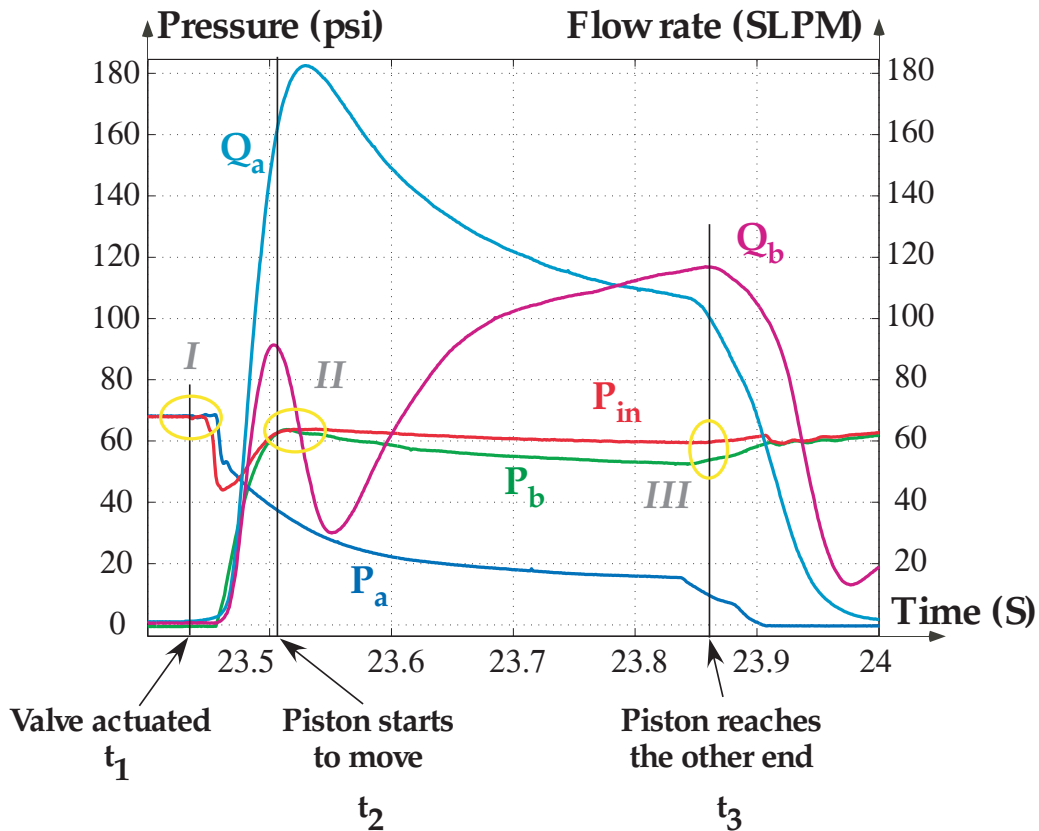
Figure 4.14: Variations of pressure and flow rate values during DNC retracting stroke

69

4.4   Discussion

The fault diagnosis consists of the determination of the type of fault, as well as the size, location, and time of the fault. In this dissertation, we focus on only one type of fault: leakage of the system. The leakage is implemented by a leakage control valve at the following locations (also see Figure 3.12):

(1) leakage in the extend line,

(2) leakage in the retract line,

(3) leakage in both extend and retract lines,

(4) leakage in supply line

The size of fault is controlled by the number of turns of the leak valve from the fully closed position (also see Section 3.2.5). The data with different positions and sizes of leakage are compared. The symptoms corresponding to different leakage configuration are generated.

4.4.1   Fluctuation of Air Supply

In an ideal condition, the system will work under constant air supply. In this experiment setup, however, the air supply are not constant due to the finite volume of tanks in house air supply system. Therefore, the change of air supply as well as its effect on the experimental results must be taken into consideration in analysis. The signals obtained during the run-time operation of our pneumatic system are shown in Figure 4.15. Three signals (supply pressure, extending pressure, and retracting pressure) are compared to determine if they have different fluctuation. From Figure 4.15, we observe that the supply pressure fluctuates with a big range in the first 5 minutes. However, the extending and retracting pressures show consistent pattern during the entire 10 minutes with small variations in certain areas.

The signals with different leakage size are also studied, which also have similar fluctuation due to the house air. The signals obtained in different time intervals are studied to determine if
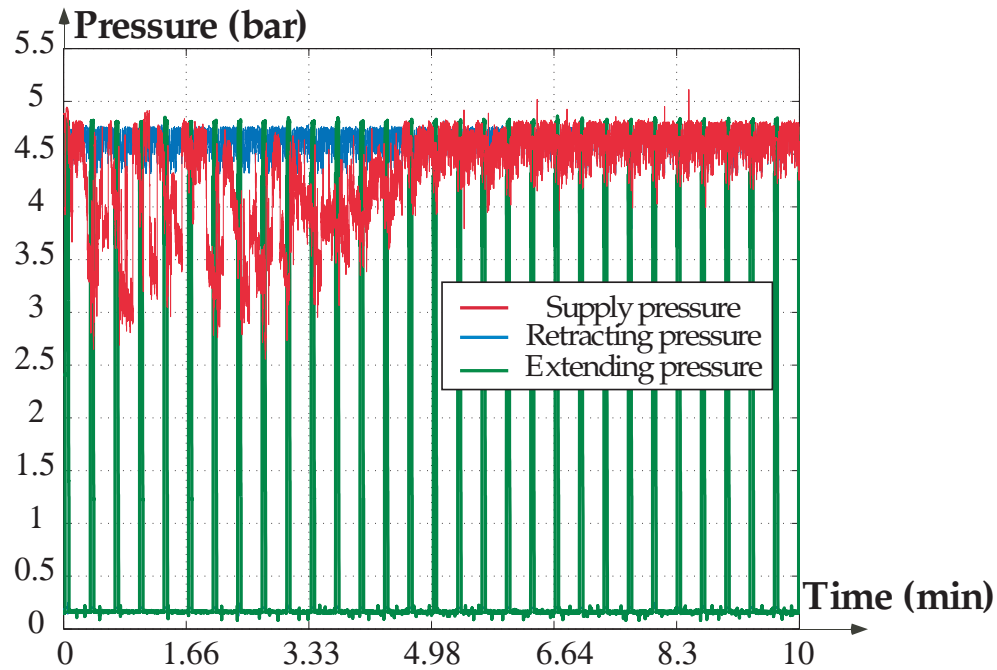
Figure 4.15: Signals of flow rate and pressures obtained in 10 minutes

the average value within the time intervals can be used in fault detection and diagnosis. Based on Figure 4.15, we use the average of last 5five minutes of data for analysis

4.4.2 Valve Model Standards

Two parameters are used to define the valve capacity (performance) in industry: flow coefficient, often used by U.S. and European companies and sonic conductance, often used by Asian companies [86] [48] [49] [78]. Correspondingly there are two standards (ANSI and ISO).

To gain a better understanding of valve-rating standards, it is useful to look at how test methods have evolved over the past few decades. One important flow-rating tool is effective area, S, an expression defined by previous versions of JIS (Japanese Industrial Standards Committee). It is based on a typical pneumatic system using solenoid valves to actuate cylinders. Researchers conducted experiments to determine the most suitable way of expressing airflow characteristics that directly correspond to the drive characteristics of cylinders. Results of this research showed

that the full stroke time of a pneumatic cylinder is inversely proportional to the maximum exhaust flow rate [86].

While the system supplies compressed air to a valve at a constant upstream pressure, the ratio between downstream and upstream pressure ($\frac{P_2}{P_1}$) decreases (the differential pressure increases) as the flow rate increases. Flow rate will increase and pressure ratio decrease until the system reaches sonic velocity and the flow rate stabilizes. Beyond this point, called the choked flow, downstream pressure drop continues without increasing flow rate. Thus, a distinctive value for representing the maximum constant flow at choked flow (the sonic velocity flow) was established by the Japanese Industrial Standard, JIS C 9312 (1964) as a way of expressing flow characteristics of solenoid valves. Termed the effective area $S(mm^2)$, this value also expresses a valve's size (or performance) in direct relation to the cylinder's drive speed.

At the same time, the process-control industry was applying the term "coefficient of volume flow" or C_V to gases, after applying a density conversion factor. The parameter C_V is a measure of water flow rate at a minimum differential pressure (1 psi) through the valve. Calculating flow rate using the C_V factor is comparable to calculating the subsonic flow rate using S. Mathematically, $C_V = \frac{S}{18}$.

In 1989, the International Organization for Standardization published ISO 6358, a standard that succeeded in expressing the entire area flow characteristics for pneumatic equipment using sonic conductance C and critical pressure ratio b. Sonic conductance represents the maximum flow rate at choked flow, and has much the same definition as that of effective area S. In experimental test, $S = 5C$.

Also, critical pressure ratio can vary from one type of valve to another, which shows that subsonic-flow characteristics depend on valve construction. Thus, ISO and JIS standards are comparable and JIS B 8390 (June 2000) is consistent with ISO 6358. The National Fluid Power Assn. (NFPA) takes a different approach. Technical committee ANSI/NFPA T3.21.3 adopted C_V as a standard measure of the flow coefficient in pneumatic equipment in 1990, a year after ISO 6358 was established. Unfortunately, C_V (ANSI) presents only one representative flow-rate value, and

calculates it by using a small differential pressure (pressure ratio 0.98 to 0.99) at the extreme end of the subsonic flow regime.

The best way to get a handle on different rating methods is through actual testing. Results of C and C_V(ANSI) measurements taken from many solenoid valves using ISO testing equipment (similar to ANSI/NFPA) indicate that the ratio of $\frac{5C}{C_V}$(ANSI) is "large" if the valves have a small b value, and "small" if b is large. It is not identical. The reference conversion $\frac{S}{C_V}$ = 18 which had been applied by Japanese companies corresponds to valves with b = 0.3 to 0.5.

Maximum flow rate can vary with valve construction even when different valves have identical C_V(ANSI) ratings. That is because C_V(ANSI) does not correspond exactly to C (or S). A good example is to look at the characteristics of an actuating cylinder driven by valves with identical C_V but different b values. Characteristics of an actuating cylinder shows flow behavior of three solenoid valves, all with measured C_V(ANSI) = 0.2 [86]. The maximum flow rate differs more than 30% between valve A with $b = 0.1$ and valve C with $b = 0.5$. A valve with a larger maximum flow rate permits quicker cylinder response. Even when ANSI methods measure the same C_V it is apparent that there are big differences in a cylinder's full stroke time. This clearly demonstrates that C_V alone is insufficient as a selection criterion for specifying components in a pneumatic actuating system.

Engineers should also keep in mind that it is rare for published flow rates to exactly equal actual valve performance in the field. Flow-rate characteristics appearing in any catalog are only representative values for a particular valve series. All of the standards mentioned - ISO, JIS, and ANSI/NFPA - prescribe an allowable variation of 15%. Thus, it is necessary to include this variance in any design. SMC feels the best way to find flow-rate characteristics for a valve is to use test equipment and methods according to ISO 6358. The company can also provide up-to-date information if current catalogs do not reflect the latest information.

4.5   Summary

In this Chapter, the system model of a pneumatic system is derived, including the valve, cylinder, tube and fault control valve, based on the experimental data. Methods of pneumatic analogy, logistic table, and system model are applied in detecting and diagnosing leakage location and level. The system leakage and performance can be evaluated qualitatively and quantitatively by flow rate, pressure, accumulated flow, and stroke time information. Two major different valve rating standards are compared and a correlation between the factors governing the standards is discussed. The effects of supply air fluctuation and the considerations of selecting an appropriate threshold value are also discussed.

Applications of signal-based approaches will be discussed in next chapter to offer another point of view in fault detection and diagnosis for pneumatic systems.

Chapter 5

SIGNAL-BASED FAULT DETECTION AND DIAGNOSIS FOR PNEUMATIC SYSTEMS

5.1   Introduction

Signal processing [72] or *feature-based approach* [25] is another way to deal with fault diagnosis. This approach usually avoids specific system modeling problems, especially, when a systematic model is difficult to construct due to the nonlinearity such as compressed air system. Signals may be studied either by using time-domain method, using frequency-domain method or methods with both time and frequency domains. The difficulty common to all such approaches is to ensure that a change in some quantity is due to a particular fault [73], which means that the selected symptom / feature should be appropriated and trained well to indicate the corresponding property of specific fault. All of these topics are covered in this chapter.

Signal processing based fault diagnosis: on the assumption that certain process signals carry information about the faults of interest and this information is presented in the form of symptoms, a fault diagnosis can be achieved by a suitable signal processing. Typical symptoms are time domain functions like magnitudes, arithmetic or quadratic mean values, limit values, trends, statistical moments of the amplitude distribution or envelope, or frequency domain functions like spectral power densities, frequency spectral lines, ceptrum, etc. The signal processing based schemes are mainly used for those processes in the steady state, and their efficiency for the detection of faults in dynamic systems, which are of a wide operating range due to the possible variation of input signals,

Signal-Based Fault Diagnosis System
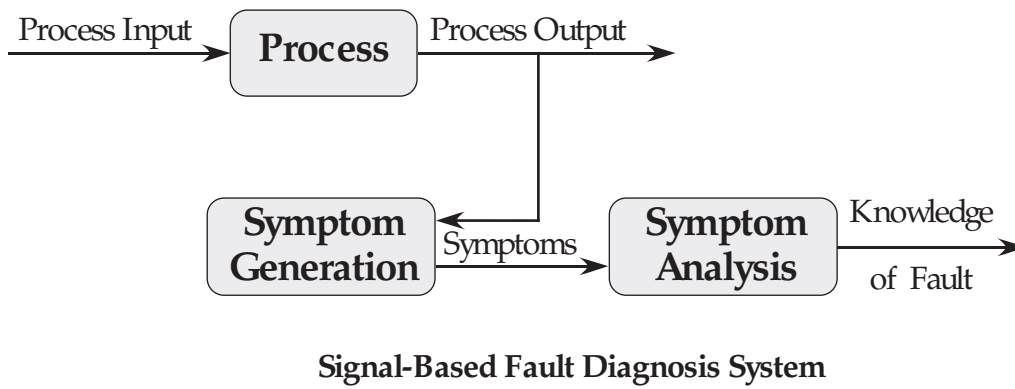
Figure 5.1: Schematic description of signal-based fault diagnosis scheme

is considerably limited. Figure 5.1 illustrates the basic idea of the signal processing schemes.

5.1.1 Fault Diagnosis Methods

Fault diagnosis is defined as the determination of the kind, size, location, and time of detection of a fault. It follows fault detection which includes fault detection and identification. The inputs, shown in Figure 5.1, to the knowledge-based fault-inferencing system are all available symptoms, and the fault-relevant knowledge about the process, including analytical symptoms, heuristic symptoms, process history and fault statistics, unified symptom representation, and fault-symptom relationships. Isermann [73] used a different way to classify the diagnosis methods from that of Leger [87]. Diagnosis methods are divided into two groups:

(1) Classification methods:

- Geometrical distance and probabilistic methods

- Pattern recognition

- Artificial neural networks

- Fuzzy clustering

(2) Typical approximate reasoning methods:

- Probabilistic reasoning

- Possibilistic reasoning with fuzzy logic

- Reasoning with artificial neural networks

Considered as one of the classification methods, pattern recognition is the scientific discipline whose primary goal is the classification of objects into a number of categories or classes. These objects can be signal waveforms, images or any type of measurements that need to be classified. The objects are referred to as patterns and the primary goal of pattern recognition is supervised or unsupervised classification. Statistical approach has been most intensively studied and used in practice [88]. Recently, neural networks have obtained more attention. The design of a recognition system requires careful attention to the following issues: definition of pattern classes, sensory environment, pattern representation, feature extraction and selection, cluster analysis, classifier design and leaning, selection of training and test samples, and performance evaluation [88, 85].

In the following sections, we will discuss various method backgrounds used in pattern recognition and their applications in pneumatic system FDD, statistical method in Section 5.2.1, wavelet transform in Section 5.2.2, and classifier in Section 5.2.3.

5.2   Theoretical Background

5.2.1   Statistical Approach

In this section, mathematical background of statistic methods are described for the analysis of signals. In typical systems, measured signals repeat themselves and show oscillations that are both of harmonic and stochastic natures. If changes in these signals are related to faults in the process, actuators or sensors, a signal analysis is a further source of information. The extraction of fault-relevant signal characteristics can in many cases be restricted to the amplitudes or amplitude densities of the signal by band-pass filters.

In utilizing the statistical approach, the measured signals are stochastic variables $S_i(t)$ (a recorded signal changing with time variation), with mean value and variance [73]

77

$$\bar{S}_i = E\{S_i(t)\} \ ; \ \bar{\sigma}_i^2 = E\{[S_i(t) - \bar{S}_i]^2\} \tag{5.1}$$

where $\bar{S}_i$ is the average of $S_i(t)$, $\bar{\sigma}$ is the standard deviation of $S_i(t)$, and $E\{S_i(t)\}$ represents expectation of $S_i(t)$. The pair $\{\bar{S}_i, \bar{\sigma}_i\}$ are used as normal values for the non-faulty process. Analytical symptoms are then obtained as changes with respect to the normal values in equation (5.1), expressed as

$$\Delta S_i = E\{S_i(t) - \bar{S}_i\} \ ; \ \Delta \sigma_i = E\{\sigma_i(t) - \bar{\sigma}_i\} \ t \succ T_F \tag{5.2}$$

Usually, the time instants T_F of fault occurrences are unknown. To distinguish faulty behavior from normal condition, a threshold value must be defined:

$$\Delta S_{tol} = \varepsilon \bar{\sigma}_S \ \ \varepsilon \geq 2 \tag{5.3}$$

Here we use a fixed threshold value for simplification. A fuzzy threshold method [73, 89] may be obtained by a gradual measure for exceeding a threshold which is not discussed in this study. If ΔS is greater than ΔS_{tol}, then some faults will be reported. By this means, a compromise has to be made between the detection of small faults and false alarms because of disturbance [73]. Another possibility is to represent the features as a fuzzy set $\mu_S(S)$. By matching the current value $\mu_{S'}$ with the feature's membership function, the "increased" $\mu_{S+}(S)$,

$$\mu_S = max_S[min(\mu_{S'}(S) \ , \ \mu_{S+}(S))] \tag{5.4}$$

5.2.2　Wavelet Transform

A feature-based process is more suitable to a complex process where waveform signals are used for process diagnosis. In such a system, features are considered as random variables. Feature extraction and feature subset selection are critical steps to reduce the number of attributes or data dimensions considered in the decision-making step. Here wavelet transform is a useful in feature extraction due to its multi-resolution nature, its localized properties in both time and frequency
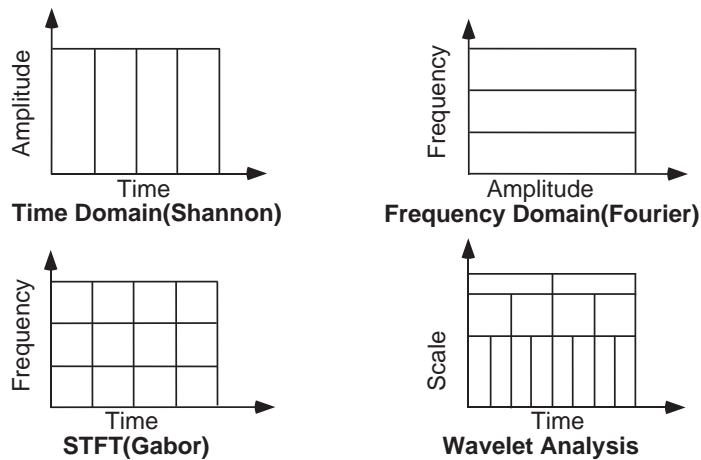
Figure 5.2: Comparison of Fourier transform , short time Fourier transform, and wavelet transform

domains, its fast algorithms ready for an on-line implementation, and its efficient data compression for feature extraction [90, 25, 91, 92, 93]. In this chapter, wavelet transform will be discussed.

The wavelet transform is a tool that cuts up data or function into different frequency components, and then studies each component with a resolution matched to its scale. In many applications, given a signal $f(t)$, one is interested in its frequency contents locally in time. The standard Fourier transform gives a representation of the frequency contents of $f(t)$. But Fourier analysis has a serious drawback, the time domain information is lost when transformed to the frequency domain. Short-Time Fourier Transform (STFT), maps a signal into a two-dimensional function of time and frequency, representing a trade-off between the time-based and frequency-based views of a signal. However, the information can only be obtained with limited precision, and that precision is determined by the size of the window [94]. Many signals require a more flexible approach – one where we can vary the window size to determine more accurately either time or frequency. Wavelet analysis represents the next logical step: a windowing technique with variable-sized regions. Wavelet analysis allows the use of long time intervals where more precise low-frequency information is required, and shorter regions where high-frequency information is required. The different view of signal is illustrated in Figure 5.2 [95, 94].

The wavelet transform of a signal, $f(t)$, is defined as an inner product of the signal and the wavelet bases

$$W(a,b) = \ <f(t), \psi_{a,b}(t)> \ = |a|^{-\frac{1}{2}} \int_{-\infty}^{\infty} f(t) \psi \frac{t-b}{a} dx \tag{5.5}$$

where $\psi_{a,b}(t)$ is referred to as the wavelet bases and $W(a,b)$ is the wavelet transform coefficients of the signal $f(t)$ [96, 95]. The wavelet bases are formed from translation and shifting of the mother wavelet, $\psi(t)$. The mother wavelet $\psi(t)$ can be any real function satisfying the following condition that C_ψ is finite; that is,

$$C_\psi = \int_{-\infty}^{\infty} \frac{|\hat{\psi}(\omega)|^2}{|\omega|} d\omega < \infty \tag{5.6}$$

where $\hat{\psi}(\omega)$ is the Fourier transform of $\psi(t)$, and ω is the Fourier domain variable. Note that since ω appears in the denominator of the integrand in equation (5.6), C_ψ can only be finite if $\hat{\psi}(0) = 0$, which results in

$$\int_{-\infty}^{\infty} \psi(t)dt = 0 \tag{5.7}$$

Equation (5.7) suggests that the mother wavelet, $\psi(t)$, must oscillate and have 0 as an average value, that is why it is called "wavelet".

If the dilation and translation parameters a and b vary continuously, this transform is called *continuous wavelet transform*. The scale and shift parameter, a and b in equation (5.5), can also be discretized to integer values; *i.e.*, $a = a_0^j$ and $b = a_0^j k$, where $a_0 \geq 2$ and $-\infty < j,k < \infty$ are integers. Then a discrete wavelet bases $\psi_{j,k}(n)$ can be formed

$$\psi_{j,k}(n) = \frac{1}{\sqrt{a_0^j}} \psi \left(\frac{n - a_0^j k}{a_0^j} \right) \tag{5.8}$$

where n is an integer [97]. Based on the discrete wavelet bases, a *discrete wavelet transform* (DWT) of a finite energy sequence with N samples, $f(n)$, can be computed as

$$W_{j,k} = \frac{1}{a_0^j} \sum_{n=0}^{N-1} \psi \left(\frac{n - a_0^j k}{a_0^j} \right) f(n) \tag{5.9}$$

where $W_{j,k}$ are referred to as the DWT coefficients of the sequence $f(n)$. There are many kinds of discrete wavelet transforms for comparison between the two transforms. One such algorithm is illustrated in Figure 5.3. The algorithm is usually referred to as the *fast wavelet transform* (FWT). The basic idea behind the FWT algorithm is to represent the mother wavelet as a set of high-pass and low-pass filters in a filter bank, through which the signal is passed. Following the filtering, the signal is decimated by a factor of 2. The outputs of the low-pass branch are called *wavelet approximation coefficients*. The outputs of the high-pass branch are called *wavelet detail coefficients*. At each iteration step, the approximation coefficients from the previous step will be used as the input of the filter bank. As the decomposition process iterates, with successive approximations decomposed in turn, one signal is broken down into many lower resolution components. Refer to [95] for more information on the inverse wavelet transform. This is called the wavelet decomposition tree, as shown in Figure 5.3, where *cA* and *cD* are the approximation and detail coefficients for each step, respectively [94].

The signal can be perfectly reconstructed from the wavelet approximation and detail coefficients using the inverse FWT. Since only the FWT is used in this dissertation to obtain the wavelet coefficient of a signal for feature extraction, IFWT will not be introduced in this chapter. Refer to [95] for more information on the inverse wavelet transform.
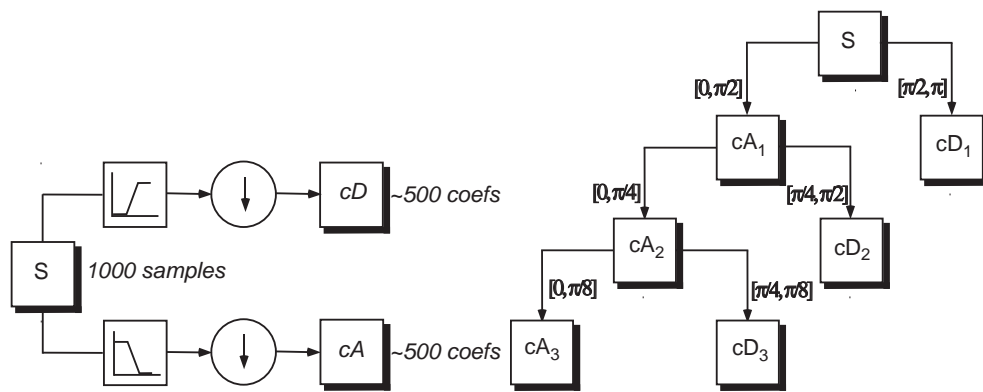

Figure 5.3: Two channel decomposition and decomposition tree

Scale is used instead of time in wavelet transform. Thus, we are interested in the relationship between scale and frequency. This answer can only be given in a broad sense, with the pseudo-

frequency corresponding to a scale. A way to do it is to compute the center frequency, F_c, of a wavelet and to use the following relationship to calculate the pseudo-frequency of a given scale

$$F_a = \frac{\Delta F_c}{a} \tag{5.10}$$

where a is a scale, Δ is the sample frequency, and F_c is the center frequency of a wavelet in Hz which maximizes the FFT of the wavelet modulus. The frequency, F_a, obtained from equation (5.10) is the pseudo-frequency corresponding to the scale a, in Hz. The idea is to associate a given wavelet with a purely periodic signal of frequency, F_c [98, 94]. The center-frequency-based approximation captures the main wavelet oscillations. It is a convenient and simple characterization of the dominant frequency of the wavelet. When the wavelet is dilated by a factor a, this center frequency of the dilated wavelet becomes F_c/a. Lastly, if the underlying sampling frequency is defined, it is natural to associate the scale a, to the frequency.

The wavelet transform will be used in the following chapter for feature selection.

5.2.3   Classifier

The four best known pattern recognition approaches are:

- template matching

- statistical classification

- syntactic or structural matching

- neural networks

Statistical pattern recognition is rigorous and practical, and has been used successfully in a number of commercial pattern recognition systems. Most statistical pattern recognition method are based on **Bayesian** methods, which is the theory we apply in our analysis.

Bayesian Decision rule: Given a classification task of M classes, $\omega_1, \omega_2, \ldots, \omega_M$ and an unknown pattern, which is represented by a feature vector **x**, we form the M conditional probabilities,

$$P(\omega_i|\mathbf{x}), \ i = 1, 2, \cdots, M \tag{5.11}$$

which is known as *a posteriori probabilities*.

In general, the *a posteriori probabilities* are not known. But the *a priori probabilities* $P(\omega_i)$ and class-conditional probability density functions $p(\mathbf{x}|\omega_i), i = 1, 2, \ldots, M$, which describe the distribution of the feature vectors in each of the classes, are known. Based on the **Bayesian** rule [85], the *a posteriori probabilities* can be calculated as follows:

$$P(\omega_i|\mathbf{x}) = \frac{p(\mathbf{x}|\omega_i)P(\omega_i)}{p(\mathbf{x})} \tag{5.12}$$

where $p(\mathbf{x})$ is the probability density function (pdf) of $\mathbf{x}$ and for which we have

$$p(\mathbf{x}) = \sum_{i=1}^{M} p(\mathbf{x}|\omega_i)P(\omega_i) \tag{5.13}$$

An unknown pattern, represented by the feature vector $\mathbf{x}$, is assigned to class ω_i if

$$P(\omega_i|\mathbf{x}) > P(\omega_j) \quad \forall j \neq i \tag{5.14}$$

This **Bayesian** decision rule has the property that the probability of classification error is minimized, making the **Bayesian** classifier statistically superior to any other. The densities $p(\mathbf{x}|\omega_k)$ are multivariate normal (Gaussian). The major reasons for this popularity are its computational tractability, and the fact that it models adequately a large number of cases. The pdf function is

$$p(\mathbf{x}|\omega_i) = \frac{1}{(2\pi)^{1/2}|\Sigma_i|^{1/2}} \exp\left[-\frac{1}{2}(\mathbf{x} - \mu_{\mathbf{i}})\Sigma_i^{-1}(\mathbf{x} - \mu_{\mathbf{i}})\right], i = 1, 2, \cdots, M \tag{5.15}$$

where $\mu_{\mathbf{i}} = E(\mathbf{x})$ is the mean value of the ω_i class and Σ_i is the local $l \times l$ *covariance matrix* defined as

$$\Sigma_i = E\left[(\mathbf{x} - \mu_i)(\mathbf{x} - \mu_i)^T\right] \tag{5.16}$$

Sample patterns taken from a normal distribution tend to fall in a single cluster with its center determined by the mean vector and its shape defined by the covariance matrix. Because of the exponential nature of the normal density function, it is preferable to work with the following discriminant functions, which involve the logarithmic function $\ln(\cdot)$

$$g_i(\mathbf{x}) = \ln(p(\mathbf{x}|\omega_i)P(\omega_i)) = \ln p(\mathbf{x}|\omega) + \ln P(\omega_i) \tag{5.17}$$

Substituting equation (5.15) into equation (5.17), we obtain

$$g_i(\mathbf{x}) = \ln P(\omega_i) - \frac{1}{2}\ln 2\pi - \frac{1}{2}\ln|\Sigma_i| - \frac{1}{2}(\mathbf{x} - \mu_{\mathbf{i}})^T\Sigma_i^{-1}(\mathbf{x} - \mu_{\mathbf{i}}) \tag{5.18}$$

which is the **Bayesian** decision function for normally distributed patterns. Assuming equi-probable classes with the same covariance matrix, the function $g_i(\mathbf{x})$ in equation (5.18) is simplified to

$$g_i(\mathbf{x}) = -\frac{1}{2}(\mathbf{x} - \mu_{\mathbf{i}})^T\Sigma^{-1}(\mathbf{x} - \mu_i) \tag{5.19}$$

The classifier based on this equation is called *minimum distance classifiers*. If $\Sigma = \sigma^2 I$, the maximum $g_i(\mathbf{x})$ implies minimum Euclidean distance

$$d_\varepsilon = ||\mathbf{x} - \mu_{\mathbf{i}}|| \tag{5.20}$$

where d_ε is the Euclidean distance between the feature vector $\mathbf{x}$ and μ_i the mean value of class ω_i. Thus, feature vectors are assigned to classes assorting to their Euclidean distance from the respective mean points. It was the same as the **Nearest Neighbor** rule introduced in Section 5.3.5. The theoretical basis of using the **Nearest Neighbor** search method in classifying a test feature vector is minimum distance classifiers, that is how the **Bayesian** method works in pneumatic FDD system.

5.3 Fault Detection and Diagnosis using Signal-Based Approaches

In this section, we apply various methods to perform signal-based fault detection and diagnosis in pneumatic systems. They are:

- Signal pre-processing and fingerprint analysis

- Statistical method and threshold value

- Classification of leakage types using wavelet

- Vectorized map

- Voronoi diagram

5.3.1 Signal Preprocessing and Fingerprint Analysis

In this section, results of experiments are presented with analysis, followed by discussions. The complex and intertwined system with 58 steps of operation was successfully diagnosed with the sources, location, and size of leakage fault. It also turns out that knowledge about an individual pneumatic cylinder can be employed, after the operations steps are properly separated by utilizing the sensory information. Data recorded in Festo (US) including reference (no leak) and leakage is adopted for analysis. Every figure presented in this Section is plotted based on an average of 100 repeated tests under the same situation to avoid any possible fluctuation of experimental conditions and results.

5.3.1.1 Comparison of flow rates and the need for pre-processing

First of all, the 100 data files for the reference[1] and leaked data are averaged, respectively, in order to eliminate the variances from each operation of the equipment. The two averages of the

---

[1] Reference means relatively no leakage condition because considering there is no perfect leakage free system and our pneumatic system only runs limited operation cycles.

reference and leaked data of flow rates are brought to comparison directly by plotting the average and the difference between them. The blue dashed and the solid red lines in Figures 5.4 and Figure 5.5 represent the average of 100 operation cycles of the system without and with leakage, respectively. The curve below the two curves is the difference between the leaked and the reference average flow rates. The vertical axis is the flow rate in standard liter per minute, with the green curve at the lower, starting at $0 \ l/min$ before the operation starts.

The reference flow rates at the corresponding point are expected to be always equal to or smaller than the leaked flow rate. Thus, the difference between the leaked and reference data, as represented by the green curve in the lower half in Figure 5.4, should always be larger than or equal to zero. However, this appears to be not the case in Figure 5.4 because the green curve, while starting at zero, fluctuates both at negative and positive values.

It turns out that the continuous stream of data of the flow rate for the leaked case always lag behind the reference because of the leakage, resulting in longer time to complete an extending or retracting cycle of a pneumatic cylinder. It is easy to understand because when a leakage is introduced to the system, the compressed air supply is not able to provide the flow rate needed to fulfill the motion assignment. In addition, part of the air is drawn by the leakage branch. Furthermore, the time lag accumulates from one step to the other. This causes a fundamental issue in data comparison in Figure 5.4. This also applied to the pressure data in Figure 5.5. The raw data cannot be compared directly to render any useful information for diagnosis. We have a dilemma.

The answer to this problem in comparing the data obtained and plotted in Figure 5.4 and Figure 5.5 lies in the sensory information from the sensor network associated with pneumatic cylinders. In order to eliminate the variation of data in the time domain due to time lag accumulated from each step, a pre-processor is needed to remove the accumulated lag, and to synchronize the reference with the leaked data for comparison.

In other words, each step of both leaked and reference data should be synchronized, by removing the lag and accumulated lags, in order for them to be brought to compare. Here, it is necessary to introduce the digital sensor data that records the logic states of each valve and/or
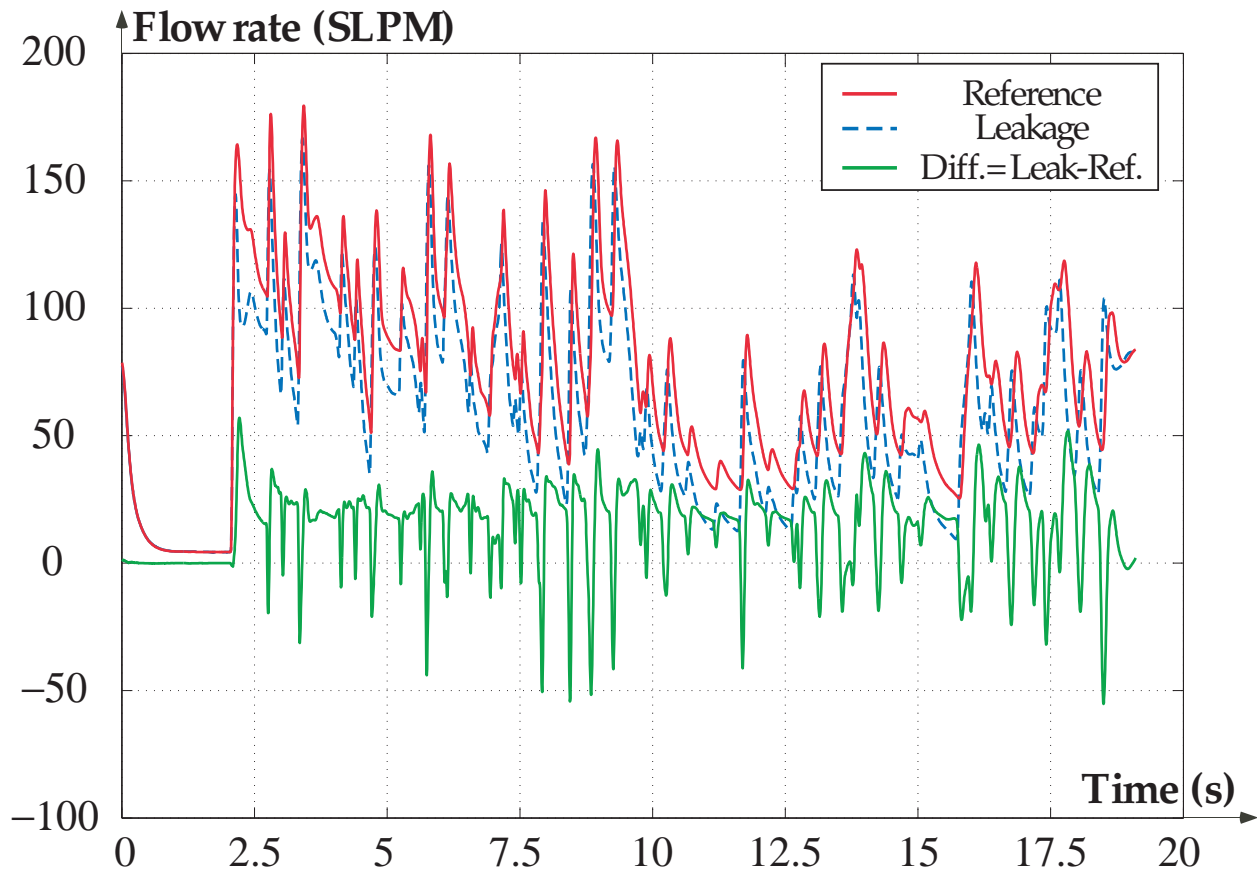
Figure 5.4: The average flow rate of the entire operating cycle. In the plot, the blue dashed and the solid red lines represent the average of 100 operations of the system without and with leakage, respectively. The curve below the two curves is the difference between the leaked and the reference data average

each proximity sensor in the data file. Each step, starting with the relevant valve firing, should be synchronized. This lag removal can be done by using such digital sensory information.

In Figure 5.6, the averaged flow rates without pre-processing of synchronization of steps 2 and 3 are plotted in the left and right plots. While step 2 provides fair comparison because this is the very first step of actual operation, step 3 inherited a time lag due to leakage from step 2, and shows a negative value for certain period of time, which is not a true reflection of the reality. It is obvious that the two average flow rate curves are not synchronized, as shown in the right plot in
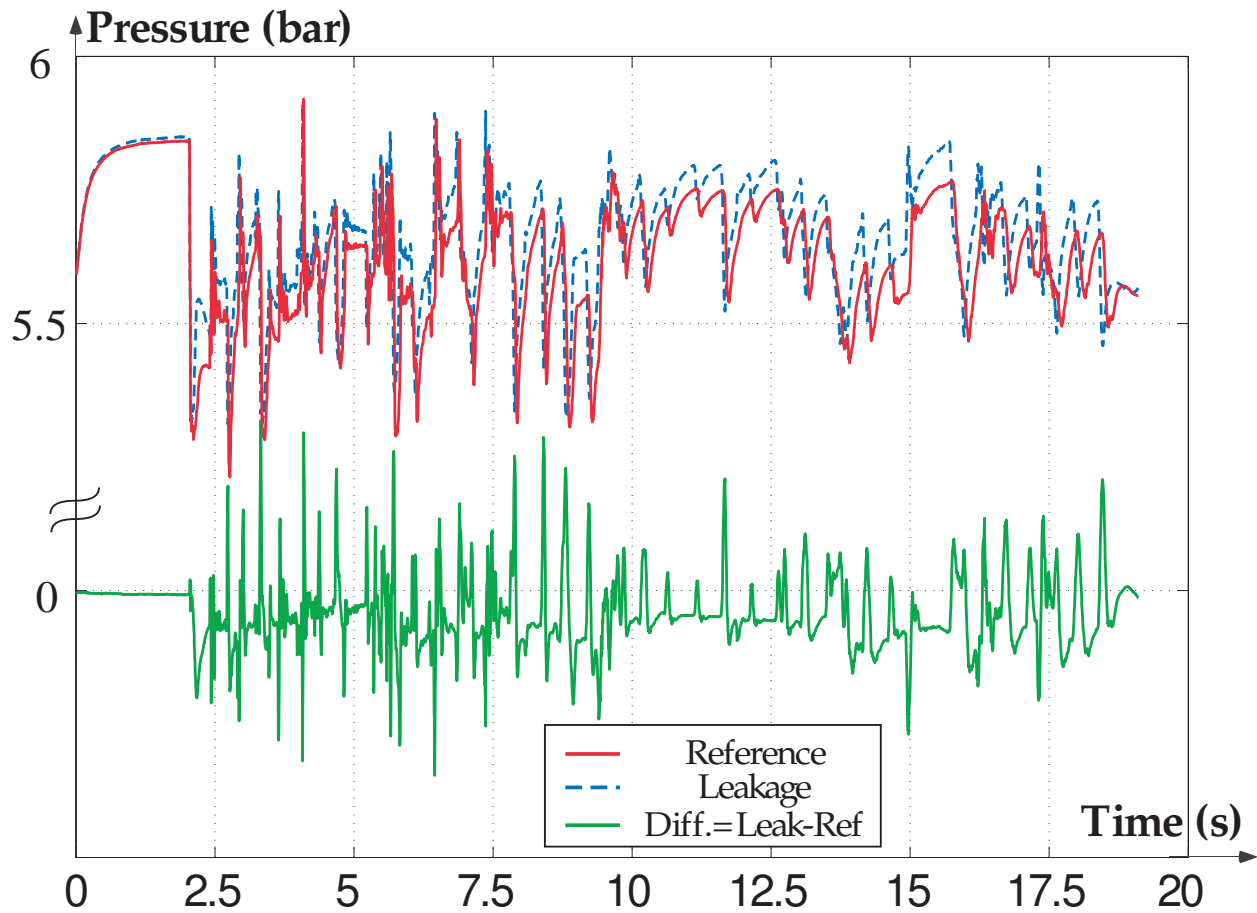
Figure 5.5: The average pressure of the entire operating cycle from 100 data files

Figure 5.6.

Figure 5.7 rectifies the problem presented in Figure 5.6 by utilizing the timing signals from the sensory information of valve's logic states or proximity sensors. With proper adjustment to remove the time lag, one finds that the difference in step 3 at approximately the same value of about 20 l/min. Step 2 starts zero, and quickly escalates to a peak value of about 60 l/min, before it gradually reduces and reaches 20 l/min.
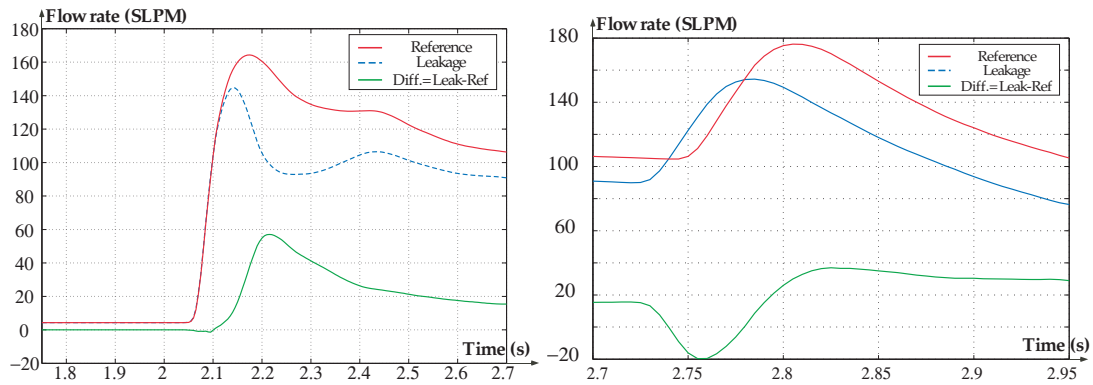
Figure 5.6: Comparison of the raw data of average flow rates without pre-processing of synchronization. The two steps shown are (*left*) step 2 and (*right*) step 3 before preprocessing for synchronization
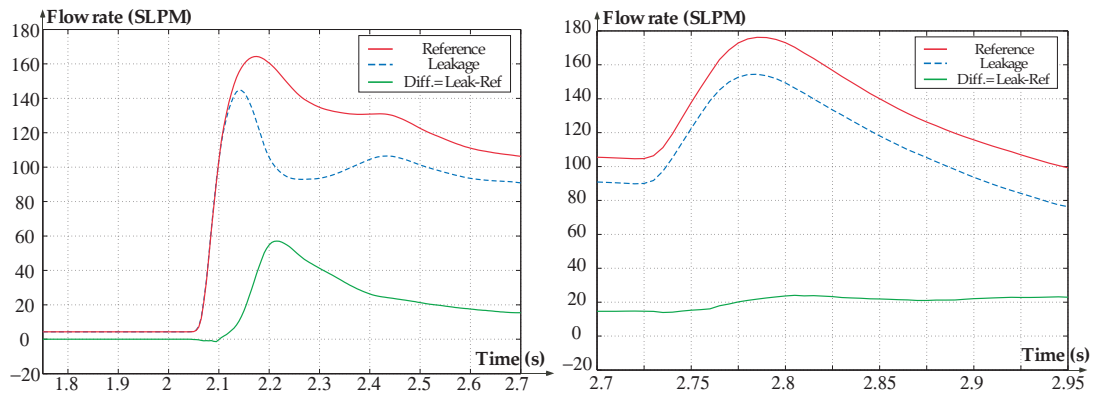
Figure 5.7: Comparison of average flow rates after pre-processing for synchronization. (*left*) step 2 and (*right*) step 3. It is noted that step 3 is significantly different from the corresponding plot in Figure 5.6

5.3.1.2   Consistent leakage–supply fault

There are 58 steps in a complete cycle of operation and movement. To determine the leakage fault of the system, the investigation and comparison of flow rate of each step is required. With the unique and/or consistent features analyzed, the intelligent detection method can be established.

Once the pre-processing is imposed, it can be readily recognized from all 58 steps that there

is always a systematic leakage at a consistent level of about 20 *l/min*. This consistent leakage throughout the entire operation is due to a leakage at the supply. As illustrated by the three steps in Figure 5.8, a systematic leakage is identified throughout the process. This consistent leakage cannot be attributed to any single pneumatic cylinder, other than the leakage at the supply of house air within the pneumatic circuit shown in Figure 3.12.
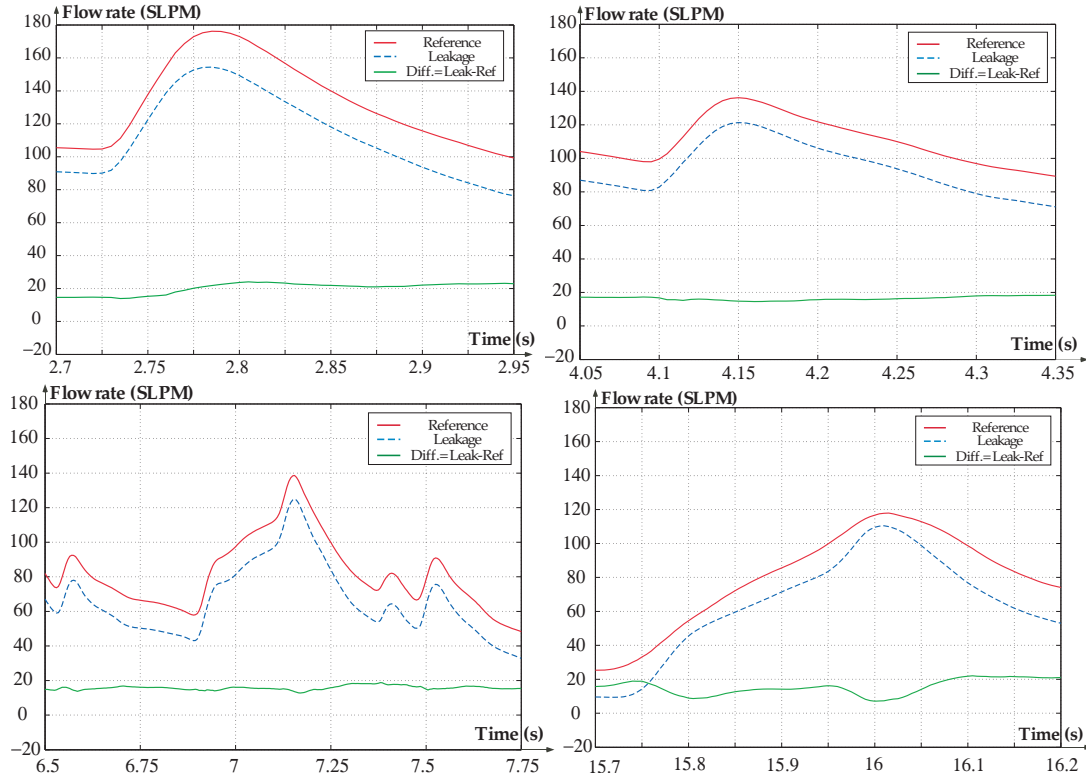
Figure 5.8: Systematic leakage at supply of house air: (*top left*) step 3, (*top right*) step 7, (*bottom right*) step 16, and (*bottom right*) step 46

5.3.1.3 Localized fault–leakage at DNC_B

In addition to the systematic leakage fault identified in Section 5.3.1.2, we proceed to detect localized leakage fault which is introduced on the branch lines of the system. As illustrated in Figure 5.9, both steps 2 and 58 involve a different pattern compared to all other cycles, such as those in Figure 5.8. Both steps involve the pneumatic cylinder and actuation valve identified as DNC_B (the rod side tube connecting to the DNC cylinder). The plots of flow rates and their
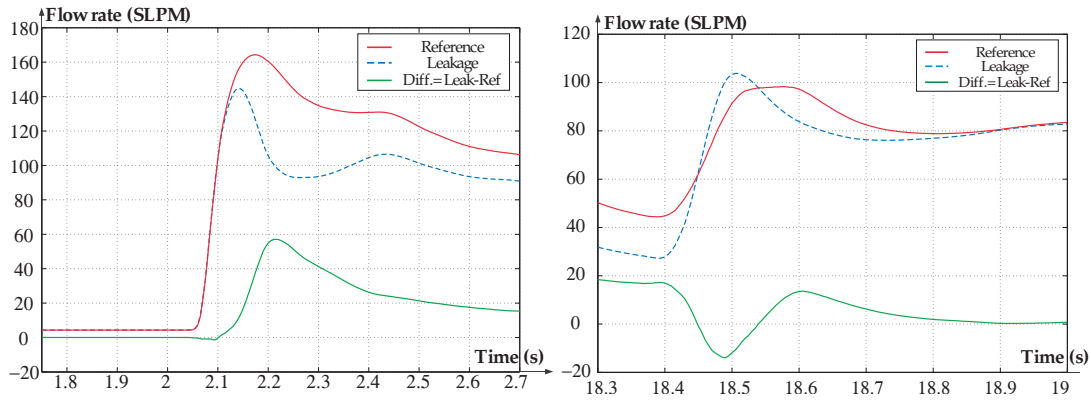
Figure 5.9: Localized leakage fault detected at DNC_B with extending and retracting, respectively. Plots shown here are (*left*) step 2 and (*right*) step 58

differences are shown in Figure 5.9.

As illustrated in Figure 3.12, the leakage at the DNC_B side of the DNC pneumatic cylinder causes more air to flow at higher flow rate in order for DNC to retract at step 2. This results in a sudden surge of flow into DNC_B to compensate for the leakage in order to actuate the retracting movement. On the other hand, step 58 is the extending movement going against the DNC_B with leak, making it easier to extend in a faster speed. This results in a smaller flow rate compared to reference data; hence, the leaked flow is lower than the reference flow for a brief period of time.

5.3.1.4   Patterns of flow rates for fingerprint analysis

One step (step 6) from the dataset is chosen to show the difference between the data without leak and with leak and the relationship between recorded data and the actuator movement. The two plots in Figure 5.10 share similar fingerprint of data, as expected. This means that the actuator dynamic motion determines the curve shape / characteristics of flow rate of and the leakage affects the curves quantitatively.

5.3.1.5   Location and size of the leakage fault

The results presented so far illustrate the ability of the proposed methodology to diagnose the location of the leakage fault as well as the quantity of the leakage fault using the FDD method.
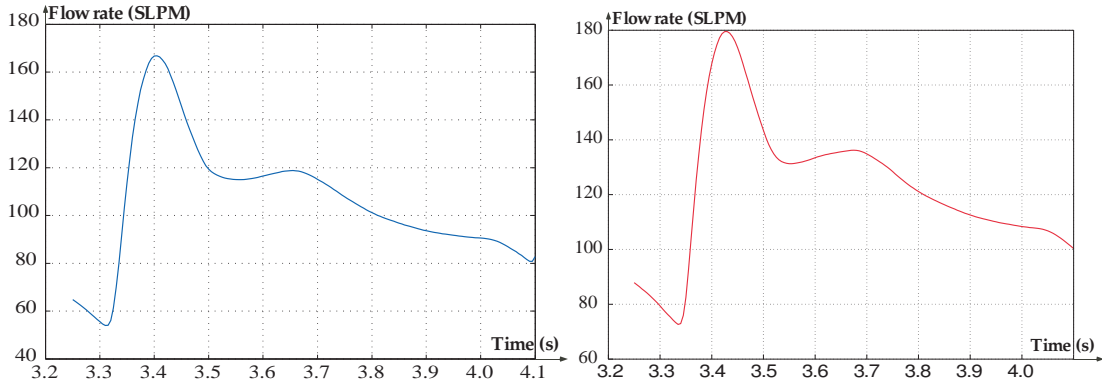
Figure 5.10: Comparison of the flow rates of step 6: (*left*) without leak (reference), and (*right*) with leakage

First, the location of fault is detected when the distinct fingerprint of difference data is found. The obviously varying difference between the data in steps 2 and 58 shows that only these two steps are involved in the movement of actuator having leakage. The detailed sensory information of steps 2 and 58 helps to further pinpoint the exact location of a leakage. Secondly, it is evident that there is a constant leak in all steps. This can be found from the other 56 steps without the target leakage. It is considered as the supply leak with an amount of 28 SLPM. For the local fault of DNC_B, the size of leakage is 55 SLPM derived from step 2. Because of extra amount of air other than the 28 SLPM constant supply leak is obvious only when air is pushed into DNC_B side not extending the cylinder.

5.3.2 Apply Statistical Method in Fault Detection

The statistical method presented in Section 5.2.1 is useful in finding a fixed threshold value to determine the upper and lower bounds of normal operation condition. For repeatedly tested cycles, Equation(5.1) can also be expressed as

$$\bar{S}_{i,j} = E\{S_{i,j}(t)\} \; ; \; \bar{\sigma}_{i,j}^2 = E\{[S_{i,j}(t) - \bar{S}_{i,j}]^2\} \tag{5.21}$$

where *i* represents one of the 6 signal types:

(1) "1" for extending pressure

(2) "2" for retracting pressure

(3) "3" for extending flow rate

(4) "4" for retracting flow rate

(5) "5" for supply flow rate

(6) "6" for supply pressure

The subscript j represents the jth sample in a complete cycle. It ranges from 1 to the longest size of a cycle. Figure 5.11 shows $S_{2,50}$ in different cycles from recorded data. Figure 5.12 is the histograph of the data plotted in Figure 5.11.
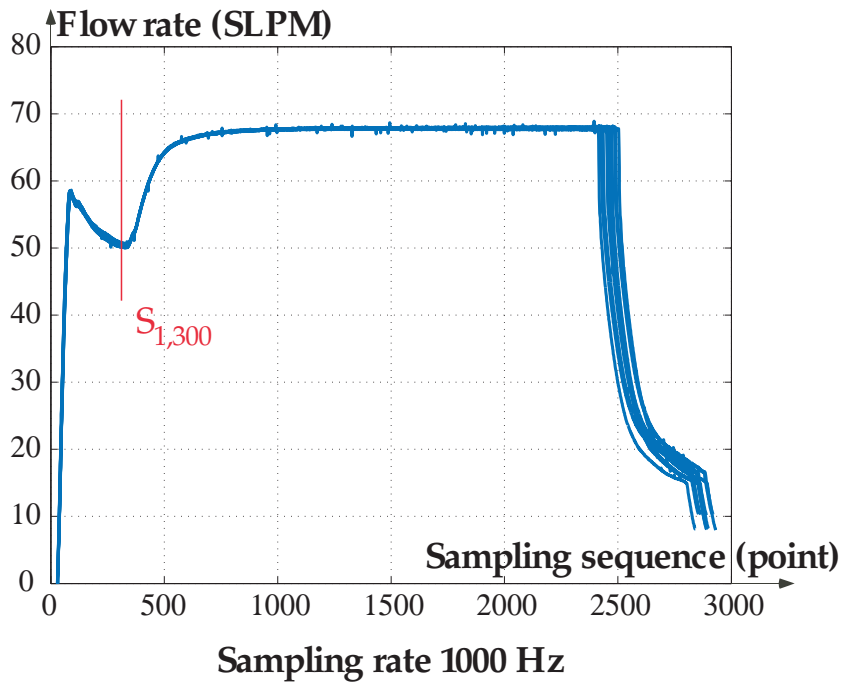
Figure 5.11: Vertical line show the 300th sample point during a complete cylinder DNC cycle. Many cycles are overlaid to show the extending pressure variation of $S_1, 300$

The parameter ε in equation (5.3) is usually a number between 2 and 3. In this dissertation, both $\varepsilon = 2$ and $\varepsilon = 3$ are shown for comparison. For the coming cycle, each sampled value $S_{i,j}$ will be compared with the three-sigma ranges, $\bar{S}_{i,j} \pm 2 \times \bar{\sigma}_{i,j}$ or $3 \times \bar{\sigma}_{i,j}$, and a threshold n will be
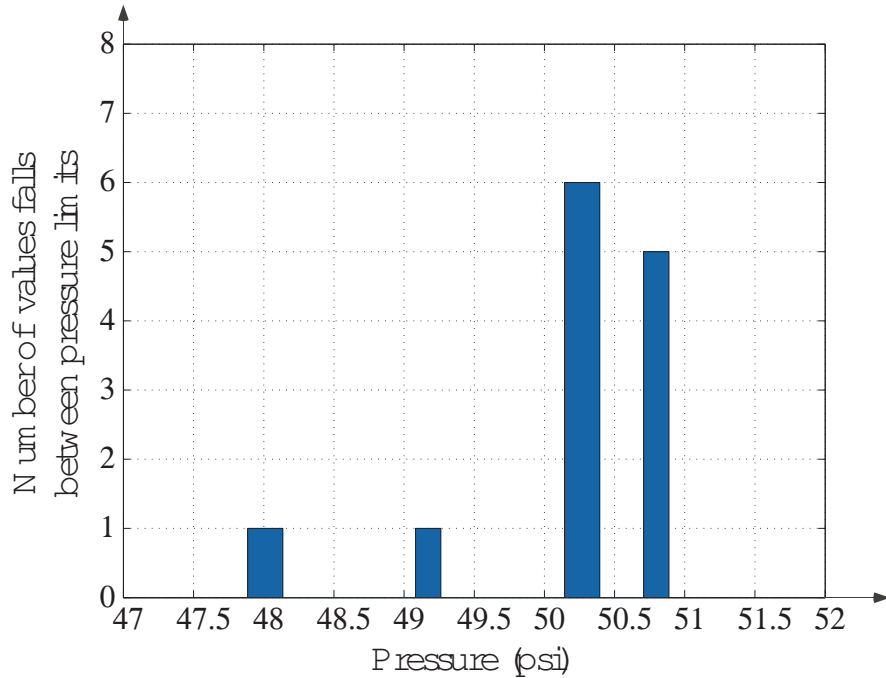
Figure 5.12: Histograph of the data points $S_1, 300$ plotted in Figure 5.11

set such that if *n%* of the coming cycle is out of the range, an error will be reported. Figure 5.13 shows both an $\varepsilon = 2$ deviation and an $\varepsilon = 2$ deviation from normal condition of DNC extending side pressure during the whole cycle as well as faulty conditions at 2, 4, 5, and 6 turns together. Figure 5.14 displays the threshold range in details, and method is very sensitive to disturbance. The right selection of a threshold value depends of the knowledge of the system, hardware setup requirements, and energy efficiency point of view.

We can also take the average of some coming cycles and use the statistic inference method, such as *Bayes decision* [99], to detect a fault. The statistic inference method obtains the average of some cycles, and is more robust to the fluctuation of the air supply. Based on the study in this chapter, a fault diagnosis system can be formed. The signals corresponding to different simulated faults form *M* classes. The algorithm for the so-called nearest neighbor rule is summarized as follows. Given an unknown feature, vector **x**, and a distance measure, then [100, 101, 102, 103, 85]

- Out of the *N* training vectors, identify the *k* nearest neighbors, irrespective of class label; *k* is chosen to be odd.

- Out of these k samples, identify the number of vectors, k_i, that belong to class ω_i, i=1,2, ..., M; obviously $\Sigma_i k_i = k$.

- Assign x to the class ω_i with the maximum number of k_i samples.

Various distance measures can be used, including the Euclidean and Mahalanobis distance. The simplest version of the algorithm is for $k = 1$, know as the Nearest Neighbor (NN) rule. In other words, a feature vector **x** is assigned to the class of its nearest neighbor.
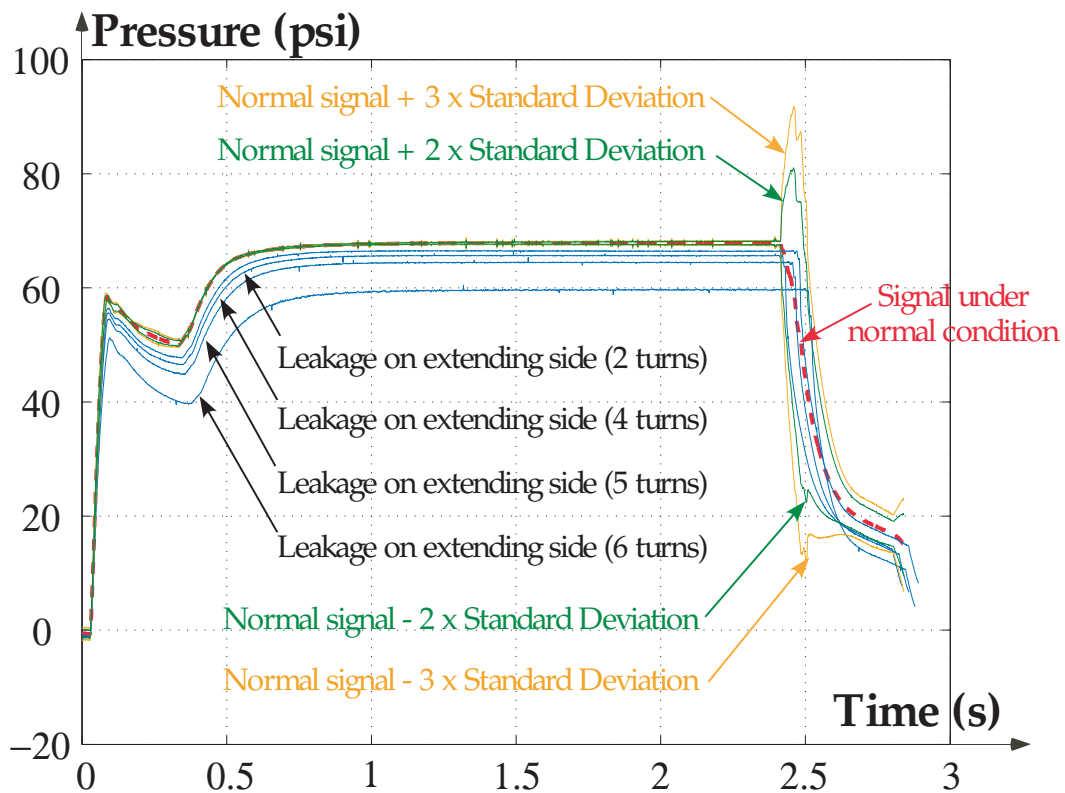
Figure 5.13: Statistical fault detection and threshold values ranges.(Extending side pressure during the whole cycle)

In this dissertation, the average, $\bar{S}_{i,j}$, from different simulated faults will be described as M different classes. The distance between incoming sampled averages, $\bar{S}'_{i,t}$ and $\bar{S}_{i,j}$, will be calculated in the following way:
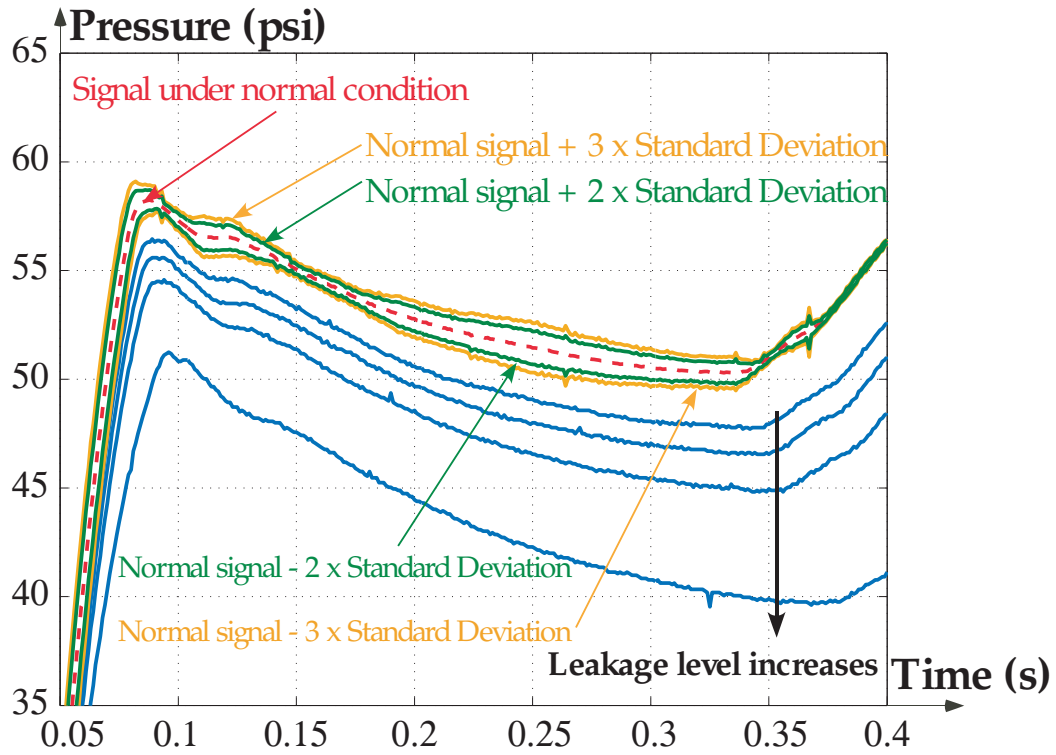
Figure 5.14: A detailed view of Figure 5.13

$$D = \left(\sum_{i=1}^{4} \sum_{j=1}^{n} (\bar{S}'_{i,j} - \bar{S}_{i,j})^2\right)^{1/2} \qquad (5.22)$$

Calculate D for all M classes, find the smallest D, and the incoming signals will be assigned to that class.

5.3.3   Apply Wavelet in Fault Classification

In this dissertation, wavelet transform is used in feature extraction and classification. Infinitely many choices of features could be extracted, including the wavelet coefficients themselves or any combination of the coefficients. When computing the DWT, two input parameters are required: (i) the choice of mother wavelet, and (ii) the level of decomposition [104]. The background information presented in Section 5.2.2 about wavelet can be summarized into two points [105]:

- The fine-scale and large-scale information in the original signal are separated into the

96

wavelet detail and approximation coefficients, respectively.

- The wavelet decomposition coefficients include all information in the original signal.

In this section, the wavelet decomposition to level 3 (cA_i and cD_i with $i = 1, 2, 3$) of a sample cycle is performed. In Figure 5.15, the wavelet analysis with $cA1$ and $cD3$ components of the flow rate signals of both reference and leaked curves associated with step 2 (DNC cylinder retracting) are presented. The $cA1$ component (left plot) suggests a delay in the leaked data with a time lag in the upper curve (leaked flow rate). It shows the same, almost overlapping rising curve when the step starts. The $cD3$ curves shows the level of valleys at the rising edge of the response, followed by a peak when the flow rates are reduced. At the end of the step, the $cD3$ plot shows the time lag in the form of similar fingerprint but shifted response.

(a) Components of cA1   (b) Components of cD3
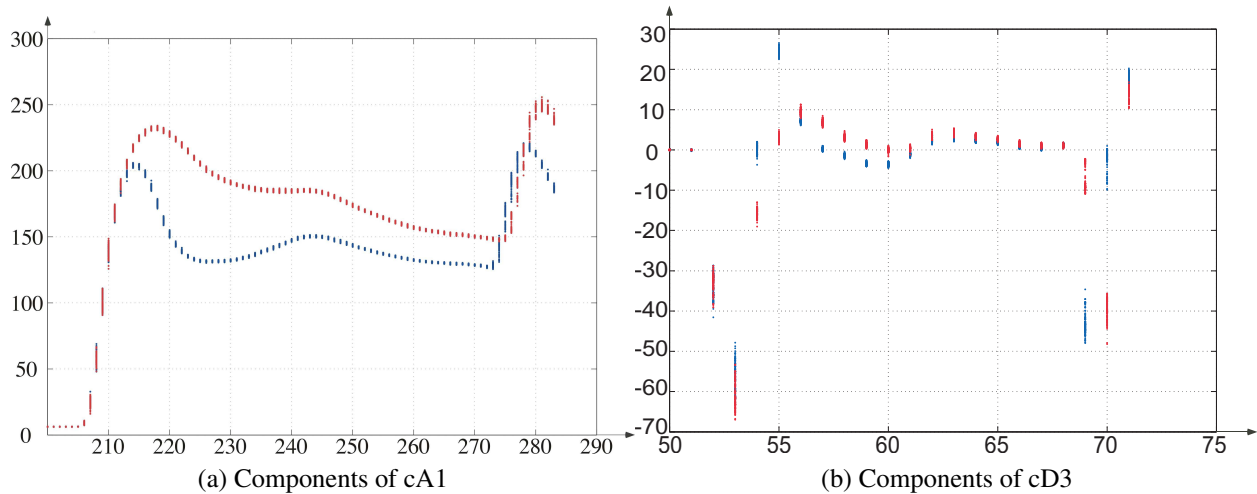
Figure 5.15: Wavelet analysis of the flow rates in step 2

Based on the individual features selected, the fingerprint of the characteristics of signals can be captured by the wavelet method. Two of such coefficients of wavelet transform are shown in Figures 5.16 and 5.17. In Figure 5.16, The leakage reflected on extending line and extracting line are compared. This coefficient effectively captures the falling edge of the P_a signal. Large leakage leads to longer time for the extending stroke and results in clusters of data that can be

used for diagnosis of the size of leakage. In the left plot of Figure 5.17, the sizes of leakage are reflected by the approximate coefficients, cA3, which captures the magnitude of P_a that decreases with increasing leakage on the extending line.
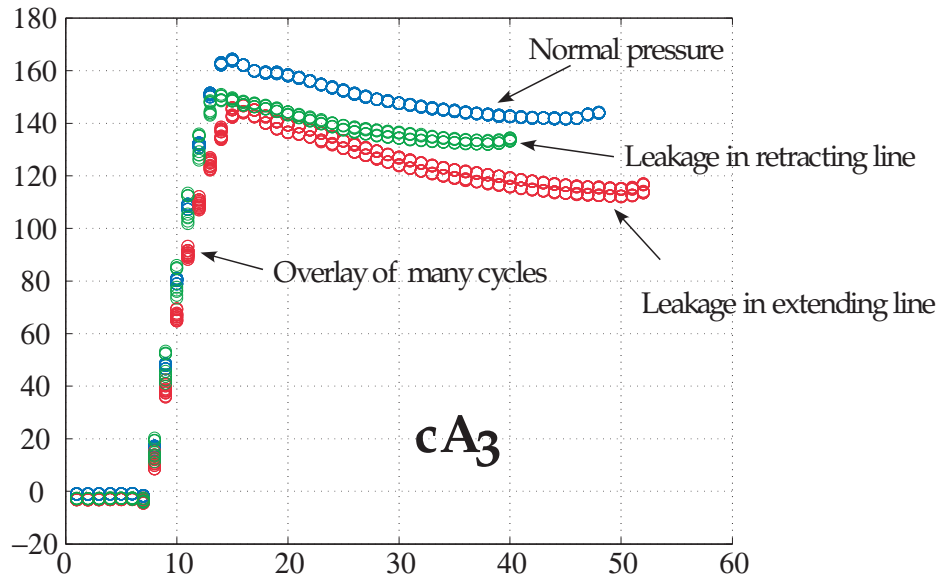
Figure 5.16: Diagnosis of the leakage location at extending and retracting lines using the wavelet approximate coefficients of extending line pressure data

5.3.4   Vectorized Map

The total flow integrated from the flow rate obtained by the flow meter (See equation(4.17)) can be employed to render a 2D plot to quantitatively determine the location and size of leakage, as shown in Figure 5.18. As presented in Xiaolin's dissertation [39], both axes in the figure above are normalized with respect to the standard flow at no leakage in respective axes. We observe that the data over more cycles tend to cluster, although occasional scatter exists. In addition, the leakage in either side (horizontal and vertical clusters enclosed by ellipses) was symmetric with respect to the near 45° clusters of data with equal amount of leakage on both extend and retract sides. The leakage levels are measured in the increasing order of 2, 4, 5, and 6 turns of the leak control valve knob, as indicated in Figure 5.18. Based on the three elliptical clusters of known sensor data, the
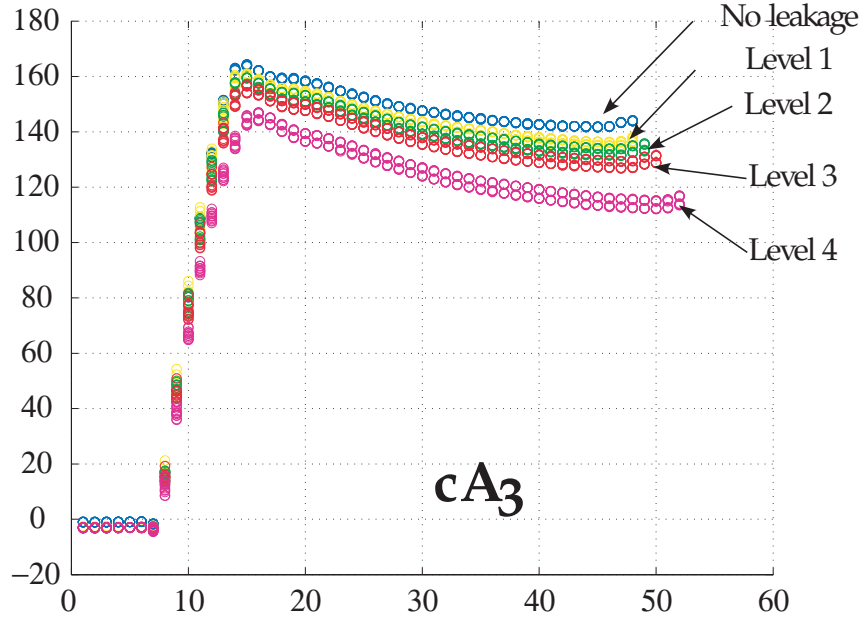
Figure 5.17: Diagnosis of various leakage size using the wavelet approximate coefficients of extending line pressure data when leakage is in extending line

four new data clusters encircled with numbers 1 to 4 can be readily diagnosed. For example, data cluster number 1 corresponds to 2 turns of extending side leakage and 5 turns of retracting side leakage. As indicated in Figure 5.18, the vector drawn to cluster 3 is almost exactly the vector sum of corresponding leakage levels on each side. Other clusters also follow the same 2D vector pattern. In a vector modeling equation, we can write

$$\overrightarrow{L}_1 = (\overrightarrow{L}_e)_2 + (\overrightarrow{L}_r)_5 \quad or \quad \overrightarrow{L} = \overrightarrow{L}_1 + \overrightarrow{L}_2 \tag{5.23}$$

$$\text{in N-manifold:} \quad \overrightarrow{L} = \overrightarrow{L}_1 + \overrightarrow{L}_2 + \cdots + \overrightarrow{L}_n \tag{5.24}$$

This is a very effective model-based technique using signal-based data for FDD because the location and size of leakage can be represented by the the vector space map using sensor data of flow rate. This technique can be potentially extended to a system of N leakages by constructing sensor data of N-manifold as indicated in equation (5.24), similar to the concept of the 2D
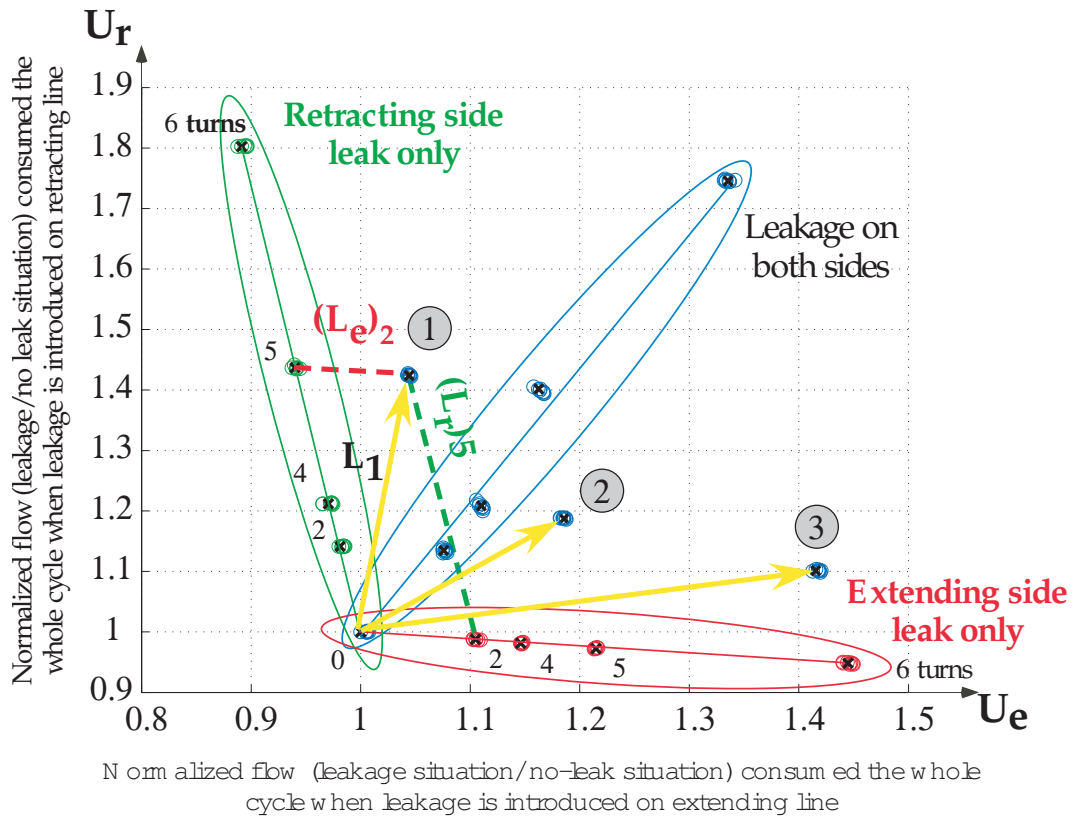
Figure 5.18: Vectorized model-based analysis of leakage location and size

case demonstrated in equation (5.23). The interpretation of sensor data will render the fault detection and diagnosis of size and location of leak. The *N*-manifold vectorized map of leakage is implemented in a stepwise method. Namely, the selected features are ordered according to their effectiveness in distinguishing the differences between leakage configurations. At the beginning of the diagnosis, only two features are used. If the vector made up of the two features succeeds in FDD, the process will stop. If there is still ambiguity, the other features will be added one by one to the vector until it succeeds in fault detection and diagnosis.

5.3.5   Voronoi Diagram

The aim of a classifier is to determine the closest feature vector to a query feature vector. The problem of finding the nearest neighbor in multidimensional space arises in several areas such as pattern classification, nonparametric estimation, information retrieval from multi-key databases,

and image and speech data compression using vector quantization. The computational complexity of the nearest-neighbor search is a major problem in these areas when the size N of the point set to be searched becomes very large. As a result, the problem of developing algorithms for fast nearest-neighbor searches has attracted significant attention. In this dissertation, the fast nearest-neighbor search is considered in the context of vector quantization.
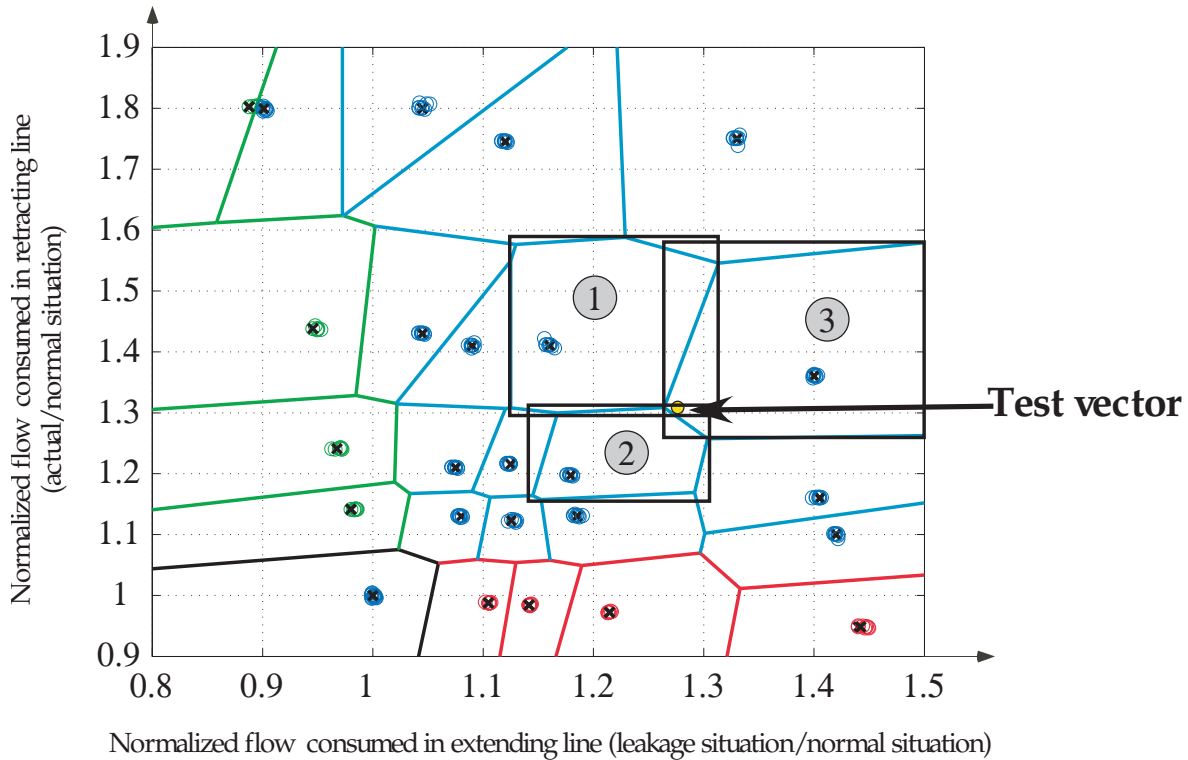
Figure 5.19: Example of Voronoi based search

Vector quantization is a powerful data compression technique used in speech coding, image coding, and speech recognition. Vector quantization has the potential to achieve classifying performance close to the rate-distortion limit with increasing vector dimension. However, the utilization of vector quantization is severely limited by its classifying complexity which increases exponentially with dimension K. Vector quantization classifying is the minimum-distortion quantization of a vector $x(x_1, ..., x_K)$ (referred to as the test vector), using a given set of N, K-dimensional classes (called the training classes C, of size N), under some distance measure $d(x, y)$. This involves finding the nearest neighbor of x in C, given by $q(x) \in c_j : d(x, c_j) < d(x, c_i)$, $i \in 1, ..., N$, which

requires N vector distance computations $d(x, c_i)$ using the exhaustive full search for classes of size N. The classes of size N are related to the dimension K, and the complexity of classifying x increases exponentially with K. The classifying complexity also constitutes the most computation intensive step in the iterative vector.

In this dissertation, a fast search method based on the Voronoi diagram is employed. The Voronoi diagram, a collection of geometric objects, is a partition of space into cells, each of which consists of points closer to one particular object than to any others. The Voronoi diagram permits the search process to be viewed as a point location problem to determine the feature vector (like a point in K dimensional space) [106, 107, 108]. In this method, the search space is partitioned into a number of classes – a set of non-overlapped regions. Each test point falling inside one region is said to belong to that region.

The fast search using the Voronoi diagram consists of two steps:

(1) construction of the Voronoi diagram: a preprocessing phase of constructing the Voronoi diagram, and

(2) identification of the vector location.

This is typically the situation in pattern classification application, where it is required to classify a test vector with long sequences in time using a given classifier. All currently known solutions for large dimensions pose major practical difficulties in term of high preprocessing, storage, and overhead costs in constructing and using the Voronoi diagram, despite their excellent asymptotic search time obtained theoretically. In this dissertation, we employ a method called *stepwise Voronoi search* to implement the fast search method. Stepwise Voronoi search overcomes this shortcoming of the high dimensional Voronoi method.

Two features are used to create the Voronoi diagram. The fast search using the stepwise Voronoi can be viewed as consisting of two steps:

(1) determine the candidate set of class vectors whose boxes contain the test feature vector, and

(2) perform a full-search in the candidate set to obtain the actual nearest-neighbor of test feature vector.

The basic structure of the search using the Voronoi diagram is illustrated by an example in 2-dimension in Figure 5.19. The 2-D Voronoi region forming the box enclosing the class vector is 1, 2, 3. Consider a test vector x, the test vector is located inside the boxes of 1, 2, 3. These are the only boxes containing the test vector, and hence form the final candidate set which has to be searched to find the actual nearest neighbor with a reduced complexity of 3 distance computations against the 25 for required full search.

The main complexity of the fast search using the Voronoi diagram, in terms of the number of distances computed, is the size of the candidate set. This is determined by the average number of boxes that contain a test vector for a given test data distribution. However, the total complexity of the algorithm is highly dependent on the cost of step 1 in determining the candidate set of vectors for a given training set. Step 1 essentially contributes to the overhead computation of the fast search and it is important to obtain efficient procedures for carrying out this step in order to reduce the overall complexity of the algorithm.

5.4   Summary

In this chapter, we have discussed the construction of intelligent FDD systems based on the pattern recognition techniques. First, a signal preprocessing and synchronization step is introduced due to existence of lag in leakage signals by using proper sensory information. And the method of training set selection and feature extraction is discussed. After that, method of vectorized map is introduced for FDD in feature classification. Next, the Voronoi diagrams are presented with stepwise Voronoi to accelerate the diagnosis process. Finally, system evaluation and improvement suggestions are discussed. This methodology works well on our experimental testing data. Future work involving sensor reduction and optimization, an extension from signal-based diagnostic approaches, are discussed in Section 6.2.2.

Chapter 6

CONCLUSIONS AND FUTURE WORK

In this dissertation, fault (especially leakage) detection and diagnosis in pneumatic systems is studied. The research topics include system components (valve, cylinder, tube, and leakage fault) modeling, preprocessing and utilization of sensory information, pinpoint fault location and indicated fault level using model-based approaches including pneumatic analogy, logistic table, and system model as well as signal-based methods including statistical methods, wavelet classification, vectorized map, and voronoi diagram in a multi-actuator PLC control pneumatic system. The conclusions and future work are given in the following.

6.1   Conclusions

The supervision of systems is very important in modern manufacturing automation. This dissertation discusses of building a fault detection and diagnosis (FDD) system for complicated pneumatic systems, which is widely in demand and used in automation. Two major categories of approaches are employed in the development of the diagnostic system: Model-based approach and signal-based approach.

First of all, a PLC control industrial multi-actuator pneumatic system is implemented to study potential fault effect on the system. Properties of the system are recorded using various sensors locating the place we interested in. Leakage is introduced in the system at different locations (extending line of a cylinder, retracting line of a cylinder, and supply line) and at different levels.

Secondly, based on the model-based analysis, the pressure and the flow of the system varies as a time function with some characteristics / fingerprints when leakage is introduced. During the experiment, we also capture the variations of system components dynamics by our pressure sensors, flow meters, and LVDT. Furthermore, digital sensors including proximity sensors and valve sensors offer the opportunity to separate motion steps in respect to one or several specific cylinders in the preprocessing of sensory information. Pneumatic analogy and the logistic table are introduced to diagnose a leakage qualitatively based on appropriately selected features. System modeling explains the properties of leakage in relationship to the parameters governing this pneumatic system quantitatively. Every method shows trustworthy results based on experimental data.

Finally, signal-based approaches are also employed in pneumatic system FDD. Statistical method is employed in deciding the threshold value for a faulty condition. Tuning the statistical parameters, the result of fault detection and diagnosis will change as well. Since redundancy exist in the sampled signal, wavelet transform is applied to reduce the redundancy of the sampled signal. After the transform, the dimension of the signal still needed to be reduced in order to construct a useful FDD algorithm. The relationship between the feature vector of signals and the fault situation in the system is revealed during diagnostic processing. It consists of two steps: the first step is to construct the relationship between signal features and known potential existing faults (like a training process) and the second step is to assign a feature vector with an unknown fault to a fault class. With the features successfully trained, a vectorized map based classifier is built to complete the diagnostic job. A feature vector from the signal with unknown fault is located on the vectorized map within the correct fault level and location area it belongs to. A stepwise Voronoi is adopted to search where the new coming feature with unknown fault should be located to and assign it to an existing fault class with a fast pace.

6.2   Future Work

6.2.1   Energy Efficiency in Compressed Air Systems

Besides leakage as an important factor of energy (money) waste, energy efficiency and efficient management of power usage also play significant roles in energy saving in compressed air systems. Even a system with zero leaks can be optimized to increase energy savings. During a recent Festo Air Consumption Analysis, it was observed that a factorys total air consumption was exceedingly high because the total system pressure was excessively increased in order to power a single cylinder that required a much higher pressure than the rest [62]. This means energy is wasted on performing an undesired job which accounts for 10% of major energy saving potential according to a technical report from the European Union [7]. Based on a U.S. Department of Energy study, every 2 psi decrease of system pressure translates to nearly 1% of energy savings.

A suitable example of saving energy through ideally sizing pneumatic components to optimally perform the function required is the pressure level required to actuate a pneumatic actuator to fulfill on assignment. The recommendation offered was to replace the double acting cylinders with single acting, spring return cylinders. As a result, the 5/3 way valve was replaced with a lower cost 3/2 way valve, and the one flow control valve was eliminated as shown in Figure 6.1. This brought the total number of connections from 9 to 5. The total air consumption was reduced by nearly 50%, and the potential sources of leakage were reduced by 44%. But, there are disadvantages to this solution which have to be taken into account:

- need to use a larger bore cylinder than the double acting cylinder to overcome spring force,

- unable to increase spring return time,

- lower retracting force, and

- shorter stroke only.

The flow control valve located on the exhaust line can be adjusted according to work requirement. If there is no strict time limitation for the operation cycle, the flow control valve can

be set in lower turns to allow the cylinder to move slower resulting in less consumption of air and smaller maximum flow rate during the operation.
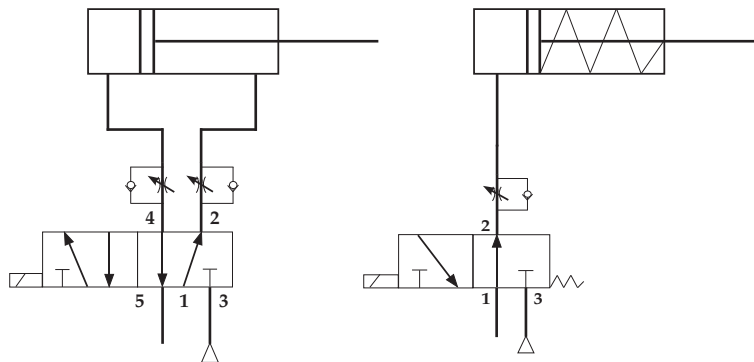
Figure 6.1: Change from double acting to single acting cylinder for energy saving purposes

A combination using both the FDD and the energy efficiency method for pneumatic system diagnosis has a procedure including: first, the installation of the measuring equipment into the main air line, followed by consumption measurements of the machine in running and standby mode; second, identifying leakage using ultrasonic equipment or FDD approaches. Every leak location is inspected and methods for future prevention of leaks in this specific location are indicated. The third step is to check every pneumatic component for correct sizing and application. After the improvements have been implemented, a second measurement is done for the purpose of cost savings analysis.

6.2.2   Sensor Reduction in Fault Detection and Diagnosis

By the help of massive sensory information, our FDD was able to be finished. However, for industrial system, flow meters and pressure sensors at any branch lines are not allowed to be installed. This leads to a huge cost of system installation especially for the flow meter. Typically, the only lines connecting on important equipment or sophisticated devices as well as the inlet line are monitored. This will make our FDD approaches impossible to realize. Sensory information is key to successful FDD and fingerprint analysis. To this end, we will study the placement of sensors (e.g., the location of flow meters in the pneumatic circuit) and their arrangement (e.g., the

107

number of pressure sensors, up-stream or down-stream of flow paths). One key idea is to arrange sensors to enhance observability, utility, and separability [109]. Certain performance indices can be formulated to characterize the ability of the system to perform intelligent FDD. Sensors can be located based on the minimization of these performance indices, as well as consideration of sensor costs, severity of faults, frequency of occurrence of different faults, and so on. As an example, we are expecting to determine the fault location and size using inlet line sensors even there are multiple cylinders working in the same cycle. The coupled information from various cylinders need to be decoupled based on the established knowledge of individual cylinder models and characteristics. Certainly, information from digital sensors cannot be omitted and it is also a necessary basis for system automation control.

Flow meter is considered an intrusive device to the system when it is installed in the flow path for the purpose of diagnosis or monitoring, and it changes the characteristics (generating laminar flow to measure flow rate) and performance of the system. To this end, continuing study and exploration of pneumatic systems without intrusive flow meters, for example, pressure sensors only, can be helpful in FDD.

Bibliography

[1] I. J. Busch-Vishniac. *Electro-mechanical Sensors and Actuators*. Mechanical Engineering Series, Series Editor, Frederic F. Ling, Springer, 1999.

[2] J. E. Bobrow and F. Jabbari. Adaptive pneumatic force actuation and position control. *ASME Journal of Dynamic Systems, Measurement, and Control*, 113:267–272, June 1991.

[3] A. R. Plummer R. Richardson and M. D. Brown. Self-tuning control of a lowfriction pneumatic actuator under the influence of gravity. *IEEE Transactions on Control System Technology*, 9, Issue 2:330–334, 2001.

[4] XENERGY Inc. Assessment of the market for compressed air efficiency services. Technical report, U.S. Department of EnergyU.S. Department of Energy, June 2001.

[5] A. Esposito. *Fluid Power with Applications*. Prentice-Hall, Inc., 4 th edition, 1997.

[6] DOEs Industrial Technologies Program and CAC. Compressed air tip sheet 3 - minimize comprssed air leaks. Technical report, U. S. Department of Energy, August 2004.

[7] P. Radgen and E. Blausein. Compressed air systems in the european union. Technical report, European Commission, Oct. 2000.

[8] J. J. Gertler. *Fault Detection and Diagnosis in Engineering Systems*. Marcel Dekker, Inc., 1998.

[9] David M. Himmelblau. *Fault detection and diagnosis in chemical and petrochemical processes*. Elsevier Scientific Pub. Co., 1978.

[10] F. Akbaryan and P. R. Bishnoi. Fault diagnosis of multivariate systems using pattern recognition and multisensor data analysis technique. *Computers and Chemical Engineering*, 25:1313–1339, 2001.

[11] H. Kumamoto, K. Ikenchi, K. Inoue, and E. J. Henley. Application of expert system techniques to fault diagnosis. *The Chemical Engineering Journal*, 29:1–9, 1984.

[12] J. L. Shearer. Study of pneumatic processes in the continuous control of motion with compressed air, parts i and ii. *Trans. of the ASME*, Feb.:233–249, 1956.

[13] D. McCloy and H. R. Martin. *Control of Fluid Power: Analysis and Design*. Ellis Horwood Limited, 1980.

[14] E. Richer and Y. Hurmuzlu. A high performance pneumatic force actuator system: Part i - nonlinear mathematical model. *Transactions of the ASME*, 122:416–425, Sept. 2000.

[15] E. Richer and Y. Hurmuzlu. A high performance pneumatic force actuator system: Part ii - nonlinear controller design. *Transactions of the ASME*, 122:426–434, Sept. 2000.

[16] Shu Ning and Gary M. Bone. Development of a nonlinear dynamic model for a servo pneumatic positioning system. In *Proceedings of the IEEE International Conference on Mechatronics & Automation*, July 2005.

[17] P. Ball and D. Fuessel. Close-loop fault diagnosis based on a nonlinear process model and automatic fuzzy rule generation. *Engineering Application of Artificial Intelligence*, 13:695–704, 2000.

[18] C. Lin S. Chang and C. Chang. A fuzzy diagnosis approach using dynamic fault trees. *Chemical Engineering Science*, 57:2971–2985, 2002.

[19] Y. M. Chen and M. L. Lee. Neural networks-based scheme for system failure detection and diagnosis. *Mathematics and Computers in Simulation*, 58:101–109, 2002.

[20] M. A. Kramer and J. A. Leonard. Diagnosis using backpropagation neural networks-analysis and criticism. *Computers Chem. Eng.*, 14(12):1323–1338, 1990.

[21] J. McGhee, I. A. Henderson, and A. Baird. Neural networks applied for the identification and fault diagnosis of process valves and actuators. *Measurement*, 20(4):267–275, 1997.

[22] E. N. Skoundrianos and S. G. Tzafestas. Fault diagnosis via local neural networks. *Mathematics and Computers in Simulation*, 60:169–180, 2002.

[23] C. Tsai and C. Chang. Dynamic process diagnosis via integrated neural networks. *Computers Chem. Eng.*, 19,Suppl:747–752, 1995.

[24] V. Venkatasubramanian, R. Vaidyanathan, and Y. Yamamoto. Process fault detection and diagnosis using neural networks-i. steady-state processes. *Computers Chem. Eng.*, 14(7):699–712, 1990.

[25] J. Jin and J. Shi. Automatic feature extraction of waveform signal for in-process diagnostic performance improvement. *Journal of Intelligent Manufacturing*, 12:257–268, 2001.

[26] K. Takeda Y. Tsuge, K. Hiratsuka and H. Matsuyama. A fault detection and diagnosis for the continuous process with load-fluctuations using orthogonal wavelets. *Computers and Chemical Engineering*, 24:761–767, 2000.

[27] P. M. Silveiria, R. Seara, and H. H. Zurn. An approach using wavelet transform for fault type identification in digital relaying. In *Power Engineering Society Summer Meeting*, pages 937–942, July 1999.

[28] Q. Sun and Y. Tang. Singularity analysis using continuous wavelet transform for bearing fault diagnosis. *Mechanical Systems and Signal Processing*, 16(6):1025–1041, 2002.

[29] M. A. Demetriou and M. M. Polycarpou. Fault detection, diagnosis and accommodation of dynamical systems with actuator failure via on-line approximators. In *Proceedings of American Control Conference*, pages 2879–2883, June 1998.

[30] S. P. Varma, A. Papandreou-Suppappola, and S. B. Suppapploa. Detecting faults in structures using time-frequency techniques. In *Acoustics, Speech, and Signal Processing,2001. Proceedings*, pages 3593–3596, May 2001.

[31] B. Li, G. Goddu, and M. Y. Chow. Detection of common motor bearing faults using frequency-domain vibration signals and a neural network based approach. In *Proceedings of the American Control Conference*, pages 2032–2036, June 1998.

[32] S. Jakubek and H. P. Jörgl. Fault-diagnosis and fault-compensation for nonlinear systems. In *Proceedings of the American Control Conference*, pages 3198–3202, June 2000.

[33] V. Venkatasubramanian, R. Rengaswamy, and S. N. Kavuri. A review of process fault detection and diagnosis part i: Quantitative model-based method. *Computers Chem. Eng.*, 27:293–311, 2003.

[34] V. Venkatasubramanian, R. Rengaswamy, and S. N. Kavuri. A review of process fault detection and diagnosis part ii: Qualitative models and search strategies. *Computers Chem. Eng.*, 27:313–326, 2003.

[35] V. Venkatasubramanian, R. Rengaswamy, and S. N. Kavuri. A review of process fault detection and diagnosis part iii: Qualitative process history based methods. *Computers Chem. Eng.*, 27:327–346, 2003.

[36] Xiaolin Li and Imin Kao. Analytical fault detection and diagnosis (FDD) for pneumatic systems in robotics and manufacturing automation. In *Proceedings of 2005 IEEE/RSJ International Conference*, 2005.

[37] Imin Kao, Xiaolin Li, and J. Binder. Fault detection and diagnosis of pneumatic systems. Technical report, NFPAs Educator/Industry Summit, October 2003.

[38] Xiaolin Li and Imin Kao. Fault detection and diagnosis for pneumatic system using wavelet transform and feature extraction. In *SCI-2004, the 8th World Multi-Conference on Systemics, Cybernetics, and Informatics*, July 18-21 2004.

[39] Xiaolin Li. *Intelligent fault detection and diagnosis of mechanical-pneumatic systems*. PhD thesis, Stony Brook University, 2005.

[40] S. Liu and J. E. Bobrow. An analysis of a pneumatic servo system and its application to a computer-controlled robot. *ASME Journal of Dynamic Systems, Measurement, and Control*, 110:228–235, September 1988.

[41] Y. T. Wang and R. Singh. Pneumatic chamber nonlinearities. *ASME Journal of Applied Mechanics*, 53:956–958, December 1986.

[42] I. T. Hong and R. K. Tessmann. The dynamic analysis of pneumatic systems using hypneu. In *International Fluid Power Exposition and Technical Conference*, April 1996.

[43] A. Anglani, D. Gnoni, A. Grieco, and M. Pacella. A cad environment for the nmerical simulation of servopneumatic actuator systems. *7th International Workshop on Advanced Motion Control*, 7:593–598, 2002.

[44] J. S. Pu and R. H. Weston. Steady state analysis of pneumatic servo drives. *Proceedings of the Institute of Mechanical Engineers*, 204:377–387, 1990.

[45] W. Backe and O. Ohligschlager. A model of heat transfer in pneumatic chambers. *Journal of Fluid Control*, 20:61–78, 1989.

[46] Y. Kawakami, J. Akao, S. Kawai, and T. Machiyama. Some considerations on the dynamic characteristics of pneumatic cylinders. *Journal of Fluid Control*, 19 (2):22–36, September 1988.

[47] M. B. Thomas. *Advanced Servo Control of A Pneumatic Actuator*. PhD thesis, The Ohio State University, 2003.

[48] American National Standards. Flow equations for sizing control valves. In *The Instrumentation, Systems, and Automation Society ANSI/ISA-75.01.01-2002 (IEC 60534-2-1 Mod)*. The Instrumentation, Systems, and Automation Society, 2002.

[49] International Organization for Standerdization. Pneumatic fluid power - components using compressible fluids. In *ISO 6538: 1989 (E)*. International Organization for Standerdization, 1989.

[50] B. W. McDonell and J. E. Bobrow. Modeling, identification, and control of a pneumatically actuated robot. In *IEEE International Conference on Robotics and Automation*, pages 124–129, May 1997.

[51] J. S. Pu, P. R. Moore, and R. H. Weston. Digital servo motion control of air motors. *International Journal of Production Research*, 29 (3):599–618, 1991.

[52] J. Wang, J. S. Pu, P. R. Moore, and Z. Zhang. Modeling study and servo control or air motor systems. *International Journal of Control*, 71 (3):459–476, 1998.

[53] N. D. Vaughan and J. B. Gamble. The modeling and simulation of a proportional solenoid valve. *ASME Journal of Dynamic Systems, Measurement, and Control*, 118:120–125, March 1996.

[54] J. B.Gamble and N. D. Vaughan. Comparison of sliding mode control with state feedback and pid control applied to a proportional solenoid valve. *ASME Journal of Dynamic Systems, Measurement, and Control*, 118:434–438, September 1996.

[55] G. H. Pfruendschuh, V. Kumar, and T. G. Sugar. Design and control of a 3 dof in-parallel actuated manipulator. In *IEEE International Conference on Robotics and Automation*, pages 1659–1664, 1991.

[56] C. T. Johnson and R. D. Lorenz. Experimental identification of friction and its compensation in precise, position-controlled mechanisms. *IEEE Transactions on Industrial Applications*, 28 (6):1392–1398, 1992.

[57] C. Canudas de Wit, P. Noel, A. Aubin, and B. Brogliato. Adaptive friction compensation in robot manipulator: low velocities. *International Journal of Robotics Research*, 10:189–199, 1991.

[58] Y. T. Wang and R. W. Longman. Limit cycle behavior and convergence to zero error in learning control with stick-slip friction. In *IEEE Conference on Systems, Man, and Cybernetics*, pages 2774–2779, 1994.

[59] W. B. Dunbar, R. A. de Callafon, and J. B. Kosmatka. Coulomb and viscous friction fault detection with application to a pneumatic actuator. In *IEEE/ASME International Conference on Advanced Intelligent Mechatronics*, pages 1239–1244, Como, Italy, July 2001.

[60] D. G. Caldwell, T. D. Badihi, and G. A. Medrano-Cerda. Pneumatic muscle actuator technology a light weight power system for a humanoid robot. In *IEEE International Conference on Robotica and Automation*, pages 3053–3058, Leuven, Belgium, May 1998.

[61] Festo. Festo services GFDM. Technical report, Festo (US) Services, 2008.

[62] P. Klaschka. White paper - air services reduce operational costs of pneumatic systems. Technical report, Festo Corporation, January 2008.

[63] Festo. Air is money. In *Trends in Automation*. Festo Corporation, February 2010.

[64] Festo Corporation. Trend in automation 13. Technical report, Festo Corporation, 2009.

[65] SAMSON. *Positioner Series 3730 and Series 3731, EXPERT/EXPERT+ Valve Diagnostics*. SAMSON, February 2007. T 8388 EN.

[66] Enertech. *Diagnostic and Test Equipment*. Enertech, 2950 Birch Street, Brea, CA 92821 USA. Form 321.

[67] R. Isermann and P. Balle. Trends in the application of model-based fault detection and diagnosis of technical processes. *Control Eng. Practice*, 5, NO. 5:709–719, 1997.

[68] S. Simani, C. Fantuzzi, and R. J. Patton. *Model-based Fault Diagnosis in Dynamic System Using Identification Techniques*. Springer, 2003.

[69] X. Li and I. Kao. Computer-based pneumatic system: System integration and diagnosis. Technical report, SUNY at Stony Brook, Department of Mechanical Engineering, Stony Brook, NY 11794-2300, September 2002.

[70] A. Barber. *Pneumatic Handbook*. Elsevier Advanced Technology, 1997.

[71] SMC. *Air Cylinders' Drive System: Full Stroke time & Stroke End Velocity*.

[72] C. Combastel, S. Lesecq, S. Peteropol, and S. Gentil. Model-based and wavelet approaches to induction motor on-line fault detection. *Control Engineering Practice*, 10:493–509, 2002.

[73] R. Isermann. Supervision, fault-detection and fault-diagnosis methods - an introduction. *Control Engineering Practice*, 5(5):639–652, 1997.

[74] S. Simani, C. Fantuzzi, and R. J. Patton. *Model-based Fault Diagnosis in Dynamic System Using Identification Techniques*. Springer, 2003.

[75] D. Ben-Dov and S. E. Salcudean. A force-controlled pneumatic actuator. *IEEE Trans. Rob. Autom.*, 11 (6):906–911, 1995.

[76] S. Drakunov, G. D. Hanchin, W. C. Su, and U. Ozguner. Nonlinear control of a rodless pneumatic servoactuator, or sliding modes versus coulomb friction. *Automatica*, 33, no. 7:1401–1408, 1997.

[77] J. H. Thomas. Proper valve size helps determine flow. Technical report, Control Engineering, 2000.

[78] Japanese Industrial Standards Committee. Pneumatic fluid power - components using compressible fluids - determination of flow-rate characteristics. In *Japanese Standards Association - JIS B 8390: 2000*, 2000.

[79] American National Standards. Flow equations for sizing control valves. In *The Instrumentation, Systems, and Automation Society ANSI/ISA-75.01.01-2007 (IEC 60534-2-1 Mod)*. The Instrumentation, Systems, and Automation Society, 2007.

[80] E. Richard and S. Scavarda. Comparison between linear and nonlinear control of an electropneumatic servodrive. *ASME J. Dyn. Syst., Meas., Control*, 118, Issue 2:245–252, 1996.

[81] A. M. Al-Ibrahim. Transient air temperature and pressure measurements during the charging and discharging processes of an actuating pneumatic cylinder. Master's thesis, University of Wisconsin - Madison, 1991.

[82] D. A. Hullender and R. L. Woods. Modeling of fluid control components. In *Proceedings of the First Conference on Fluid Control and Measurement, FLUCOME 85, Pergamon Press, Tokyo, London.*, 1985.

[83] A. M. Al-Ibrahim and D. R. Otis. Transient air temperature and pressure measurements during the charging and discharging processes of an actuating pneumatic cylinder. In *Proceedings of the 45th National Conference on Fluid Power*, 1992.

[84] B. Armstrong-Helouvry, P. Dupont, and C. Canudas de Wit. A survey of models, analysis tools, and compensation methods for the control of machines with friction. *Automatica*, 30 (7):1083–1138, 1994.

[85] S. Theodoridis and K. Koutroumbas. *Pattern Recognition*. Academic Press, 2003.

[86] N. Oneyama. Japanese test methods better predict pneumatic valve performance. In *Machine Design*, October 2001.

[87] R. P. Leger, W. J. Garland, and W. F. S. Poehlman. Fault detection and diagnosis using statistical control charts and artificial neural networks. *Artificial Intelligence in Engineer*, 12:35–47, 1998.

[88] A. K. Jain, R. P. W. Duin, and J. Mao. Statistical pattern recognition: A review. *IEEE Trans. on Pattern Analysis and Machine Intelligence*, 22(1):4–37, January 2000.

[89] R. Isermann. On fuzzy logic application for automatic control, supervision, and fault diagnosis. *IEEE Transaction on Systems, Man, and Cybernetics — Part A: Systems and Humans*, 28(2):221–235, March 1998.

[90] Q. Q. Huynn, L. N. Cooper, N. Intrator, and H. Shouval. Classification of underwater mammals using feature extraction based on time-frequency analysis and bcm theory. *IEEE Transactions on Signal Processing*, 46(5):1202–1207, 1998.

[91] S. Perrin, E. Duflos, P. Vanheeghe, and A. Bibaut. Multisensor fusion in the frame of evidence theory for landmines detection. *IEEE Transactions on Systems, Man and Cybernetics, Part C*, 34(4):485–498, November 2004.

[92] C. Pun and M. Lee. Extraction of shift invariant wavelet features for classification of images with different sizes. *IEEE Transactions on Pattern Analysis and Machine Intelligenc*, 26(9):1228–1233, September 2004.

[93] J. R. Sveinsson, M. O. Ulfarsson, and J. A. Benediktsson. Cluster-based feature extraction and data fusion in the wavelet domain. In *Geoscience and Remote Sensing Symposium*, pages 867–869, June 2001.

[94] The MathWorks In. *MATLAB help*, 1999.

[95] I. Daubechies. *Ten lectures on wavelets*. Society for Industrial and Applied Mathematics, 1992.

[96] C. K. Chui. *An Introduction to Wavelets*. Academic Press, 1992.

[97] C. E. Heil and D. F. Walnet. Continuous and discrete wavelet transforms. *Siam Review*, 31(4):628–666, December 1989.

[98] P. Abry. *Ondelettes et turbulence. Multirsolutions, algorithmes de dcomposition, invariance d'chelles*. Diderot Editeur, 1997.

[99] R. O. Duda and P.E. Hart. *Pattern Classification and Scene Analysis*. John Wiley and Sons, Inc., 1973.

[100] T. A. Brown and J. Kolpitz. The weighted nearest neighbor rule for class dependent samples sizes. *IEEE Trans. Information Theory*, 25:617–619, 1979.

[101] T. M. Cover. Estimation by the nearest neighbor rule. *IEEE Transactions on Information Theory*, IT-14(1):50–55, 1968.

[102] T. M. Cover and P. E. Hart. Nearest neighbor pattern classification. *IEEE Transactions on Information Theory*, IT-13(1):21–27, 1967.

[103] R. D. Short and K. Fukunaga. A new nearest neighbor distance measure. In *Proc. Fifth IEEE Int"l Conf. Pattern Recognition*, pages 81–86, 1980.

[104] A. Jensen and A. la Cour-harbo. *Ripples in Mathematics: The Discrete Wavelet Transform*. Springer, 2001.

[105] L. M. Bruce, C. H. Koger, and J. Li. Dimensionality reduction of hyperspectral data using discrete wavelet transform feature extraction. *IEEE Transaction on Geoscience and Remote Sensing*, 40(10):2331–2338, October 2002.

[106] F. Aurenhammer. Voronoi diagrams - a survey of a fundamental geometric data structure. *ACM Computing Surveys*, 23(3):346–405, 1991.

[107] M. de Berg, M. van Kreveld, M. Overmars, and O. Schwarzkopf. *Computational Geometry: algorithms and Applications*. Springer, 2000.

[108] V. Ramasubramanian and K. K. Paliwal. Voronoi projection-based fast nearest-neighbor search algorithms: Box-search and mapping table-based search techniques. *Digital Signal Processing*, 7:260–277, 1997.

[109] S. Tanaka. *Diagnosability of systems and optimal sensor location*. NY: Prentice Hall, 1989.

Appendix A

NOMENCLATURE FOR PNEUMATIC SYSTEMS

Symbols

A	Area
b	Critical pressure ratio
C	Sonic conductance
C_D	Discharge coefficient
C_V	Flow coefficient
C_{vf}	Coefficient of viscous friction
D	Diameter
E	Expectation
F_f	Friction force
F_{sf}	Stick-slip friction force
F_{cf}	Coulomb friction force
i	Current
k	Specific heat ratio, k=1.4 for air
L	Piston stroke
L	Vector in vectorized maps
l	Pipe length
M_P	Piston and rod assembly mass
m	Mass

$\dot{m}_v$	Mass flow rate through a valve
N	Numbers of cycle (one cycle including extending and retracting strokes)
P	Pressure
Q	Volumetric flow rate
Q_S	Flow rate in SLPM (standard liter per minute)
q	Heat transfer term
R	Ideal gas constant
S	Effective area
$S(t)$	Measured signal
T	Temperature
t	Time
U	Change of internal energy
U_c	Average flow per cycle for N cycles
V	Volume
V_c	Inactive volume at the end of stroke
W	Rate of change in the work
X_T	Pressure differential ratio factor
x	Displacement
$\dot{x}$	First derivative of x (velocity)
$\ddot{x}$	Second derivation of x (acceleration)
α	Adjustable factor between 1 and k
γ	Pressure momentum
δ	Changes with respect to normal values
ρ	Density
$\bar{\sigma}$	Standard deviation

Subscripts

1	Port 1
2	Port 2
a	Chamber A, cylinder blind side
b	Chamber B, cylinder rod side
air	Air
atm	Atmosphere
cr	Critical
dn	Downstream
in	Entering a chamber
L	Load
m	Meter measured
out	Leaving a chamber
Ref	Reference
up	Upstream
S	Standard condition
s	Supply